

A high-resolution spectropolarimetric survey of Herbig Ae/Be stars[★]

I. Observations and measurements

E. Alecian^{1,2,†}, G.A. Wade², C. Catala¹, J.H. Grunhut^{2,3}, J.D. Landstreet^{4,5}, S. Bagnulo⁵,
T. Böhm^{6,7}, C.P. Folsom⁵, S. Marsden^{8,9}, I. Waite⁹

¹LESIA-Observatoire de Paris, CNRS, UPMC Univ., Univ. Paris-Diderot, 5 place Jules Janssen, F-92195 Meudon Principal Cedex, France,

²Dept. of Physics, Royal Military College of Canada, PO Box 17000, Stn Forces, Kingston K7K 7B4, Canada

³Department of Physics, Queen's University, Kingston, Canada

⁴Dept. of Physics & Astronomy, University of Western Ontario, London N6A 3K7, Canada

⁵Armagh Observatory, College Hill, Armagh BT61 9DG, Northern Ireland, UK

⁶Université de Toulouse; UPS-OMP; IRAP; Toulouse, France

⁷CNRS; IRAP; 14, avenue Edouard Belin, F-31400 Toulouse, France

⁸Centre for Astronomy, School of Engineering and Physical Sciences, James Cook University, Townsville, 4811, Australia

⁹Faculty of Sciences, University of Southern Queensland, Toowoomba, 4350, Australia

Accepted . Received ; in original form

ABSTRACT

This is the first in a series of papers in which we describe and report the analysis of a large survey of Herbig Ae/Be stars in circular spectropolarimetry. Using the ESPaDOnS and Narval high-resolution spectropolarimeters at the Canada-France-Hawaii and Bernard Lyot Telescopes, respectively, we have acquired 132 circularly-polarised spectra of 70 Herbig Ae/Be stars and Herbig candidates. The large majority of these spectra are characterised by a resolving power of about 65,000, and a spectral coverage from about 3700 Å to 1 μm. The peak signal-to-noise ratio per CCD pixel ranges from below 100 (for the faintest targets) to over 1000 (for the brightest). The observations were acquired with the primary aim of searching for magnetic fields in these objects. However, our spectra are suitable for a variety of other important measurements, including rotational properties, variability, binarity, chemical abundances, circumstellar environment conditions and structure, etc. In this first paper, we describe the sample selection, the observations and their reduction, and the measurements that will comprise the basis of much of our following analysis. We describe the determination of fundamental parameters for each target. We detail the Least-Squares Deconvolution that we have applied to each of our spectra, including the selection, editing and tuning of the LSD line masks. We describe the fitting of the LSD Stokes *I* profiles using a multi-component model that yields the rotationally-broadened photospheric profile (providing the projected rotational velocity and radial velocity for each observation) as well as circumstellar emission and absorption components. Finally, we diagnose the longitudinal Zeeman effect via the measured circular polarisation, and report the longitudinal magnetic field and Stokes *V* Zeeman signature detection probability. As an appendix, we provide a detailed review of each star observed.

Key words: Stars : pre-main-sequence – Stars : early-type – Stars : magnetic fields – Stars : binaries : spectroscopic.

1 INTRODUCTION

Herbig (1960) was the first to perform a systematic study of a

certain class of stars that we call now Herbig Ae/Be (HAeBe) stars, and whose observational parameters are as follows :

- (i) the spectral type is A or earlier, with emission lines,
- (ii) the star lies in an obscured region of space, and
- (iii) the star illuminates fairly bright nebulosity in its immediate vicinity.

Herbig selected these characteristics following the observational properties of the lower-mass counterparts of HAeBe stars -

[★]. Based on observations obtained at the Canada-France-Hawaii Telescope (CFHT) which is operated by the National Research Council of Canada, the Institut National des Sciences de l'Univers of the Centre National de la Recherche Scientifique of France, and the University of Hawaii

[†]. E-mail: evelyne.alecian@obspm.fr

T Tauri stars - and built a list of 26 HAeBe stars satisfying these criteria. This list, as well as the Herbig characteristics, have been extended since this original study (e.g. Herbig & Bell 1988, Thé et al. 1994, Vieira et al. 2003), and we now know of more than a hundred HAeBe stars of spectral type earlier than F5. All of them do not necessarily show all Herbig characteristics, but all of them have infrared excess with an abnormal extinction law (compared to classical Be stars).

The characteristics enumerated above suggest that HAeBe stars are very young, still surrounded by dust and gas in an envelope or disk. However, it was the spectroscopic study of Ström et al. (1972) that brought the first solid evidence that Herbig Ae/Be stars are in the pre-main sequence (PMS) phase of quasi-static contraction, by showing that their surface gravities are systematically lower than those of their main sequence (MS) counterparts. Herbig Ae/Be stars are therefore generally believed to be the evolutionary progenitors of main sequence (MS) intermediate mass (A/B) stars.

Before the work of Palla & Stahler in the early 90's, intermediate-mass stars with masses above $3 M_{\odot}$ were believed to not experience a pre-main sequence phase similar to that of lower-mass stars (Larson 1972). More detailed calculations performed by Palla & Stahler (1990, 1991, 1992, 1993), including deuterium burning during the protostellar collapse and the pre-main sequence phase, show that optically-visible pre-main sequence stars could be observed, up to masses of about $8 M_{\odot}$. Their calculations considered a constant mass accretion rate during the protostellar collapse, and from the upper envelope of the distribution of Herbig Ae/Be stars in the HR diagram, they concluded that all stars with masses lower than $8 M_{\odot}$ are formed with a similar mass accretion rate of the order of $10^{-5} M_{\odot} \text{yr}^{-1}$.

However, following this work, many Herbig Be stars with masses larger than $8 M_{\odot}$ have been discovered in the field of the Galaxy (see e.g. Fig. 4 of this paper), as well as in very young clusters (e.g. Martayan et al. 2008), implying that the simplified model of Palla & Stahler - with a constant mass accretion rate at all masses - may be insufficient to explain the observations. In fact, Palla & Stahler themselves proposed that the mass accretion rate should be time-dependent. Norberg & Maeder (2000, NM00 hereinafter), then Behrend & Maeder (2001, BM01 hereinafter) proposed that the mass accretion rate depends on the mass or the luminosity of the growing star. As a result, the mass accretion rate should increase while the star is growing and gaining in mass and luminosity, until the circumstellar (CS) matter become sufficiently rare and the massive accretion phase stops. Whereas a unique accretion rate of $10^{-5} M_{\odot} \text{yr}^{-1}$ as proposed by Palla & Stahler (1993) results in a maximum PMS star mass of around $8 M_{\odot}$, a modulated mass accretion rate, as proposed by NM00 and BM01, allows the birth-line to reach the zero-age main sequence (ZAMS) at much higher masses (above $20 M_{\odot}$).

Herbig Ae/Be stars are indeed observed with masses as large as $20 M_{\odot}$, with a distribution more concentrated between 1.5 and $3 M_{\odot}$ (see Table 2 and Figure 4 of this paper). Their spectral types are found between F5 and B2 (Vieira et al. 2003), and many of them show some spectroscopic and photometric activity, reflective of their young age. Many types of activity can be found among Herbig Ae/Be stars, but their origins are not well understood. Among them we find the UX Ori stars, with the Herbig Ae star UX Ori as the prototype. These stars are characterised by a very strong photometric variability (up to 3 magnitudes in the V band), and by the presence of transient absorption features in their spectra that may be due to episodic accretion events (e.g. Mora et al. 2002). While some authors think that these charac-

teristics are created by the infall of cometary bodies onto the star (e.g. Grady et al. 2000b), others are more convinced by the theory of accretion from a disk, either via the intermediary of a magnetic field, or not (Natta et al. 2000; Mora et al. 2004). The presence of winds is detected in many HAeBe stars through P Cygni profiles observed in $H\alpha$ and sometimes in metallic and He lines (e.g. Finkenzeller & Mundt 1984; Bouret et al. 1997; Bouret & Catala 1998). Some authors have proposed that these winds have a stellar origin (e.g. Böhm & Catala 1994), while others believe that a disc wind is present (e.g. Corcoran & Ray 1998; Vieira et al. 2003). However, strong variability in $H\alpha$ emission profiles is observed in a few HAeBe stars, some of them at times showing double-peaked profiles, and sometimes P Cygni profiles (e.g. Thé et al. 1985a; Catala et al. 1986a). These stars show periodic cyclical modulations of their $H\alpha$ emission, but also of metallic lines such as the UV Mg II h & k doublet (e.g. Catala et al. 1989), as well as of their X-ray emission (e.g. Testa et al. 2008). Their spectra also show UV emission lines of highly-ionised species such as N V and O VI (e.g. Bouret et al. 1997). Bouret et al. (1997) proposed that these characteristics are due to the presence of a non-axisymmetric wind controlled by a stellar magnetic field. Various non-photospheric spectral features, in addition to those discussed above, are observed in the spectra of HAeBe stars, some with variability and others without. However, the interpretation of each one of these features, as well as their diversity, is not understood at all. The fact that HAeBe stars cover such a large range of mass, temperatures, age and evolutionary state, as well as the fact that these stars evolve at a variety of rates, certainly must be connected with the large variety of observed HAeBe activity phenomena and our difficulties to interpret them.

HAeBe stars are important astrophysical objects because they represent the late formative stages of intermediate mass stars. They are therefore significant for understanding general and specific phenomena involved in star formation. Moreover, HAeBe stars can help us to understand a number of perplexing properties of their main sequence (MS) descendants : in particular chemical peculiarities, very slow rotation, and magnetic fields, observed in individually or in combination in a significant fraction of MS A/B stars.

Among the MS A/B stars, a significant fraction shows photospheric abundance anomalies (as compared to solar abundances, and to the abundances of the majority of MS A/B stars). These anomalies are believed to result from atomic diffusion within their surface layers due to the competition between radiative levitation and gravitational settling (e.g. Michaud 1970). One important condition necessary to allow this phenomenon to occur is the absence of strong deep mixing in those layers, which would tend to overwhelm these separation processes. As rotation-driven circulation is an important source of such mixing, this condition implies that such chemically peculiar stars should be slow rotators. It has been observed that nearly all chemically peculiar Am, Ap/Bp and HgMn stars are characterised by slow rotation (rotation periods longer than ~ 1 day) compared to the "normal" (non-peculiar) A/B stars (Abt & Morrell 1995). The origin of this slow rotation is not well understood. In the case of Am and HgMn stars, slow rotation might be the result of tidal interaction occurring in close binary systems (i.e. those with orbital periods shorter than 100 days; e.g. Abt 2009). The mechanism responsible for the slow rotation of Ap/Bp stars is likely related to their strong magnetic fields. Stępień (2000) discussed different theories aimed at explaining this slow rotation, and he concluded that magnetic braking must occur during the PMS phase in order to reproduce the rotational angular momenta of MS A/B stars. Stępień demonstrated that magnetic coupling of a PMS

star with its accretion disk would slow the rotation of the star and increase its rotation period to a few days. In order to produce the very slowest rotators - those with observed rotation periods greater than about one month - the disk must disappear sufficiently early during the PMS phase to allow strong magnetised winds to carry away a large quantity of angular momentum before the star reaches the ZAMS.

Until recently we had very few observational constraints on the magnetic fields and the rotation of Herbig Ae/Be stars. To our knowledge, only two thorough observational studies of the evolution of the angular momentum of intermediate-mass stars during the PMS phase have been undertaken. Böhm & Catala (1995) concluded that if these stars rotate as solid bodies, the evolution of the angular momentum must depend on stellar mass, while if the internal rotation varies as (radius)⁻², the observations of HAeBe and MS A/B stars in young clusters are consistent with conservation of total angular momentum at all masses. Wolff et al. (2004) concluded that PMS intermediate-mass stars lose angular momentum before they start the PMS phase, while angular momentum is conserved during the radiative phase of PMS evolution. Both of these analyses provided very interesting results that should be discussed in the framework of a scenario of angular momentum evolution that includes magnetic fields.

A number of studies have been attempted to detect magnetic fields in Herbig Ae/Be stars, without much success (e.g. Catala et al. 1993; Hubrig et al. 2004). Apart from a marginal detection in HD 104237 reported by (Donati et al. 1997), and a possible detection in HD 101412 proposed by (Wade et al. 2007) (both being now firmly confirmed magnetic stars : Alecian et al. in prep.), no other convincing magnetic detections have been reported before the present survey. The reason is likely limited precision and an insufficiently large stellar sample as a consequence of limited observational capabilities. Fortunately, many of these limitations are overcome by today's spectropolarimetric facilities : telescopes with large collecting area, high-efficiency instruments, large spectral range, and high spectral resolution.

In order to thoroughly investigate magnetism and rotation in HAeBe stars, we have performed a large survey of 70 stars using the newest high-resolution spectropolarimetric instruments : ESPaDOnS (at the Canada-France-Hawaii telescope, CFHT, USA) and Narval (at the T lescope Bernard Lyot, TBL, France). Within the context of this survey we have detected a small number of new magnetic stars and confirmed the presence of a magnetic field already discovered during a parallel ESPaDOnS program focused on massive stars in Orion (LP Ori, Petit et al. 2008). Those discoveries (HD 190073, HD 200775, HD 72106, V380 Ori and LP Ori), and the analysis we performed to characterise their magnetic fields and related properties, have already or will be described in other papers (Wade et al. 2005; Catala et al. 2007; Alecian et al. 2008a; Folsom et al. 2008; Petit et al. 2008; Alecian et al. 2009b, Petit et al. in prep.). While this survey is focusing on HAeBe stars in the field of the Galaxy, we have also performed a similar survey of HAeBe stars in three young clusters and detected three more magnetic stars : NGC 6611 601, NGC 2244 201 and NGC 2264 83 (Alecian et al. 2008b, 2009a). The description of this cluster survey will be presented in an upcoming paper (Alecian et al. in prep.).

We are now publishing a series of papers describing the complete sample of observed field stars, discussing the observations and their analysis (this paper, paper I), an analysis of their rotation velocities (Alecian et al. 2012, paper II), an analysis of their magnetic properties (Wade et al. in prep., paper III), and the characterisation

of the CS contributions to the spectra of the sample (Alecian et al. in prep., paper IV).

This paper is organised as follows. In Sect. 2 we review the sample selection, and in Sect. 3 the observational procedure and data reduction, and summarise the characteristics and quality of the reduced spectra. In Sect. 4 we determine fundamental parameters for the stars of the sample, and in Sect. 5 describe the extraction and fitting of the Least-Squares Deconvolved profiles that we use for the majority of our analysis. In Sect. 6 we discuss the magnetic field diagnosis carried out in a number of different ways. Sect. 7 provides a discussion of the results and conclusions relevant to the analysis to be reported in papers II, III and IV.

2 SAMPLE SELECTION

Our study required the selection of a relatively large number of HAeBe stars to allow us to derive statistically meaningful conclusions about the presence of magnetic fields in these stars. Various literature sources were used for target selection, primarily the catalogues of HAeBe stars and HAeBe candidates by Th  et al. (1994) and by Vieira et al. (2003).

The catalogue of Th  et al. (1994) contains six categories of stars ; the stars selected for our study were obtained only from the first category, which contains stars historically known as HAeBe stars, or strong candidates of the group. According to the authors, all of these stars possess near- or far-infrared excess and emission lines, associated with the presence of CS dust, discs and energetic outflows which are usually found in HAeBe stellar environments. On the other hand, Vieira et al. (2003) produced a catalogue of HAeBe stars and probable candidates from an initial search for new T Tauri stars (pre-main sequence stars of lower mass) using the Infrared Astronomical Satellite (*IRAS*) point source catalogue¹. Because the initial search was based on CS dust properties, it included HAeBe stars along with T Tauri stars. Vieira et al. extracted the HAeBe stars by filtering the data using specific requirements such as a spectral type earlier than F5, emission at H α , and a minimum level of infrared emission. The majority of the stars were associated by the authors with a star forming region. Based on the quality of these two literature sources and the arguments presented by their authors, we conclude that all of the stars in our sample are *bona fide* HAeBe stars. In total, 70 HAeBe stars have been selected with visual magnitudes lower than 12, spanning in spectral type from F5 to B0.

Measurements with high-resolution spectropolarimeters (such as ESPaDOnS@CFHT or Narval@TBL) have a high enough resolving power to take advantage of the information contained in the line profiles of metallic lines, as has already been demonstrated in earlier studies with the MuSiCoS spectropolarimeter (e.g. Wade et al. 2000, Petit et al. 2004). ESPaDOnS magnetic field measurements have standard errors which decrease strongly with decreasing $v \sin i$ and with increasing richness and strength of the metallic line spectrum (c.f. Landstreet 1982 ; Shorlin et al. 2002). To fully exploit this dependence, and thus to obtain the most precise measurements possible, we have preferentially selected our targets for low $v \sin i$ ($\lesssim 100 \text{ km.s}^{-1}$) where available $v \sin i$ data allowed us to perform such a selection. However, because accurate measurements of $v \sin i$ are not available for many HAeBe stars, a significant frac-

¹ <http://irsa.ipac.caltech.edu/>

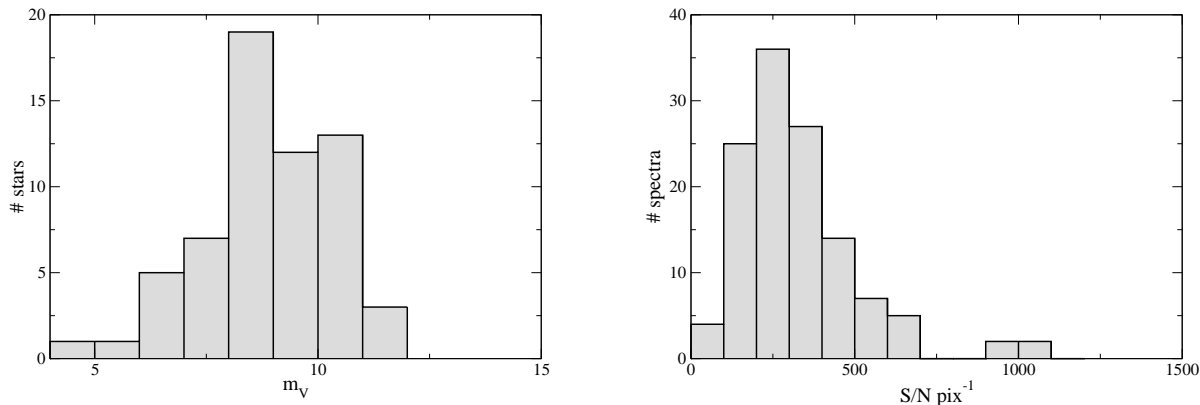


Figure 1. Distributions of m_V (left) and SNR (right) of the sample stars.

tion of our targets (about one-third) turn out to be relatively rapid rotators.

3 OBSERVATIONS AND DATA REDUCTION

The 132 program star observations reported here were obtained between 2004 and 2010 using two high-resolution spectropolarimeters : the ESPaDOnS spectropolarimeter at the Canada-France-Hawaii Telescope (80 spectra), and the Narval spectropolarimeter at the T ellescope Bernard Lyot (52 spectra). The ESPaDOnS observations were obtained during 6 observing runs in 2004 (technical and commissioning runs), 2005 and 2006 (competitively-allocated PI time), including the first scientific ESPaDOnS run. The Narval observations were obtained during 7 observing runs between 2007 and 2010 (competitively-allocated PI time).

The basic technical characteristics of ESPaDOnS and Narval are nearly identical. The polarisation analysis unit is located at the Cassegrain focus of the telescope. The stellar image is formed on an aperture followed by a collimating lens. The beam then passes through a rotatable $\lambda/2$ retarder, a fixed $\lambda/4$ retarder, a second rotatable $\lambda/2$ retarder, and finally a small-angle Wollaston prism, followed by a lens which refocuses the (now double) star image on the inputs of two optical fibres. This relatively complex polarisation analyser is necessary because one of the fundamental design parameters for ESPaDOnS/Narval was very wide wavelength coverage (approximately 3700 \AA to $1.04 \mu\text{m}$). To have retarders which are approximately achromatic over this wide range, ESPaDOnS uses Fresnel rhombs. A single Fresnel rhomb acts as a $\lambda/4$ retarder, but deviates the beam, while two Fresnel rhombs in series form a $\lambda/2$ plate without beam deviation. To minimise mechanical complications, only the double (non-deviating) Fresnel rhombs are allowed to rotate ; the configuration chosen is the minimum which allows one to analyse all of the Stokes polarisation components (Q, U, V) by appropriate orientation of the axes of the successive retarders.

The two output beams from the Wollaston prism, which have been split into the two components of circular polarisation (for this study) by appropriate retarder orientations, are then carried by the pair of optical fibres to a stationary and temperature-controlled cross-dispersed spectrograph where two interleaved spectra are formed, covering virtually the entire desired wavelength range with a resolving power of $R \approx 65000$. The I component of the stellar

Stokes vector is formed by adding the two corresponding spectra, while the desired polarisation component (Q, U, V) is obtained essentially from the difference of the two spectra. To minimise systematic errors due to small misalignments, differences in transmission, effects of seeing, etc., one complete observation of a star consists of four successive sub exposures ; for the second and third, the retarder orientations are changed so as to exchange the beam paths of the two analysed spectra (see Donati et al. 1997).

The actual reduction of observations is carried out at the observatory using the dedicated software package Libre-ESPRIT. Libre-Esprit subtracts bias, locates the various spectral orders on the CCD image, measures the shape of each order and models the (varying) slit geometry, identifies comparison lines for each order and computes a global wavelength model of all orders, performs an optimal extraction of each order, and combines the resulting spectra to obtain one-dimensional intensity (Stokes I) and circular polarisation (Stokes V) spectra. The Stokes V spectrum normally has the continuum polarisation removed, as this arises mainly from instrumental effects and carries little information about the star. Each spectrum is corrected to the heliocentric frame of reference, and may optionally be divided by a flat field and be approximately normalised (see Donati et al. 1997, and ESPaDOnS www pages²). Due to the presence of strong emission lines in the spectra of many of our targets, the automatic Libre-Esprit normalisation fails to achieve a satisfactory rectification of the continuum. We have therefore turned off this option in Libre-Esprit, and normalised the final reduced one-dimensional spectra manually, order-by-order.

Diagnostic null spectra called N spectra, computed by combining the four successive sub exposures of polarisation in such a way as to have the real polarisation cancel out (Donati et al. 1997), are also calculated by Libre-Esprit. The N spectra test the system for spurious polarisation signals. In all of our observations, the N spectra are quite featureless, as expected. The final spectra consist of ascii files tabulating $I/I_c, V/I_c, N/I_c$, and estimated uncertainty per pixel as a function of wavelength, order by order.

The log of spectropolarimetric observations is reported in Table 1. The 132 observations include 112 observations of 64 apparently non-magnetic program stars, 9 observations of 5 magnetic program stars (the discovery and/or confirmation observations of

² <http://www.cfht.hawaii.edu/Instruments/Spectroscopy/Espadons>

each), and 11 observations of one possibly newly-detected magnetic program star (HD 35929).

Because the program stars observed in this study are characterised by a large range of visual magnitudes (reflecting their diverse luminosities, distances and extinctions due to their surrounding environments), the distribution of their apparent magnitudes m_V (shown in Fig. 1, left panel) is rather broad (with a mean of 8.9, a minimum of 4.2 and a maximum of 11.9). As a consequence, our data yield a broad distribution of signal-to-noise ratios (SNRs, illustrated in Fig. 1, right panel), ranging from below 100 per CCD pixel to over 1000.

4 FUNDAMENTAL PARAMETERS

4.1 Effective temperature and surface gravity determination

The temperature and gravity, as well as their errors, of each star was first taken from the literature, and has then been compared to our data as follows. For effective temperatures below 15000 K, we have calculated synthetic spectra in the local thermodynamic equilibrium (LTE) approximation, using the code SYNTH of Piskunov (1992). SYNTH requires, as input, atmosphere models, obtained using the ATLAS 9 code (Kurucz 1993), and a list of spectral line data obtained from the Vienna Atomic Line Database³ (VALD, Piskunov et al. 1995; Kupka et al. 1999; Ryabchikova et al. 1999). Above 15000 K we used TLUSTY non-LTE atmosphere models and the SYNPEC code (Hubeny 1988; Hubeny & Lanz 1992, 1995), to calculate synthetic spectra. At all temperatures the synthetic spectra have been computed with a solar metallicity (see Sec. 4.2). Then we compared, by eye, the observed to the synthetic spectra, and if necessary adjusted the temperature (holding $\log g = 4.0$ constant) until a best fit was achieved. For some stars, the temperatures found in the literature were not able to reproduce our spectra, and therefore we give here new determinations of T_{eff} .

In this procedure we fixed the surface gravity $\log g = 4.0$ because for most of the stars of our sample, the determination of $\log g$ using our data is not possible for the following reasons. First, the continuum level is very difficult to determine in echelle spectra and most of the Balmer lines are spread over two orders, making the determination of $\log g$ from the wings of the Balmer lines very imprecise. Then, the spectrum of many of our targets are heavily contaminated with CS emission/absorption and especially in the spectral lines of Fe, Ti, Si, Cr, which makes impossible the determination of surface gravity from the ionisation equilibrium of abundant species. Typical values of $\log g$ in HAeBe stars are comprised between 3.5 and 4.5 (e.g. Folsom et al. 2012). We have therefore adopted a value of 4.0 for all stars for which a determination from our observations was not possible.

For a few Herbig stars whose metallic spectral lines are only very faintly contaminated with CS emission/absorption, we obtained very high quality, high resolution spectra. To determine accurate effective temperature and gravity in these few cases, we developed an automatic procedure, based on a comparison of the observed spectrum to a grid of model spectra. The grid is composed of LTE SYNTH3 models (Kochukhov 2007), computed using Kurucz's ATLAS 9 atmospheres. The models assume solar abundances and no macroturbulence, while the grid varies the microturbulence between 0, 1, 2, 3, 4, and 5 km s⁻¹. The atomic line lists were extracted from VALD, for all lines with a predicted line

depth greater than 0.01 times the continuum. The models in our grid range from an effective temperature of 6500 K to 15000 K, in steps of 100 K. In addition, the models range from 3.0 to 5.0 dex in $\log(g)$ in 0.5 dex steps. The rotational broadening and disk integration of the SYNTH3 models used for comparison with the observed spectra was carried out using the code S3DIV (Kochukhov 2007).

For this procedure the spectral region between 420 nm and 520 nm was modeled, as lines in this region show the strongest sensitivity to temperature variations for stars with temperatures within our grid range. We used a brute-force search for the lowest χ^2 by comparing the observation to each model within a pre-selected parameter space (corresponding to a predefined temperature range, a predefined range in $\log(g)$, and each value of microturbulence) of the grid. The initial search parameters were chosen based on photometric or spectroscopic literature estimates. For each model, we fit the $v \sin i$ to the observations using a χ^2 minimisation routine as well. The Balmer line regions were ignored due to imprecise continuum normalisation of the short echelle orders, and strong local emission.

Once the best-fit model was identified, we carried out a visual comparison between the model and the observation to determine which regions (if any) were poorly fit, likely due to contamination from CS material. We then re-ran our spectrum fitting procedure with these regions ignored to improve our fits. If an observation showed strong emission in metallic lines, this procedure would not provide a realistic estimate on the stellar parameters. Examples demonstrating the quality of fit we are able to achieve, for both a low $v \sin i$ and high $v \sin i$ star, are shown in Fig. 2. The parameters derived in this way were used to check those obtained for the same stars from visual comparison and to refine the visual matching process.

We note that the effective temperatures derived from the visual comparison method depend on the assumed (solar) abundance and fixed $\log g = 4.0$. To check the sensitivity of our atmospheric parameter determinations to these assumptions, we compare our T_{eff} values with the results of Folsom et al. (2012), who derive T_{eff} and $\log g$ from detailed spectrum synthesis of a sample of approximately 20 HAeBe stars, simultaneously determining the abundance table and microturbulence parameter. As is illustrated in Fig. 3, the results of our more approximate procedures are in reasonable agreement with those from detailed fitting. Ultimately, the results of the LSD procedure, which is used in particular to determine $v \sin i$, to identify circumstellar and interstellar line features, and to diagnose the magnetic field, are only weakly sensitive to the details of the line mask, and errors in the adopted parameters of up to about $\pm 10 - 20\%$ have little impact on the results.

The adopted effective temperatures and surface gravities are summarised in Table 2. The stars whose effective temperature and surface gravity have been determined using a visual inspection or the automatic procedure are labelled with a dagger (†) or a double dagger (‡) respectively. In these two cases no uncertainties have been determined in $\log g$, and the indicated values are estimated at the model grid precision, i.e. ± 0.5 dex.

4.2 Metallicities

In this work we have assumed a solar metallicity for all our objects (except one, HD 34282, that shows a very low metallicity, Merin et al. 2004) for the following reasons. The spectra of most of the stars of our sample are heavily contaminated with CS emission and/or absorption, making difficult a reliable abundance analysis, and therefore a metallicity determination. However, Folsom et al. (2012), using our data, have isolated the 20 stars of our sample

³ <http://ams.astro.univie.ac.at/~vald/>

Table 1. Log of observations of the HAAeBe program stars. Columns 1 and 2 give the designations of the stars. The date, Universal Time (UT), and Heliocentric Julian Date (HJD) of the start of the observation are given in columns 3 and 4. The total exposure time is given in column 5. Columns 6 gives the peak SNR per CCD pixel at the wavelength indicated in column 7. Columns 8 to 11 give the number of lines used to compute the LSD profiles with the full and cleaned masks and the SNR in the LSD V profile. The final column indicates the instrument associated to the observation.

HD or BD number	Other name	Date (d/m/y) UT time	HJD - 2450000	Total exp. time (s)	Peak SNR	λ (nm)	Full mask		Cleaned mask		Instrument
							# LSD lines	LSD SNR	# LSD lines	LSD SNR	
BD-06 1259	BF Ori	21/02/05 09 :17	3422.88915	4800	192	515	2401	1986	466	1426	ESPaDOnS
		12/03/09 19 :41	4903.32074	4640	83	567	2398	3224	397	874	Narval
		12/03/09 21 :03	4903.37805	4640	88	731					Narval
BD-06 1253	V380 Ori	20/02/05 09 :32	3421.90001	4800	144	781					ESPaDOnS
BD-05 1329	T Ori	24/08/05 14 :53	3607.11832	3600	245	731	1487	2890	662	2201	ESPaDOnS
BD-05 1324	NV Ori	12/01/06 04 :56	3747.71083	3200	163	708	5896	2759	368	860	ESPaDOnS
BD+41 3731		26/08/05 09 :03	3608.88285	4000	309	527	362	1564	320	2552	ESPaDOnS
		06/11/07 21 :54	4411.41380	5800	178	552	382	2675	310	1444	Narval
BD+46 3471	V1578 Cyg	26/08/05 10 :59	3608.96354	4800	304	708	1274	3540	586	2811	ESPaDOnS
BD+61 154	V594 Cas	22/02/05 05 :56	3423.74367	3600	144	730	550	1332	12	148	ESPaDOnS
		24/08/05 11 :01	3606.96314	5600	208	515	570	870	12	355	ESPaDOnS
BD+65 1637	V361 Cep	11/06/06 14 :49	3898.11845	2400	237	730	371	1728	86	738	ESPaDOnS
		24/09/09 21 :43	5099.40934	8400	276	731	343	2151	73	911	Narval
BD+72 1031	SV Cep	12/06/06 15 :00	3899.12535	1600	159	730	967	1547	561	1301	ESPaDOnS
		11/11/07 21 :46	4416.40939	6400	139	731	1025	1394	543	1228	Narval
HD 9672	49 Cet	25/08/05 11 :40	3607.98968	800	910	515	2079	17572	2079	17572	ESPaDOnS
HD 17081	π Cet	20/02/05 05 :29	3421.72749	480	925	515	518	8006	234	4885	ESPaDOnS
		21/02/05 05 :31	3422.72864	480	1049	515	517	9158	234	5837	ESPaDOnS
HD 31293	AB Aur						1525	5293	590	6641	ESPaDOnS
		20/02/05 05 :53	3421.74513	1200	395	527	1536	8391	559	3500	ESPaDOnS
		22/02/05 08 :26	3423.85121	2400	547	527	1604	9895	559	5575	ESPaDOnS
HD 31648	MWC 480	22/02/05 09 :13	3423.88401	2400	389	527	3411	9335	1073	6583	ESPaDOnS
		25/08/05 12 :45	3608.03208	2000	435	708	3420	9671	1067	6934	ESPaDOnS
		25/08/05 13 :57	3608.07957	4000	246	708	2924	4904	2924	4904	ESPaDOnS
HD 34282		26/08/05 13 :13	3609.05072	2000	360	708	2104	5967	1383	5466	ESPaDOnS
HD 35187 B		13/11/07 00 :50	4417.53905	4000	415	566	4853	12302	3055	10076	Narval
HD 35929		14/11/07 00 :29	4418.52488	2000	213	708	4962	11800	3050	4999	Narval
		20/02/09 19 :33	4883.31686	2000	335	731					Narval
		20/02/09 20 :12	4883.34386	2000	341	731	4951	5830	3010	14214	Narval
		20/02/09 20 :49	4883.36939	2000	323	731					Narval
		21/02/09 19 :13	4884.30273	2000	309	731					Narval
		21/02/09 19 :49	4884.32826	2000	298	731	4852	16589	3007	12287	Narval
		21/02/09 20 :26	4884.35380	2000	281	731					Narval
		11/03/09 19 :31	4902.31377	2000	284	731					Narval
		11/03/09 20 :08	4902.33930	2000	250	731	4851	14318	3006	10574	Narval
		11/03/09 20 :44	4902.36482	2000	265	731					Narval
HD 36112	MWC 758						3758	7123	284	2792	ESPaDOnS
		20/02/05 06 :30	3421.77182	2400	322	708	4185	9217	271	2236	ESPaDOnS
HD 36910	CQ Tau	04/04/08 20 :12	4561.33902	6000	198	731	5671	5037	1219	3209	Narval
HD 36917	V372 Ori	08/11/07 23 :48	4413.49636	4000	208	552	1064	2477	1064	2477	Narval
HD 36982	LP Ori	09/11/07 01 :05	4413.54984	4000	136	552	614	3430	187	937	Narval
		10/11/07 00 :56	4414.54299	6000	306	552	615	3270	187	2178	Narval
		11/11/07 00 :03	4415.50631	4400	264	552					Narval
		11/11/07 01 :21	4415.56085	4400	314	552	609	4838	187	2088	Narval
		12/11/07 01 :05	4416.54958	6000	426	552	579	1447	187	3091	Narval
HD 37258	V586 Ori	24/02/09 19 :15	4887.30404	6600	292	553	1872	5262	559	3215	Narval
HD 37357		24/02/09 22 :15	4887.42954	4440	270	553	1965	4795	723	3550	Narval
HD 37806	MWC 120	25/08/05 15 :10	3608.13042	2000	468	515	577	4293	53	1793	ESPaDOnS
HD 38120		13/03/09 22 :23	4904.43316	3600	230	553	1400	3152	1436	3021	Narval
HD 38238	V351 Ori	16/03/07 20 :16	4176.34501	4680	247	731	4790	6822	3356	6190	Narval
HD 50083	V742 Mon	13/11/07 01 :50	4417.57965	2000	487	553	584	5699	157	2508	Narval
		03/04/08 20 :58	4560.37363	2000	500	553	628	7080	147	2287	Narval
HD 52721		07/11/07 03 :33	4411.65007	2000	523	553	628	5350	273	4090	Narval
		03/04/08 20 :14	4560.34420	2000	467	553	662	6253	250	3590	Narval
HD 53367		20/02/05 10 :31	3421.94295	1200	363	708	545	2646	59	977	ESPaDOnS
		21/02/05 10 :25	3422.93832	2400	505	566	548	4289	59	1621	ESPaDOnS
HD 68695		22/02/05 10 :53	3423.95853	2400	128	527	1550	1579	1550	1575	ESPaDOnS
HD 72106		22/02/05 10 :04	3423.92478	2400	236	515					ESPaDOnS
HD 76534 A		22/02/05 11 :40	3423.99189	1800	221	708	436	1578	11	353	ESPaDOnS

Table 1 – *continued*

HD or BD number	Other name	Date (d/m/y) UT time	HJD - 2450000	Total exp. time (s)	Peak SNR	λ (nm)	Full mask		Cleaned mask		Instrument
							# LSD lines	LSD SNR	# LSD lines	LSD SNR	
HD 98922		21/02/05 11 :54	3423.00115	1600	451	527	683	3089	578	2872	ESPaDOnS
HD 114981	V958 Cen	20/02/05 12 :13	3422.01396	1600	329	515	518	6680	210	1756	ESPaDOnS
		12/01/06 15 :01	3748.12665	2400	633	515	531	3018	211	4060	ESPaDOnS
HD 135344		10/01/06 15 :40	3746.15200	2400	128	731	6631	2555	6631	2555	ESPaDOnS
HD 139614		20/02/05 13 :50	3422.07904	3600	298	708	3495	5853	7023	9542	ESPaDOnS
		21/02/05 13 :46	3423.07633	2800	274	708	3519	5587	7004	9242	ESPaDOnS
		22/02/05 14 :14	3424.09588	2400	294	708	3513	6592	7020	10579	ESPaDOnS
HD 141569		13/02/06 12 :29	3780.02056	4000	301	708	1496	2821	1418	2723	ESPaDOnS
		07/03/07 13 :20	4167.05806	5400	1053	566	1478	16345	1395	15985	ESPaDOnS
HD 142666	V1026 Sco	20/02/05 12 :54	3422.03917	2400	237	708	3855	4123	2496	3711	ESPaDOnS
		22/02/05 13 :16	3424.05441	3600	338	708	3885	7184	2549	6402	ESPaDOnS
		22/05/05 07 :50	3512.83235	3600	292	708	3866	6005	2543	5381	ESPaDOnS
		22/05/05 08 :55	3512.87760	3600	293	708	3867	5141	2506	5365	ESPaDOnS
		23/05/05 08 :25	3513.85638	3600	256	708	3920	6425	2507	4593	ESPaDOnS
		24/05/05 07 :54	3514.83487	3600	308	708	3893	5863	2530	5725	ESPaDOnS
		25/05/05 08 :02	3515.84083	3600	282	708	4775	7989	2507	5209	ESPaDOnS
HD 144432			20/02/05 14 :47	3422.11732	2400	323	708	4792	9430	1751	5893
		21/02/05 14 :46	3423.11688	3200	368	708	3426	12788	1742	7118	ESPaDOnS
HD 144668	HR 5999	24/08/05 05 :38	3606.73345	1200	569	708	3863	8503	2821	12340	ESPaDOnS
HD 145718	V718 Sco	26/08/05 05 :32	3608.72972	2800	403	730	1760	6149	2284	7274	ESPaDOnS
HD 150193	V2307 Oph	24/08/05 06 :20	3606.76406	2800	453	730	1768	9845	1541	6043	ESPaDOnS
HD 152404	AK Sco	15/02/06 14 :46	3782.11538	3600	393	708	6684	10308	2634	7454	ESPaDOnS
HD 163296		22/05/05 09 :54	3512.91769	2400	588	527	1764	7008	1123	8391	ESPaDOnS
		23/05/05 10 :02	3513.92318	3600	460	515	1801	10426	1112	5924	ESPaDOnS
		24/05/05 09 :49	3514.91391	3600	615	515	1798	7439	1157	8981	ESPaDOnS
		24/05/05 14 :48	3515.12170	2400	448	515	1714	3678	1121	6362	ESPaDOnS
		25/05/05 09 :52	3515.91662	3600	617	527	1791	10394	1097	8744	ESPaDOnS
		25/05/05 14 :53	3516.12540	2400	436	566	1753	11221	1056	6092	ESPaDOnS
		25/08/05 05 :39	3607.73704	1200	641	515	5421	6488	1104	9561	ESPaDOnS
HD 169142		20/02/05 15 :34	3422.14750	2400	270	708	5450	5421	3718	5865	ESPaDOnS
		22/02/05 15 :01	3424.12494	2400	208	708	5502	8648	3788	4861	ESPaDOnS
		22/05/05 10 :41	3512.95012	2400	311	708	5479	14187	3737	7728	ESPaDOnS
		24/08/05 07 :10	3606.80061	2000	473	708	554	1926	3751	12614	ESPaDOnS
HD 174571	MWC 610	17/03/07 03 :51	4176.65909	3600	283	731	586	2557	343	2086	Narval
		16/04/08 02 :35	4572.60859	3900	245	731	626	5359	342	1621	Narval
HD 176386		25/08/05 06 :09	3607.75872	1600	573	708	820	9459	601	5297	ESPaDOnS
HD 179218		21/02/05 15 :30	3423.14213	1200	298	527	849	2949	271	2117	ESPaDOnS
		26/08/05 08 :10	3608.84465	1600	631	515	841	6965	271	4945	ESPaDOnS
		03/10/09 20 :53	5108.37217	7200	866	553	1768	5059	255	6667	Narval
HD 190073	V1295 Aql	22/05/05 11 :40	3512.98887	3290	411	527					ESPaDOnS
HD 200775	MWC 361	22/05/05 14 :35	3513.10716	3600	555	731					ESPaDOnS
HD 203024		24/08/05 09 :38	3606.90562	2800	365	515	1765	5954	1238	5567	ESPaDOnS
		07/11/07 22 :17	4412.43070	4800	307	552	1799	2353	1238	4811	Narval
HD 216629	IL Cep	10/06/06 15 :06	3897.12935	1200	301	730	437	1773	90	910	ESPaDOnS
		08/12/06 07 :09	4077.79899	1200	227	708	438	2115	81	758	ESPaDOnS
		05/11/07 21 :18	4410.39095	5700	339	731	2871	3856	90	1112	Narval
HD 244314	V1409 Ori	05/11/07 23 :19	4410.47647	6000	158	552	3449	7804	1799	2363	Narval
HD 244604	V1410 Ori	24/08/05 13 :47	3607.07333	3600	329	527	1736	2631	2016	6964	ESPaDOnS
HD 245185	V1271 Ori	20/02/05 07 :39	3421.82069	4800	192	515	1971	2213	1736	2631	ESPaDOnS
HD 249879		05/04/08 21 :03	4562.37504	6000	133	553	492	1726	982	1951	Narval
HD 250550	V1307 Ori	08/11/07 00 :23	4412.52023	5360	202	553	416	2282	387	1403	Narval
HD 259431	V700 Mon	17/03/07 22 :40	4177.44524	5100	302	731	402	1528	261	1583	Narval
		24/02/09 23 :31	4887.48247	2400	274	731	404	2078	253	1473	Narval
		17/03/10 20 :23	5273.35057	2400	199	731	1100	1072	258	1178	Narval
HD 275877	XY Per	11/12/06 06 :24	4080.77111	3600	348	708	2897	6912	453	3058	ESPaDOnS
		25/09/09 00 :46	5099.53643	7200	299	731	2715	5390	412	2419	Narval
HD 278937	IP Per	21/02/05 06 :26	3422.76644	4800	195	666	2892	3084	2871	3856	ESPaDOnS
		21/02/05 07 :50	3422.82473	4800	171	527	2924	2735	2892	3084	ESPaDOnS
		22/02/05 07 :14	3423.79948	4800	172	708	395	30034	2924	2735	ESPaDOnS
HD 287823		17/03/07 21 :16	4177.38573	3120	112	552	3671	2836	1100	1072	Narval
HD 287841	V346 Ori	20/02/09 22 :23	4883.43440	7740	151	731	2112	2979	3671	2836	Narval
HD 290409			07/11/07 00 :17	4411.51658	6000	171	552	1983	1315	2112	2979

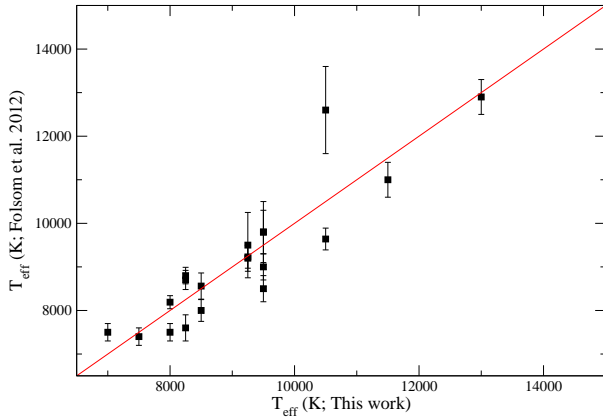


Figure 3. Comparison of effective temperature T_{eff} derived by Folsom et al. (2012) for a sample of ~ 20 HAeBe stars, and those derived in this study. The solid line indicates a perfect agreement.

both components are been obtained by Alencar et al. (2003). It was therefore possible to derive an error bare on the luminosity ratio of the system, and therefore on the individual luminosities (see Appendix A and Table2).

All the quantities are summarised in Table 2, while the sources of the data are detailed, star by star, in Appendix A. For three stars (HD 50083, HD 52721, HD 174571) no reliable distance could be found in the literature. We have therefore estimated their luminosity from their effective temperature and surface gravity by comparing their position in a $\log g - T_{\text{eff}}$ diagram with theoretical evolutionary tracks (described in Sec. 4.4).

4.4 Mass and radius determination

We placed all the stars in an HR diagram (Fig. 4), with the error bars when available, and compared their positions with evolutionary tracks calculated with the CESAM stellar evolutionary code (Morel 1997) version 2K. Using a 2D-linear interpolation and a grid of 120 evolutionary tracks with masses from 1 to $20 M_{\odot}$, and mass steps varying between 0.01 and $1 M_{\odot}$ (depending on the mass and the position of the stars in the HR diagram), we determined the mass, radius and age of each star.

The errors have been determined using the intersection of the evolutionary tracks with the error ellipses, as defined by the errors in effective temperature, luminosity or surface gravity. When the ellipses are intersecting the ZAMS or the birthline, only the portion of the ellipse between the birthline and the ZAMS was considered.

The ages have been measured from the birthline, i.e the locus in the HR diagram where the newly-formed stars become observable at optical wavelength, meaning that the CS matter in which the stars were buried during the proto-stellar phase becomes optically thin. We used the birthline of Behrend & Maeder (2001) that has been computed with a mass accretion rate increasing with the luminosity of the growing star. We favoured a birthline calculated with a modulated accretion rate (instead of a constant accretion rate as computed by Palla & Stahler 1993) as it better fits the upper envelope of the distribution of massive Herbig Be stars in the HR diagram (see Fig. 4). Furthermore, Palla & Stahler (1993, PS93 hereinafter) argue that a constant accretion rate of $10^{-5} M_{\odot} \cdot \text{yr}^{-1}$ during

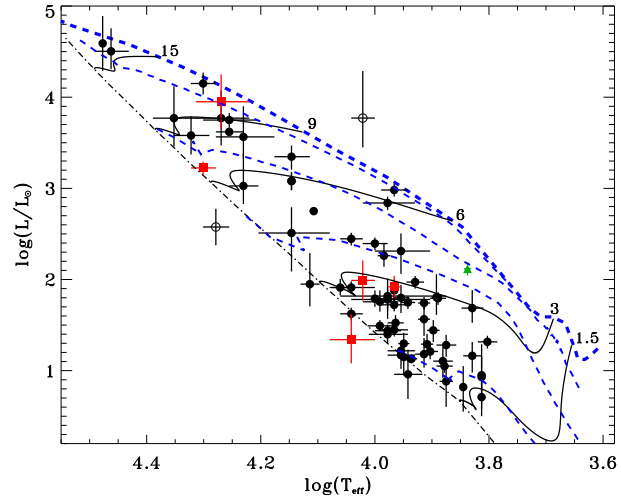


Figure 4. Magnetic (red squares) and non-magnetic (black circle) Herbig Ae/Be stars plotted in an HR diagram. The green triangle is the candidate magnetic star HD 35929. Open circles correspond to HD 98922 (above the birthline) and IL Cep (below the ZAMS) that fall outside of the PMS region of the HR diagram, whose positions cannot be reproduced with the theoretical evolutionary tracks considered in this paper. The CESAM PMS evolutionary tracks for 1.5, 3, 6, 9 and $15 M_{\odot}$ (black full lines), 0.01, 0.1, 1 and 10 Myr isochrones (blue thin dashed lines), and ZAMS (black dot-dashed line) are also plotted. The birthline taken from Behrend & Maeder (2001) is plotted with a blue thick dashed line.

the proto-stellar phase is a good approximation as it fits well the upper envelope of the known Herbig Ae/Be stars. However their work was only including HAeBe stars of masses lower than $6 M_{\odot}$. Since their work, more massive stars have been identified as Herbig Be (e.g. Vieira et al. 2003; Martayan et al. 2008), while intermediate-mass T Tauri stars that are cooler and younger than Herbig Ae/Be star and that are identified as the progenitors of the Herbig Ae/Be phases, have also been found (e.g. Wolff et al. 2004; Hussain et al. 2009). The latter are filling the right part of the HR diagram (with $\log T_{\text{eff}} \leq 3.8$) and are evolving along the Hayashi track up to the radiative phase of the PMS evolution. We are therefore convinced that the BM01 birthline is a reasonable assumption for the start of the PMS phase at all masses.

In Fig. 4 all the stars of our sample are plotted, with circles for non-magnetic stars, squares for magnetic stars, and a triangle for the candidate-magnetic star. The BM01 birthline and the CESAM zero-age-main-sequence (ZAMS) are also overplotted. We observe that two points (the open circles) are situated way outside of the theoretical limits of the PMS region (from the birthline to the ZAMS), even taking into account their error bars. For the two corresponding stars (HD 98922 and IL Cep) we are therefore not able to estimate their mass, radius and age using the CESAM theoretical tracks. For stars situated just below the ZAMS, we have estimated the ranges of the parameters covered by the intersection area between the error ellipse and the HR diagram, and took the middle values. For the four magnetic stars, HD 190073, HD 200775, HD 72106 and V380 Ori, we have adopted the masses and radii reported in the papers that describe their spectroscopic and magnetic analyses (Catala et al. 2007; Alecian et al. 2008a; Folsom et al. 2008; Alecian et al. 2009b). However we have re-determined their ages as different birthlines were used in these papers.

This method does not take into account the uncertainties in the metallicity (however see Sec. 4.2), nor the choice of the birth-

Table 2. Photometric and fundamental parameters. Columns 1 and 2 give the stars designations. Columns 3 to 6 give the effective temperature, the surface gravity and their origin. The Johnson V magnitude and $(B - V)$ color and the reference are indicated in columns 7 to 9. The visual extinction and magnitude corrected from extinction are given in columns 10 and 11. The distance and its reference are given in column 12 and 13. The luminosity is given in column 14. Columns 11, 12 and 13 give the mass, radius and age, while the PMS duration and the predicted radius on the ZAMS are indicated in columns 14 and 15. The measured $v \sin i$ and v_{rad} are given in columns 16 and 17. In the column 14 to 21, a reference is given when it was not determined in this work. An asterisk (*) indicates a note at the end of the table. All references are indicated at the end of the table.

HD or BD number	Other Name	T_{eff} (K)	Ref	$\log g$ (cgs)	Ref	V (mag)	$(B - V)$ (mag)	Ref	A_V (mag)	V_0 (mag)	d (pc)	Ref
(1)	(2)	(3)	(4)	(5)	(6)	(7)	(8)	(9)	(10)	(11)	(12)	(13)
BD-06 1259	BF Ori	8750±250	ar	4.0±0.5	ar	7.85	-0.028	j	-0.57	8.42	375 ⁺³⁰ ₋₃₀	d
BD-06 1253 A	V380 Ori A	10500±500	b	4.0		10.34	0.689	j	3.74	6.59	400 ⁺⁴⁰ ₋₄₀	b
BD-05 1329	T Ori	8500±300	ao	4.2±0.3	ao	10.63	0.53	r	2.64	7.99	375 ⁺³⁰ ₋₃₀	d
BD-05 1324	NV Ori	6350±250	ay	4.0		9.90	0.46	r	0.45	9.45	375 ⁺³⁰ ₋₃₀	d
BD+41 3731		17000±1000	†	4.0		9.90	0.052	j	1.06	8.84	980 ⁺⁵⁰⁰ ₋₂₀₀	ai
BD+46 3471	V1578 Cyg	9500±1000	aq	4.0		10.14	0.436	j	2.25	7.89	950 ⁺⁸⁰ ₋₈₀	p
BD+61 154	V594 Cas	13000±500	†	4.0		10.51	0.566	j	3.29	7.22	202 ⁺⁹⁷ ₋₄₉	al
BD+65 1637	V361 Cep	18000±1000	†	4.0		10.83	0.429	j	2.94	7.89	1250 ⁺⁵⁰ ₋₅₀	ah
BD+72 1031	SV Cep	9500±2000	aq	4.0		10.48	0.344	ag	1.87	8.61	400 ⁺¹⁰⁰ ₋₁₀₀	v
HD 9672	49 Cet	8900±200	‡	4.5	‡	5.62	0.066	j	0.05	5.57	59 ^{+1.0} _{-1.0}	al
HD 17081	π Cet	12800±200	as	3.77±0.15	as	4.24	-0.122	j	-0.06	4.30	120 ⁺³ ₋₃	al
HD 31293	AB Aur	9800±700	ao	3.9±0.3	ao	7.03	0.132	j	0.65	6.38	139 ⁺²¹ ₋₁₆	al
HD 31648	MWC 480	8200±300	‡	4.0	‡	7.73	0.160	j	0.10	7.63	137 ⁺³¹ ₋₂₁	al
HD 34282		8625±200	x	4.2±0.20	x	9.92	0.299	j	1.00	8.93	191 ⁺⁸⁹ ₋₄₆	al
HD 35187 B		8900±200	‡	4.0	‡	8.169	0.218	j	0.81	7.36	114 ⁺⁴¹ ₋₂₄	al
HD 35929		6800±100	at	3.3±0.1	at	8.11	0.438	j	0.69	7.42	375 ⁺³⁰ ₋₃₀	d
HD 36112	MWC 758	7800±150	‡	4.0	‡	8.27	0.317	j	0.69	7.59	279 ⁺⁹⁴ ₋₅₆	al
HD 36910	CQ Tau	6750±300	aq	4.0		8.77	0.94	j	2.85	5.92	113 ⁺²⁹ ₋₁₉	al
HD 36917	V372 Ori	10000±500	†	4.0		8.03	0.17	an	1.00	7.03	375 ⁺³⁰ ₋₃₀	d
HD 36982	LP Ori	20000±1000	†	4.0		8.46	0.09	an	1.55	6.91	375 ⁺³⁰ ₋₃₀	d
HD 37258	V586 Ori	9500±500	†	4.0		9.64	0.140	g	0.41	9.23	375 ⁺³⁰ ₋₃₀	d
HD 37357		9250±500	am	4.0		8.88	0.13	am	0.37	8.52	375 ⁺³⁰ ₋₃₀	d
HD 37806	MWC 120	11000±500	†	4.0		7.91	0.025	j	0.58	7.32	375 ⁺³⁰ ₋₃₀	d
HD 38120		11000±500	†	4.0		9.07	0.044	j	0.21	8.86	375 ⁺³⁰ ₋₃₀	d
HD 38238	V351 Ori	7750±250	†	4.0		8.89	0.381	j	0.65	8.23	375 ⁺³⁰ ₋₃₀	d
HD 50083	V742 Mon	20000±1000	m	3.43±0.15	m	6.91	0.008	j	1.09	5.82	1000 ⁺¹⁰⁰ ₋₁₀₀	
HD 52721		22500±2000	m	3.99±0.20	m	6.54	0.016	j	1.28	5.26	670 ⁺¹⁴⁰ ₋₁₁₀	
HD 53367		29000±2000	†	4.0		6.97	0.357	j	3.29	3.68	255 ⁺⁸⁶ ₋₅₁	al
HD 68695		9000±300	ao	4.3±0.3	ao	9.82	0.10	am	0.49	9.33	570 ⁺¹⁰⁰ ₋₁₀₀	i
HD 72106 A		11000±1000	l	4.0±0.5	l	9.00	-0.090	k	-0.09	9.10	289 ⁺²⁰⁴ ₋₈₅	j
HD 72106 B		8750±500	l	4.0±0.5	l	9.62	0.20	k	0.10	9.52	289 ⁺²⁰⁴ ₋₈₅	j
HD 76534 A		18000±2000	†	4.0		8.35	0.107	j	1.43	6.91	870 ⁺⁸⁰ ₋₈₀	q
HD 98922		10500±500	am	4.0		6.77	0.037	j	0.54	6.24	1150 ⁺⁹³⁰ ₋₃₆₀	al
HD 114981	V958 Cen	17000±2000	†	4.0		7.16	-0.098	j	0.51	6.65	550 ⁺²⁶⁰ ₋₁₃₀	al
HD 135344		6750±250	†	4.0		8.70	0.60	ae	0.96	7.74	142 ⁺²⁷ ₋₂₇	aa
HD 139614		7600±300	ao	3.9±0.3	ao	8.40	0.24	am	0.50	7.90	142 ⁺²⁷ ₋₂₇	aa
HD 141569		9800±500	ao	4.2±0.4	ao	7.11	0.095	j	0.46	6.65	116 ⁺⁹ ₋₈	al
HD 142666	V1026 Sco	7900±200	‡	4.0	‡	8.67	0.50	am	1.60	7.07	145 ⁺²⁰ ₋₂₀	af
HD 144432		7500±300	‡	3.5	‡	8.19	0.397	j	0.74	7.45	145 ⁺²⁰ ₋₂₀	af
HD 144668	HR 5999	8200±200	‡	3.5	‡	7.00	0.190	j	0.25	6.75	142 ⁺²⁷ ₋₂₇	aa
HD 145718	V718 Sco	8100±200	‡	4.0	‡	8.83	0.456	j	1.38	7.45	145 ⁺²⁰ ₋₂₀	af
HD 150193	V2307 Oph	9500±500	†	4.0		8.79	0.522	j	2.47	6.32	145 ⁺²⁰ ₋₂₀	af

Table 2 – *continued*

ID	$\log(L/L_{\odot})$	M/M_{\odot}	R/R_{\odot}	age	t_{PMS}	R_{ZAMS}	$v \sin i$	v_{rad}
(1) or (2)	(14)	(15)	(16)	(17)	(18)	(19)	(20)	(21)
BD-06 1259	$1.75^{+0.7}_{-0.7}$	$2.58^{+0.14}_{-0.14}$	$3.26^{+0.31}_{-0.31}$	$3.15^{+0.58}_{-0.44}$	$5.1^{+1.0}_{-0.8}$	$1.88^{+0.06}_{-0.06}$	39 ± 9	22 ± 6
BD-06 1253 A	$1.99^{+0.22b}_{-0.22}$	$2.87^{+0.52b}_{-0.32}$	$3.00^{+1.1b}_{-0.8}$	$2.5^{+1.0}_{-1.0}$	$3.56^{+1.3}_{-1.5}$	$1.99^{+0.10}_{-0.10}$	6.7 ± 1.1^b	$[27.3, 28.2]^b$
BD-05 1329	$1.97^{+0.07}_{-0.07}$	$3.13^{+0.19}_{-0.19}$	$4.47^{+0.46}_{-0.46}$	$1.77^{+0.38}_{-0.32}$	$2.66^{+0.60}_{-0.49}$	$2.10^{+0.07}_{-0.07}$	147 ± 9	29 ± 8
BD-05 1324	$1.32^{+0.07}_{-0.07}$	$2.28^{+0.18}_{-0.16}$	$3.77^{+0.41}_{-0.41}$	$3.7^{+1.0}_{-0.9}$	$7.6^{+2.0}_{-1.7}$	$1.75^{+0.07}_{-0.07}$	74 ± 7	30 ± 5
BD+41 3731	$3.03^{+0.36}_{-0.20}$	$5.50^{+1.37}_{-0.38}$	$3.8^{+0.8}_{-0.8}$	$0.24^{+0.18}_{-0.15}$	$0.344^{+0.042}_{-0.119}$	$2.89^{+0.11}_{-0.11}$	345 ± 27	-14 ± 22
BD+46 3471	$2.84^{+0.07}_{-0.08}$	$5.9^{+0.6}_{-0.5}$	$9.7^{+1.9}_{-1.9}$	$0.06^{+0.06}_{-0.06}$	$0.31^{+0.05}_{-0.06}$	$3.00^{+0.15}_{-0.15}$	199 ± 11	-3 ± 9
BD+61 154	$1.95^{+0.34}_{-0.24}$	$3.41^{+0.38}_{-0.38}$	$2.42^{+0.35}_{-0.35}$	$2.2^{+0.9}_{-0.9}$	$2.2^{+0.9}_{-0.9}$	$2.20^{+0.14}_{-0.14}$	112 ± 24	-16 ± 18
BD+65 1637	$3.620^{+0.034}_{-0.035}$	$8.11^{+0.24}_{-0.23}$	$6.7^{+0.7}_{-0.7}$	$0.035^{+0.012}_{-0.010}$	$0.153^{+0.012}_{-0.010}$	$3.56^{+0.05}_{-0.05}$	278 ± 27	-26 ± 20
BD+72 1031	$1.82^{+0.19}_{-0.25}$	$2.62^{+0.59}_{-0.34}$	$3.0^{+1.1}_{-1.1}$	$3.2^{+1.9}_{-1.6}$	$4.8^{+2.8}_{-2.4}$	$1.89^{+0.14}_{-0.14}$	180 ± 15	-9 ± 11
HD 9672	$1.297^{+0.015}_{-0.014}$	$2.13^{+0.08}_{-0.07}$	$1.88^{+0.09}_{-0.09}$	$7.0^{+1.1}_{-1.3}$	$9.0^{+1.0}_{-1.0}$	$1.690^{+0.030}_{-0.030}$	195 ± 6	13.1 ± 4.6
HD 17081	$2.750^{+0.022}_{-0.022}$	$4.65^{+0.08}_{-0.08}$	$4.84^{+0.19}_{-0.19}$	$0.279^{+0.012}_{-0.023}$	$0.469^{+0.012}_{-0.021}$	$2.630^{+0.030}_{-0.030}$	19.9 ± 0.9	$[11.0, 12.7]$
HD 31293	$1.76^{+0.12}_{-0.11}$	$2.50^{+0.29}_{-0.13}$	$2.62^{+0.44}_{-0.44}$	$3.7^{+0.6}_{-0.8}$	$5.6^{+1.1}_{-1.7}$	$1.84^{+0.06}_{-0.06}$	116 ± 6	24.7 ± 4.7
HD 31648	$1.18^{+0.18}_{-0.15}$	$1.93^{+0.09}_{-0.14}$	$1.93^{+0.32}_{-0.32}$	$7.8^{+4.5}_{-1.5}$	$12.9^{+3.3}_{-1.8}$	$1.60^{+0.06}_{-0.06}$	97.5 ± 4.7	12.9 ± 3.5
HD 34282	$1.13^{+0.27x}_{-0.22}$	$1.59^{+0.30x}_{-0.07}$	$1.66^{+0.62x}_{-0.37}$	$6.4^{+2.6x}_{-1.9}$			105 ± 6	16.2 ± 4.8
HD 35187 B	$1.15^{+0.27}_{-0.20}$	$1.93^{+0.28}_{-0.04}$	$1.58^{+0.02}_{-0.02}$	$10.7^{+3.7}_{-5.2}$	$12.9^{+1.4}_{-4.5}$	$1.60^{+0.04}_{-0.04}$	93.3 ± 2.8	27.0 ± 2.1
HD 35929	$2.12^{+0.07}_{-0.07}$	$4.13^{+0.23}_{-0.24}$	$8.1^{+0.7}_{-0.7}$	$0.16^{+0.49}_{-0.08}$	$0.68^{+0.54}_{-0.13}$	$2.46^{+0.08}_{-0.08}$	61.8 ± 2.2	21.1 ± 1.8
HD 36112	$1.81^{+0.25}_{-0.19}$	$2.90^{+0.67}_{-0.43}$	$4.4^{+0.9}_{-0.9}$	$2.1^{+1.1}_{-1.1}$	$3.4^{+2.4}_{-1.8}$	$2.01^{+0.17}_{-0.17}$	54.1 ± 4.9	17.8 ± 3.7
HD 36910	$1.69^{+0.20}_{-0.16}$	$2.93^{+0.54}_{-0.37}$	$5.1^{+0.9}_{-0.9}$	$1.9^{+0.9}_{-0.8}$	$3.3^{+1.9}_{-1.5}$	$2.02^{+0.15}_{-0.15}$	98 ± 5	35.7 ± 4.5
HD 36917	$2.39^{+0.07}_{-0.07}$	$3.98^{+0.25}_{-0.24}$	$5.2^{+0.6}_{-0.6}$	$0.72^{+0.29}_{-0.42}$	$1.06^{+0.33}_{-0.45}$	$2.41^{+0.09}_{-0.09}$	127.1 ± 4.6	26.3 ± 3.6
HD 36982	$3.22^{+0.07}_{-0.07}$	$6.70^{+0.64}_{-0.37}$	$3.42^{+0.30}_{-0.30}$	$0.20^{+0.07}_{-0.07}$	$0.230^{+0.043}_{-0.030}$	$3.22^{+0.10}_{-0.10}$	88 ± 8	30 ± 6
HD 37258	$1.44^{+0.07}_{-0.07}$	$2.28^{+0.15}_{-0.16}$	$1.94^{+0.24}_{-0.24}$	$5.9^{+1.8}_{-1.5}$	$7.5^{+1.9}_{-1.4}$	$1.75^{+0.07}_{-0.07}$	200 ± 14	31 ± 12
HD 37357	$1.72^{+0.07}_{-0.07}$	$2.47^{+0.13}_{-0.11}$	$2.83^{+0.35}_{-0.35}$	$3.7^{+0.6}_{-0.5}$	$5.8^{+1.0}_{-0.9}$	$1.83^{+0.05}_{-0.05}$	124 ± 7	21.4 ± 4.7
HD 37806	$2.45^{+0.07}_{-0.07}$	$3.94^{+0.23}_{-0.23}$	$4.6^{+0.5}_{-0.5}$	$0.88^{+0.21}_{-0.51}$	$1.18^{+0.25}_{-0.53}$	$2.39^{+0.08}_{-0.08}$	120 ± 27	47 ± 21
HD 38120	$1.62^{+0.07}_{-0.07}$	$2.49^{+0.09}_{-0.09}$	$1.91^{+0.11}_{-0.11}$	$5.1^{+0.5}_{-0.5}$	$5.6^{+0.8}_{-0.8}$	$1.840^{+0.040}_{-0.040}$	97 ± 17	28 ± 12
HD 38238	$1.79^{+0.07}_{-0.07}$	$2.88^{+0.18}_{-0.18}$	$4.38^{+0.44}_{-0.44}$	$2.16^{+0.46}_{-0.38}$	$3.5^{+0.8}_{-0.6}$	$2.00^{+0.07}_{-0.07}$	99.8 ± 4.2	15.0 ± 2.9
HD 50083	$4.15^{+0.12}_{-0.12}$	$12.1^{+1.1}_{-1.1}$	$10.0^{+1.0}_{-1.0}$	$0.004^{+0.006}_{-0.006}$	$0.033^{+0.035}_{-0.035}$	$7.6^{+3.4}_{-3.4}$	233 ± 22	-0.4 ± 1.2
HD 52721	$3.77^{+0.35}_{-0.31}$	$9.1^{+2.4}_{-1.4}$	$5.0^{+1.2}_{-1.2}$	$0.044^{+0.073}_{-0.030}$	$0.12^{+0.06}_{-0.06}$	$3.78^{+0.33}_{-0.33}$	215 ± 18	21 ± 14
HD 53367	$4.50^{+0.25}_{-0.20}$	$16.1^{+2.7}_{-1.6}$	$7.1^{+1.6}_{-1.6}$	$0.008^{+0.016}_{-0.008}$	$0.036^{+0.000}_{-0.035}$	$5.13^{+0.29}_{-0.29}$	41 ± 7	47.2 ± 4.8
HD 68695	$1.80^{+0.14}_{-0.17}$	$2.64^{+0.31}_{-0.30}$	$3.3^{+0.6}_{-0.6}$	$3.0^{+1.2}_{-0.8}$	$4.7^{+2.3}_{-1.4}$	$1.90^{+0.13}_{-0.13}$	43.8 ± 2.6	20.3 ± 1.7
HD 72106 A	$1.34^{+0.28/}_{-0.26}$	$2.40^{+0.3/}_{-0.3}$	$1.3^{+0.5/}_{-0.5}$	9.0^{+4}_{-3}	9.0^{+4}_{-3}	$1.3^{+0.5}_{-0.5}$	41.0 ± 0.3^l	22 ± 1^l
HD 72106 B	$0.96^{+0.27/}_{-0.27}$	$1.9^{+0.2/}_{-0.2}$	$1.3^{+0.5/}_{-0.5}$	9.0^{+4}_{-3}	9.0^{+4}_{-3}	$1.3^{+0.5}_{-0.5}$	53.9 ± 1.0^l	22 ± 1^l
HD 76534 A	$3.75^{+0.08}_{-0.08}$	$9.0^{+0.6}_{-0.6}$	$7.7^{+1.6}_{-1.6}$	$0.021^{+0.018}_{-0.013}$	$0.122^{+0.019}_{-0.022}$	$3.76^{+0.13}_{-0.13}$	68 ± 30	23 ± 18
HD 98922	$3.77^{+0.52}_{-0.32}$						50.0 ± 3.0	0.2 ± 2.2
HD 114981	$3.56^{+0.34}_{-0.24}$	$7.9^{+2.4}_{-1.3}$	$7.0^{+2.0}_{-2.0}$	$0.038^{+0.064}_{-0.038}$	$0.16^{+0.08}_{-0.08}$	$3.51^{+0.33}_{-0.33}$	239 ± 13	-50 ± 11
HD 135344	$1.16^{+0.15}_{-0.18}$	$1.90^{+0.25}_{-0.24}$	$2.8^{+0.6}_{-0.6}$	$6.6^{+3.4}_{-2.0}$	$13.6^{+6.9}_{-4.4}$	$1.58^{+0.11}_{-0.11}$	82.4 ± 2.0	-0.0011 ± 0.0006
HD 139614	$1.10^{+0.15}_{-0.18}$	$1.76^{+0.15}_{-0.08}$	$2.06^{+0.42}_{-0.42}$	$8.8^{+4.5}_{-1.9}$	$17.2^{+2.7}_{-3.9}$	$1.520^{+0.040}_{-0.040}$	24.1 ± 3.0	0.3 ± 2.3
HD 141569	$1.49^{+0.06}_{-0.06}$	$2.33^{+0.20}_{-0.12}$	$1.94^{+0.21}_{-0.21}$	$5.7^{+1.3}_{-1.4}$	$7.1^{+1.4}_{-1.7}$	$1.77^{+0.05}_{-0.05}$	228 ± 10	-12 ± 7
HD 142666	$1.44^{+0.11}_{-0.13}$	$2.15^{+0.20}_{-0.19}$	$2.82^{+0.41}_{-0.41}$	$5.0^{+1.6}_{-1.1}$	$9.2^{+3.1}_{-2.2}$	$1.70^{+0.08}_{-0.08}$	65.3 ± 3.1	-7.0 ± 2.7
HD 144432	$1.28^{+0.11}_{-0.13}$	$1.95^{+0.18}_{-0.16}$	$2.59^{+0.40}_{-0.40}$	$6.4^{+1.8}_{-1.4}$	$12.4^{+3.7}_{-3.0}$	$1.61^{+0.07}_{-0.07}$	78.8 ± 4.2	-3.0 ± 3.5
HD 144668	$1.56^{+0.15}_{-0.18}$	$2.31^{+0.29}_{-0.28}$	$3.0^{+0.6}_{-0.6}$	$4.2^{+2.0}_{-1.2}$	$7.2^{+3.7}_{-2.3}$	$1.77^{+0.12}_{-0.12}$	199 ± 11	-10 ± 8
HD 145718	$1.29^{+0.11}_{-0.13}$	$1.93^{+0.14}_{-0.08}$	$2.25^{+0.33}_{-0.33}$	$7.4^{+0.7}_{-1.7}$	$12.8^{+1.8}_{-2.5}$	$1.60^{+0.04}_{-0.04}$	113.4 ± 3.4	-3.6 ± 2.3
HD 150193	$1.79^{+0.11}_{-0.13}$	$2.56^{+0.22}_{-0.19}$	$2.89^{+0.48}_{-0.48}$	$3.3^{+0.9}_{-0.7}$	$5.2^{+1.5}_{-1.2}$	$1.87^{+0.08}_{-0.08}$	108 ± 5	-4.9 ± 3.9

line. The inferred masses, radii and ages are therefore approximate, but will be useful when considering comparisons between the stars themselves. The masses, radii and ages are summarised in Table 2. In the same table we also give the PMS duration for each star, and the predicted radius that each star will have once it reaches the

ZAMS. Both have been calculated by assuming a mass-constant evolution for each star. The PMS duration has been computed from the birthline. In the case of HD 34282, as we did not calculate the ZAMS radius and the PMS duration because our models are of solar metallicity. HD 98922 and IL Cep fall well outside of the HR

Table 2 – *continued*

HD or BD number	Other Name	T_{eff} (K)	Ref (4)	$\log g$ (cgs)	Ref (6)	V (mag)	$(B - V)$ (mag)	Ref (9)	A_V (mag)	V_0 (mag)	d (pc)	Ref (13)
(1)	(2)	(3)	(4)	(5)	(6)	(7)	(8)	(9)	(10)	(11)	(12)	(13)
HD 152404 A	AK Sco A	6500±100	c	4.0		8.839	0.622	w	1.06	7.78	103 ⁺²⁷ ₋₁₈	al {
HD 152404 B	AK Sco B	6500±100	c	4.0								
HD 163296		9200±300	ao	4.2±0.3	ao	6.86	0.092	j	0.32	6.54	119 ⁺¹² ₋₁₀	al
HD 169142		7500±200	ao	4.3±0.2	ao	8.15	0.28	am	-0.30	8.45	145 ⁺⁴⁰ ₋₄₀	ak
HD 174571	MWC 610	21000±1500	m	4.00±0.10	m	8.87	0.610	j	4.15	4.72	540 ⁺⁸⁰ ₋₇₀	
HD 176386		11500±350	‡	4.5	‡	7.22	0.121	j	1.00	6.22	128 ⁺¹⁵ ₋₁₂	al
HD 179218		9640±250	ao	3.9±0.2	ao	7.40	0.094	j	0.77	6.63	254 ⁺⁴⁵ ₋₃₃	al
HD 190073	V1295 Aql	9250±250	e	3.5±0.5	e	7.84	0.113	j	0.43	7.41		
HD 200775 A	MWC 361 A	18600±2000	a	3.5	a	7.34	0.306	j	2.43	4.91	429 ⁺¹⁵⁶ ₋₉₀	j {
HD 200775 B	MWC 361 B	18600±2000	a	3.6	a							
HD 203024 A		9250	†	4.0		8.80	0.40	aj	1.86	6.94	420 ⁺⁵⁰ ₋₅₀	u {
HD 203024 B		6500	†	4.0								
HD 216629 A	IL Cep A	19000	†	4.0		9.34	-0.240	j	-0.25	9.59	720 ⁺¹⁹⁰ ₋₁₅₀	f
HD 216629 B	IL Cep B	19000	†	4.0								
HD 244314	V1409 Ori	9250±500	am	4.0		10.19	0.22	z	0.96	9.23	375 ⁺³⁰ ₋₃₀	d
HD 244604	V1410 Ori	8200±200	‡	4.0	‡	8.99	0.255	g	0.57	8.41	375 ⁺³⁰ ₋₃₀	d
HD 245185	V1271 Ori	9500±750	ao	4.0±0.4	ao	9.96	0.070	s	0.21	9.75	450 ⁺⁵⁰ ₋₅₀	ab
HD 249879		9000±1000	†	4.0		10.64	0.05	am	-0.04	10.68	2000 ⁺⁵⁰⁰ ₋₅₀₀	am
HD 250550	V1307 Ori	12000±1500	†	4.0		9.51	0.044	j	0.68	8.83		
HD 259431	V700 Mon	14000±1000	†	4.0		8.71	0.274	j	2.02	6.69	660 ⁺¹⁰⁰ ₋₁₀₀	t
HD 275877	XY Per	9000±500	ay	4.0		9.04	0.47	ad	1.75	7.29	120 ⁺⁸⁷ ₋₃₅	j
HD 278937	IP Per	8500±250	ao	4.1±0.2	ao	10.36	0.31	y	0.95	9.41	320 ⁺³⁰ ₋₃₀	h
HD 287823 A		10000	†	4.0		9.71	0.223	j	1.26	8.45	375 ⁺³⁰ ₋₃₀	d {
HD 287823 B		7000	†	4.0								
HD 287841	V346 Ori	7550±250	av	3.5±0.4	av	10.21	0.199	j	0.09	10.11	375 ⁺³⁰ ₋₃₀	d
HD 290409 A		9000±500	†	4.0		10.02	0.09	am	0.17	9.85	375 ⁺³⁰ ₋₃₀	o
HD 290500		9000±500	†	4.0		11.04	0.31	n	1.26	9.77	375 ⁺³⁰ ₋₃₀	d
HD 290770		11000±1000	†	4.0		9.27	0.03	am	0.61	8.66	375 ⁺³⁰ ₋₃₀	d
HD 293782	UX Ori	9250±500	ax	4.0	ax	8.53	0.615	j	3.06	5.47	375 ⁺³⁰ ₋₃₀	d
HD 344361	WW Vul	9000±1000	ar	4.0		10.74	0.41	r	2.04	8.70	700 ⁺²⁶⁰ ₋₁₅₀	ap
	LkHa 215 A	14000	†	4.0		10.54	0.52	r	3.25	7.29	900 ⁺¹⁰⁰ ₋₁₀₀	ac {
	LkHa 215 B	14000	†	4.0								
	MWC 1080	30000	aw	4.0		11.58	1.197	j	7.09	4.49	2300 ⁺⁶⁰⁰ ₋₆₀₀	
	VV Ser	14000±2000	aq	4.0		11.92	0.96	r	5.35	6.57	260 ⁺¹⁰⁰ ₋₁₀₀	az
	VX Cas	9500±1500	aq	4.0		11.28	0.32	r	1.67	9.61	620 ⁺⁶⁰ ₋₆₀	ap

diagram, even when the error on their temperatures and luminosities are taken into account. Furthermore, no distance, accurate enough to estimate a luminosity with reasonable error bars, could be found for HD 250550. Therefore no age, mass, radius, ZAMS radius and PMS duration could be estimated for these stars.

5 THE LEAST-SQUARES DECONVOLVED PROFILE ANALYSIS

5.1 The LSD method

In order to increase the signal to noise ratio of our line profiles, we applied the Least Squares Deconvolution (LSD) procedure

to all spectra (Donati et al. 1997). This procedure combines the information contained in many metal lines of the spectrum, in order to extract the mean intensity (Stokes I) and polarised (Stokes V) line profiles. In Stokes I , each line is weighted according to its central depth, while in Stokes V the profiles are weighted according to the product of the central depth, wavelength and Landé factor. These parameters are contained in a "line mask" derived from a synthetic spectrum corresponding to the effective temperature and gravity of the star given in Table 2. The construction of the line mask for each star involved several steps. First, we used Kurucz ATLAS 9 models (Kurucz 1993) to obtain generic masks of solar abundances, and of $T_{\text{eff}}/\log g$ following the Kurucz models grid. Our masks contain only lines with intrinsic depths larger or equal

Table 2 – continued

ID	$\log(L/L_{\odot})$	M/M_{\odot}	R/R_{\odot}	age	t_{PMS}	R_{ZAMS}	$v \sin i$	v_{rad}
(1) or (2)	(14)	(15)	(16)	(Myr)	(Myr)	R_{\odot}	(km.s^{-1})	(km.s^{-1})
				(17)	(18)	(19)	(20)	(21)
HD 152404 A	$0.95^{+0.21}_{-0.21}$	$1.66^{+0.29}_{-0.21}$	$2.4^{+0.5}_{-0.5}$	$9.3^{+3.8}_{-3.3}$	20^{+10}_{-8}	$1.48^{+0.10}_{-0.10}$	18.2 ± 1.7	-17.0 ± 1.3
HD 152404 B	$0.71^{+0.21}_{-0.21}$	$1.43^{+0.20}_{-0.09}$	$1.79^{+0.38}_{-0.38}$	$13.7^{+3.6}_{-4.3}$	31^{+6}_{-10}	$1.37^{+0.04}_{-0.04}$	17.6 ± 0.9	14.3 ± 0.9
HD 163296	$1.52^{+0.08}_{-0.08}$	$2.23^{+0.22}_{-0.07}$	$2.28^{+0.23}_{-0.23}$	$5.10^{+0.31}_{-0.77}$	$8.1^{+0.9}_{-2.1}$	$1.73^{+0.03}_{-0.03}$	129 ± 8	-9 ± 6
HD 169142	$0.88^{+0.21}_{-0.28}$	$1.69^{+0.06}_{-0.14}$	$1.64^{+0.20}_{-0.20}$	$13.5^{+11.2}_{-4.7}$	$19.2^{+5.5}_{-1.9}$	$1.49^{+0.06}_{-0.06}$	47.8 ± 2.3	-0.4 ± 2.0
HD 174571	$3.58^{+0.21}_{-0.21}$	$8.0^{+1.2}_{-1.0}$	$4.7^{+0.6}_{-0.6}$	$0.065^{+0.050}_{-0.026}$	$0.161^{+0.060}_{-0.043}$	$3.53^{+0.24}_{-0.24}$	219 ± 31	14 ± 24
HD 176386	$1.91^{+0.09}_{-0.09}$	$3.02^{+0.23}_{-0.26}$	$2.28^{+0.24}_{-0.24}$	$2.8^{+1.0}_{-0.8}$	$3.0^{+1.1}_{-0.7}$	$2.05^{+0.10}_{-0.10}$	175 ± 6	-2 ± 5
HD 179218	$2.26^{+0.14}_{-0.12}$	$3.66^{+0.44}_{-0.34}$	$4.8^{+0.7}_{-0.7}$	$1.08^{+0.48}_{-0.70}$	$1.5^{+0.6}_{-0.8}$	$2.29^{+0.12}_{-0.12}$	68.8 ± 2.9	15.1 ± 2.3
HD 190073	$1.92^{+0.12e}_{-0.12}$	$2.85^{+0.25e}_{-0.25}$	$3.60^{+0.5e}_{-0.5}$	$2.40^{+0.7}_{-0.6}$	$3.6^{+1.3}_{-1.0}$	$1.99^{+0.10}_{-0.10}$	$[0-8.3]^d$	0.21 ± 0.10^d
HD 200775 A	$3.95^{+0.30a}_{-0.30}$	$10.7^{+2.5a}_{-2.5}$	$10.4^{+4.9a}_{-4.9}$	$0.016^{+0.009}_{-0.009}$	$0.07^{+0.07}_{-0.07}$	$4.1^{+0.5}_{-0.5}$	26 ± 2^a	$[-23.3, 8.2]^a$
HD 200775 B	$3.77^{+0.30a}_{-0.30}$	$9.3^{+2.1a}_{-2.1}$	$8.3^{+3.9a}_{-3.9}$	$0.016^{+0.009}_{-0.009}$	$0.12^{+0.08}_{-0.06}$	$3.8^{+0.4}_{-0.4}$	59 ± 5^a	$[-21.1, 9.3]^a$
HD 203024 A	1.88	2.8	3.4	2.7	4.0	1.9	162 ± 11	-14 ± 9
HD 203024 B	0.93	1.6	2.3	9.3	21.1	1.5	57.1 ± 3.8	$[-10.5, -5.3]$
HD 216629 A	$2.58^{+0.20}_{-0.20}$	{					179 ± 27	$[-39, 31]$
HD 216629 B							152 ± 33	$[-87, -30]$
HD 244314	$1.45^{+0.07}_{-0.07}$	$2.33^{+0.08}_{-0.23}$	$2.07^{+0.26}_{-0.26}$	$4.78^{+2.40}_{-0.19}$	$7.1^{+2.8}_{-0.7}$	$1.77^{+0.10}_{-0.10}$	51.9 ± 2.2	22.5 ± 1.8
HD 244604	$1.74^{+0.07}_{-0.07}$	$2.66^{+0.15}_{-0.15}$	$3.69^{+0.34}_{-0.34}$	$2.79^{+0.52}_{-0.41}$	$4.6^{+1.0}_{-0.8}$	$1.91^{+0.06}_{-0.06}$	98.3 ± 1.8	26.8 ± 1.6
HD 245185	$1.40^{+0.09}_{-0.10}$	$2.19^{+0.27}_{-0.12}$	$1.85^{+0.20}_{-0.20}$	$6.9^{+2.0}_{-2.5}$	$8.7^{+1.8}_{-2.7}$	$1.71^{+0.06}_{-0.06}$	118 ± 22	16 ± 16
HD 249879	$2.31^{+0.19}_{-0.25}$	$4.0^{+0.8}_{-0.8}$	$5.9^{+1.8}_{-1.8}$	$0.7^{+1.0}_{-0.5}$	$1.1^{+1.3}_{-0.6}$	$2.40^{+0.27}_{-0.27}$	254 ± 26	11 ± 20
HD 250550							79 ± 9	-22 ± 8
HD 259431	$3.35^{+0.12}_{-0.14}$	$7.1^{+0.8}_{-0.8}$	$8.0^{+1.6}_{-1.6}$	$0.059^{+0.035}_{-0.041}$	$0.218^{+0.040}_{-0.053}$	$3.32^{+0.20}_{-0.20}$	83 ± 11	26 ± 8
HD 275877	$1.21^{+0.47}_{-0.30}$	$1.95^{+0.46}_{-0.09}$	$1.65^{+0.11}_{-0.11}$	10^{+6}_{-6}	$12.4^{+3.1}_{-6.2}$	$1.61^{+0.06}_{-0.06}$	224 ± 12	2 ± 10
HD 278937	$1.21^{+0.08}_{-0.09}$	$1.86^{+0.10}_{-0.06}$	$2.10^{+0.23}_{-0.23}$	$8.19^{+0.40}_{-1.18}$	$14.3^{+1.4}_{-2.2}$	$1.570^{+0.030}_{-0.030}$	79.8 ± 2.9	13.7 ± 2.1
HD 287823 A	1.79	2.5	2.6	3.5	5.2	1.9	10.3 ± 1.5	-0.3 ± 1.1
HD 287823 B	0.82	1.6	1.8	11.9	24.2	1.4	8.2 ± 3.3	54.0 ± 1.6
HD 287841	$1.05^{+0.07}_{-0.07}$	$1.72^{+0.15}_{-0.05}$	$1.96^{+0.20}_{-0.20}$	$9.3^{+0.6}_{-0.8}$	$18.2^{+1.6}_{-4.2}$	$1.510^{+0.020}_{-0.020}$	115.8 ± 4.2	20.0 ± 3.6
HD 290409 A	$1.32^{+0.06}_{-0.06}$	$2.04^{+0.18}_{-0.18}$	$1.75^{+0.20}_{-0.20}$	$10.5^{+4.8}_{-4.8}$	$11.8^{+3.5}_{-3.5}$	$1.64^{+0.09}_{-0.09}$	250 ± 120	1 ± 70
HD 290500	$1.22^{+0.07}_{-0.07}$	$1.96^{+0.21}_{-0.06}$	$1.68^{+0.09}_{-0.09}$	$9.8^{+2.9}_{-3.7}$	$12.3^{+1.3}_{-3.4}$	$1.61^{+0.03}_{-0.03}$	85 ± 15	29 ± 11
HD 290770	$1.91^{+0.07}_{-0.07}$	$2.86^{+0.27}_{-0.21}$	$2.49^{+0.44}_{-0.44}$	$2.76^{+0.86}_{-0.33}$	$3.6^{+1.0}_{-0.9}$	$1.99^{+0.08}_{-0.08}$	240 ± 100	4 ± 60
HD 293782	$2.98^{+0.07}_{-0.07}$	$6.72^{+0.42}_{-0.43}$	$12.1^{+1.5}_{-1.5}$	$0.009^{+0.027}_{-0.009}$	$0.229^{+0.034}_{-0.226}$	$3.22^{+0.12}_{-0.12}$	221 ± 13	12 ± 10
HD 344361	$2.23^{+0.27}_{-0.21}$	$3.7^{+1.0}_{-0.6}$	$5.4^{+1.4}_{-1.4}$	$0.9^{+0.9}_{-0.8}$	$1.0^{+1.0}_{-1.0}$	$2.31^{+0.22}_{-0.22}$	196 ± 8	-4 ± 8
LkHa 215 A	$3.08^{+0.10*}_{-0.10}$	5.8	5.9	0.1	0.3	3.0	210 ± 70	0 ± 40
LkHa 215 B	$3.08^{+0.10*}_{-0.10}$	5.8	5.9	0.1	0.3	3.0	11.7 ± 4.6	$[12, 22]$
MWC 1080	$5.77^{+0.20}_{-0.26}$	17.4	7.3	0.0028	0.033	5.4		
VV Ser	$2.51^{+0.28}_{-0.42}$	$4.0^{+0.8}_{-0.8}$	$3.1^{+0.9}_{-0.9}$	$0.64^{+1.91}_{-0.35}$	$0.76^{+1.78}_{-0.33}$	$2.43^{+0.29}_{-0.29}$	124 ± 24	51 ± 18
VX Cas	$1.78^{+0.08}_{-0.09}$	$2.55^{+0.37}_{-0.14}$	$2.9^{+0.8}_{-0.8}$	$3.4^{+0.6}_{-1.0}$	$5.3^{+1.0}_{-1.9}$	$1.86^{+0.06}_{-0.06}$	158 ± 23	-9 ± 18

Notes : * Assuming that both components have the same temperature, and therefore the same luminosity; References : † Visual temperature determination; ‡ Automatic temperature determination; ^a Alecian et al. (2008a); ^b Alecian et al. (2009b); ^c Alencar et al. (2003); ^d Brown et al. (1994); ^e Catala et al. (2007); ^f Crawford & Barnes (1970); ^g de Winter et al. (2001); ^h de Zeeuw et al. (1999); ⁱ Eggen (1986); ^j ESA (1997); ^k Fabricius & Makarov (2000); ^l Folsom et al. (2008); ^m Frémat et al. (2006); ⁿ Guetter (1979); ^o Guetter (1981); ^p Harvey et al. (2008); ^q Herbst (1975); ^r Herbst & Shevchenko (1999); ^s Høg et al. (2000); ^t Kharchenko et al. (2005); ^u Kun et al. (2000); ^v Kun (1998); ^w Manset et al. (2005); ^x Merin et al. (2004); ^y Miroshnichenko et al. (2001); ^z Miroshnichenko et al. (1999a); ^{aa} Müller et al. (2011); ^{ab} Murdin & Penston (1977); ^{ac} Oliver et al. (1996); ^{ad} Oudmaijer et al. (2001); ^{ae} Oudmaijer et al. (1992); ^{af} Preibisch & Mamajek (2008); ^{ag} Rostopchina et al. (2000); ^{ah} Shevchenko & Yakubov (1989); ^{ai} Shevchenko et al. (1991); ^{aj} Simbad (<http://simbad.u-strasbg.fr/simbad/>); ^{ak} Sylvester et al. (1996); ^{al} van Leeuwen (2007); ^{am} Vieira et al. (2003); ^{an} Wolff et al. (2004); ^{ao} Folsom et al. (2012); ^{ap} Montesinos et al. (2009); ^{aq} Hernández et al. (2004); ^{ar} Mora et al. (2004); ^{as} Fossati et al. (2009); ^{at} Miroshnichenko et al. (2004); ^{au} Hernández et al. (2005); ^{av} Bernabei et al. (2009); ^{aw} Hillenbrand et al. (1992); ^{ax} Mora et al. (2002); ^{ay} Mora et al. (2001); ^{az} Straižys et al. (1996)

to 0.1, which, according to the SNR of our data, is sufficient. We then excluded from the masks hydrogen Balmer lines, strong resonance lines, and lines whose Landé factor is unknown. At this stage, the mask contains all predicted lines satisfying the initial assumption of the LSD procedure, i.e. a similar shape for all spectral lines considered in the procedure. This mask will be called in the following the "full mask". Finally, each mask was carefully examined in order to exclude lines predicted by the models, but not appearing in the spectrum, as well as lines contaminated by non-photospheric features. This final "cleaning" procedure is explained in Sec. 5.2 and detailed for each star in Appendix A. Following this procedure, we executed Least-Squares Deconvolution using the full and cleaned masks and the observed spectra, obtaining for each star the mean intensity Stokes I profile, the mean circularly-polarised Stokes V profile, and the null N profile. Fig 5 shows the LSD I , V , and N profiles for two stars : one with a magnetic field detection, and one without. In both cases - as well as in all of our observations, the N profiles are null indicating the absence of spurious polarisation signals, and confirming that the Zeeman signatures detected in the magnetic stars are real. The use of two separate masks per star is justified in the following sections. The analysis of the LSD I profile and the rotation velocity measurements are described in Section 5.2, while the magnetic analysis performed using the I and V profiles is detailed in Section 6.

The LSD method implies that all lines of the spectra have a similar shape, differing only in their relative strength. The strengths depend on the central depth when the method is applied to an I spectrum, and on the central depth and Landé factor for a polarised V spectrum. This hypothesis is reasonable for purely photospheric lines. However in the case of a spectrum contaminated with CS features, these hypotheses should be discussed. The CS features contaminating the photospheric lines of the spectra of the Herbig Ae/Be stars have the same shape (except in few lines like the Balmer, Ca II h&k or Na D lines, which are removed from the mask). However, their relative strength is not dependent on the central depths of the photospheric lines, which are used to weight each line in the LSD procedure. Therefore, the LSD method, by averaging the contaminated lines, applies inappropriate weights to the CS contribution, while taking correctly into account the different weights of the photospheric lines. In the LSD procedure, using wrong weights does not change the global shape of the resulting profile, however its relative strength (with respect to the V profile, for example) cannot be trusted. Therefore, the strength of the CS contribution of our LSD I profiles must be investigated in more detail before it can be reliably used to draw any quantitative conclusions. However, its shape can be modelled and removed to be able to analyse the photospheric contribution of the I profile, which is the one of interests for this paper. We describe in the following section how the CS contamination has been handled in this study.

5.2 Fitting of the LSD I profiles

The LSD I profiles computed with the full mask reveal a rather complex average of the lines of the spectrum included in the line mask. Most HAeBe stars show CS emission and absorption in their spectrum ; these effects are also reflected in the LSD profiles. Those lines that are the most strongly contaminated by CS emission can be easily identified directly in the spectrum itself, and excluded from the mask. For some of the stars, the resulting LSD profiles show a relatively clean rotational profile indicative of simple photospheric absorption. For others, the resulting profiles still show significant CS absorption and/or emission that is not possible to remove by

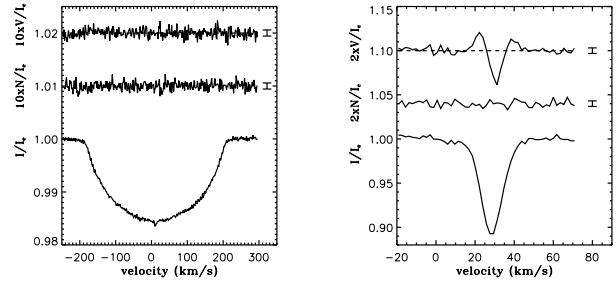


Figure 5. LSD Stokes I (bottom) and V (top) profiles of the non-magnetic Herbig Ae star 49 Cet (left), and the magnetic Herbig Ae star V380 Ori (right). The diagnostic N profile is also plotted in the middle. V and N have been shifted on the Y-axis, and magnified by a factor of 10 for 49 Cet, and 2 for V380 Ori, for display purposes.

further refinement of the line mask. However, the investigations of rotation and magnetic fields in papers II and III require that we are able to extract an approximation of the uncontaminated photospheric profiles in order to infer $v \sin i$ and to model the magnetic constraint imposed by Stokes V .

To characterise the various contributions to the LSD I profiles, we have performed a least-squares fit to each of the LSD I profiles using several models. In the first case we consider a simple photospheric profile modelled using the convolution of a rotation function (depending on the projected rotational velocity $v \sin i$ and the radial velocity of the star v_{rad}), and a Gaussian (approximating the local photospheric profile) whose width is fixed and computed from the spectral resolution and the macroturbulent velocity (Gray 1992). This convolution will be called the photospheric function. The free parameters of the fitting procedure are the line depth, $v \sin i$ and v_{rad} . In order to fit the wings of the observed LSD profiles of our sample, a macroturbulent velocity (v_{mac}) is frequently required to be added to the model. Only a few stars of our sample have LSD I profiles suitable for estimating the value of v_{mac} , and the typical value is found to be around 2 km.s^{-1} . The other stars of our sample (i.e. most of them) either display too large a Doppler broadening, and/or the wings of the profile are sufficiently contaminated by CS features, that they do not allow us to obtain useful information about v_{mac} . Nonetheless, we assumed that a macroturbulent velocity field is present near the surface of the star, and we adopted for all the stars an isotropic macroturbulent velocity of 2 km.s^{-1} . However, taking into account a $v_{\text{mac}} \sim 2 \text{ km.s}^{-1}$ seems to improve the fit, when fitting with the eye, only for stars with $v \sin i$ lower than 40 km.s^{-1} . In order to estimate the error on the $v \sin i$ introduced by fixing v_{mac} , we varied the value of v_{mac} between 0 and 4 km.s^{-1} , and we find that it introduces significant variations of $v \sin i$ only if $v \sin i$ is lower than 10 km.s^{-1} . For $v \sin i$ between 10 and 40 km.s^{-1} , changing v_{mac} modifies the value of $v \sin i$ within the error bars. For $v \sin i$ larger than 40 km.s^{-1} , changing v_{mac} has no impact on $v \sin i$. The macroturbulent velocity is therefore not a significant parameter to be considered within this fitting procedure. It has been included in all the fitted models for consistency from one star to the other, but should only be considered with caution at very low $v \sin i$ (lower than 10 km.s^{-1}).

The second model considers one or more Gaussian functions meant to model the CS features present in the LSD I profile. These functions are added to the photospheric function with the aim of providing the best reproduction of the observed profile. The parameters of each Gaussian contributing to the CS function are the

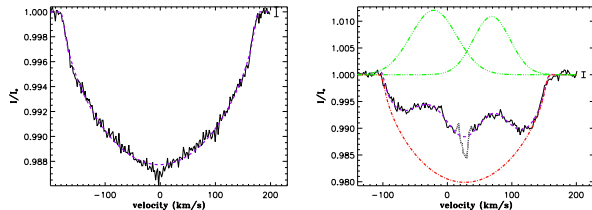


Figure 6. Examples of LSD fits (dashed purple line) using only a photospheric (red dot-dashed line) function for HD 176386 (left) and using a photospheric + two Gaussian (green dot-dot-dot-dashed line) functions for HD 36917 (right) observed on Nov. 8th 2007. In the case of HD 36917, the narrow absorption in the core of the profile (dotted line) has been excluded from the fit.

full-width at half maximum (FWHM), the centroid position, and the amplitude. The amplitude may be either positive or negative, corresponding to emission or absorption contributions. Depending on the star analysed, we require between zero and four circumstellar functions to fit the Stokes I profile. Hence, the number of fitting parameters required to reproduce the LSD I profiles ranges from 3 up to 15. For a few stars for which this simple model was unable to reproduce features in the observed profile, an alternative method we applied was to suppress from the fit the regions contaminated with CS (or other) features. We accomplished this by assigning a null weight to all points inside the affected region, and fit the profile with only a photospheric function.

The LSD profiles of our observations show systematically a continuum level lower than one (while the spectra are all normalised to one). We believe that this is due to spectral features not taken into account in the LSD procedure, and not due to poor continuum normalisation or to a reduction problem, for two reasons. First, multiple LSD profiles of a star obtained at different times show a continuum at the same level. However, multiple observations of different stars do not have the same continuum level, suggesting that the choice of the mask might determine the level of the continuum. Secondly, when we apply the LSD procedure on a simulated ESPaDOnS or Narval observation, in which the continuum is by construction perfectly normalised to one, the continuum level of the resulting I profile is also lower than one.

In order to simplify the fitting procedure and avoid additional parameters to fit, we have normalised each profile before fitting them. The continuum levels have been determined by fitting a line between two points chosen by eye on each side of the profiles. The profiles are then divided by the fitted continuum. We have checked that this normalisation process does not introduce significant errors by repeating the procedure many times and checking that the fitted parameters converge all towards the same value.

A remarkable result of this procedure is the conclusion that the mean line profiles of most HAeBe stars can be satisfactorily reproduced by a simple model consisting of the sum of a rotationally-broadened photospheric profile and a small number of local absorption/emission profiles assumed to be contributed by the CS environment. The analysis of the quantitative characteristics of the CS-contributed profiles will be described in a future paper.

As an additional complication, some stars in our sample are double-lined spectroscopic binaries (see Sec. 5.3). In these cases, we fitted the LSD I profiles using the sum of two photospheric functions, each one having independent fitting parameters. Examples of the results of the fitting procedure are shown in Fig. 6.

This fitting procedure is automatic and requires as input first

guesses for each free parameter. We checked the uniqueness of the derived fit by modifying the first guesses, and checking that whatever the first guesses, the fits always converge towards a unique solution. This verification procedure was always successful for the photospheric parameters (the photospheric line depth, $v \sin i$ and v_{rad}). However in some cases when one or more Gaussian CS functions was required, we could find multiple solutions (e.g. the addition of a Gaussian in emission or a Gaussians in absorption could give fits of comparable quality). In those cases we checked individual spectral lines in order to determine which of the solutions was the most consistent with the observed spectrum. Whenever multiple observations were obtained for the same star, we also chose the solution the most consistent over all observations.

When multiple observations were obtained for the same star with similar SNRs, we performed a simultaneous fit to the whole set of observations, by forcing the photospheric parameters (depth, $v \sin i$, v_{rad}) to be the same for each of the observations. When necessary, one or more Gaussian functions were added to the profiles, with independent parameters for each observation.

We checked that changing the effective temperature and gravity of the masks, within the error bars, do not change our determination of our $v \sin i$ values. The fit performed to reproduce the shape of the LSD I profile is dominating the uncertainties. The uncertainties on the adopted parameters (see Table 2) have therefore been determined by calculating the confidence intervals at a level of 99.73%, as described in Press et al. (1992, p. 697).

After completing the analysis of the LSD profiles, we checked that the derived $v \sin i$ were consistent with individual spectral lines in the reduced spectra. The adopted values of $v \sin i$ and v_{rad} are summarised in Table 2, and the fitting procedure for each of the spectra is described in Appendix A. In the case of MWC 1080, no photospheric lines could be identified in the spectrum, therefore no $v \sin i$ values could be measured.

5.3 The discovery of spectroscopic binaries

The inspection of the LSD profiles allowed us to easily identify a number of spectroscopic binaries among our sample. Among the stars not detected as magnetic, a total of 5 SB2 systems were identified : 3 previously known or suspected (AK Sco, HD 287823, IL Cep), and two new discoveries previously unreported in the literature (HD 203024 and HD 290409). Based on the detection of a LiI lines at 6707 Å, Corporon & Lagrange (1999) claimed the presence of a low mass companion orbiting HD 203024. However this claimed companion cannot be the spectroscopic companion that we detect because its temperature is too high. We therefore cast some doubts on the stellar nature of the feature observed at ~ 6708 Å, and leave open the interpretation of its origin.

For each of the SB2 systems, we have attempted a determination of the effective temperature of both components, as well as of their luminosity ratio. The description of each system is detailed in Appendix A.

6 MAGNETIC FIELD DIAGNOSIS

6.1 Method

Each of the spectra that we have acquired with ESPaDOnS and Narval was obtained in Stokes V polarimetric mode, in order to allow us to measure the longitudinal Zeeman effect in spectral lines. We employ two methods to detect magnetic fields in our program

and standard stars. First, we use the Stokes V spectra to measure the mean longitudinal magnetic field strength $\langle B_z \rangle$ of each star at the time of observation. This is the conventional measure of field strength normally used for detection of magnetic fields in main sequence stars (e.g. Landstreet 1982). However, because of the high value of the resolving power, we can also examine spectral lines for the presence of circular polarisation signatures : Zeeman splitting combined with Doppler broadening of lines by rotation leads to non-zero values of V within spectral lines even when the value of $\langle B_z \rangle$ is close to, or even equal to, zero. This possibility substantially increases the sensitivity of our measurements as a discriminant of whether a star is in fact a magnetic star or not, as discussed by Shorlin et al. (2002), Silvester et al. (2009) and Shultz et al. (2011).

Each set of LSD Stokes I and V profiles is therefore analysed in two ways. First, the value of $\langle B_z \rangle$ is determined by computing the first-order moment of Stokes V , normalised to the equivalent width of Stokes I (Mathys 1991; Donati et al. 1997; Wade et al. 2000) :

$$\langle B_z \rangle = -2.14 \times 10^{11} \frac{\int vV(v)dv}{\lambda \bar{g} c \int [I_c - I(v)]dv}, \quad (1)$$

where $\langle B_z \rangle$ is in G, \bar{g} is the mean Landé factor of the LSD weights in the line mask (typically 1.3 ± 0.1), and λ is the SNR-weighted mean wavelength of the LSD weights in the mask in nm (typically 520 ± 40 nm). The uncertainties σ on $\langle B_z \rangle$ have been computed by propagating the error of each pixel within the Stokes I and V profiles through Eq. (1). The limits of integration are usually chosen for each star to coincide with the observed limits of the LSD I and V profiles; using a smaller window would neglect some of the signal coming from the limb of the star, while a window larger than the actual line would increase the noise without adding any further signal, thus degrading the SNR below the optimum value achievable (see e.g. Neiner et al. 2012).

In addition, the LSD Stokes V profile is itself examined. We evaluate the false alarm probability (FAP) of V/I_c inside the line according to :

$$\text{FAP}(\chi_r^2, \nu) = 1 - P\left(\frac{\nu}{2}, \frac{\nu \chi_r^2}{2}\right), \quad (2)$$

where P is the incomplete gamma function, ν is the number of spectral points inside the line, and χ_r^2 is the reduced chi-square (χ^2/ν) computed across the V profile relative to zero (e.g. Donati et al. 1992). The FAP value gives the probability that the observed V signal inside the spectral line could be produced by chance if there is actually no field present. Thus a very small value of the FAP implies that a field is actually present. We evaluate FAP using the detection thresholds of Donati et al. (1997). We consider that an observation displays a “definite detection” (DD) of Stokes V Zeeman signature if the FAP is lower than 0.00001, a “marginal detection” (MD) if it falls between 0.001 and 0.00001, and a “null detection” (ND) otherwise. As mentioned above a *significant signal* (i.e. with a MD or DD) may occur even if $\langle B_z \rangle$ is not significantly different from zero. On the contrary, a profile can give a $\langle B_z \rangle$ different from zero at a level of 3σ or lower without displaying a marginal or a definite detection (see Fig. 10 and Sec. 6.3). For these reasons, the FAP is the most sensitive diagnostic of the presence of a magnetic field, and will be the only one applied in this paper. Table 4 summarises our measurements of FAP and the magnetic diagnosis (DD, MD or ND) for all observations, except those already published in previous papers.

If a significant signal (i.e. with a MD or DD) is detected within the line, while always remaining insignificant in the neighbouring

Table 3. Log of our first observations of HAeBe stars in which we have detected a magnetic field. Column one gives the name of the star. Columns 2, 3 and 4 report the Heliocentric Julian Date, the type of detection (MD for marginal detection and DD for definite detection) and the longitudinal field measurement reported in the literature. In the final column we indicate the first refereed publication in which the field detection was reported. Discoveries by Wade et al. (2005), Catala et al. (2007) and Alecian et al. (2008a) are derived from this survey. LP Ori was reported to be magnetic by Petit et al. (2008) as part of a parallel program. However, as it was serendipitously detected within this survey as well, we include this star as a *bona fide* blind detection in our statistics.

Name	HJD -2450000	Det	$\langle B_z \rangle \pm \sigma_B$ (G)	Discovery paper
<i>Confirmed magnetic HAeBe stars</i>				
V380 Ori	3421.900	MD	-165 ± 190	Wade et al. (2005)
HD 36982	4416.549	MD	-240 ± 70	Petit et al. (2008)
HD 72106	3423.924	DD	228 ± 50	Wade et al. (2005)
HD 190073	3607.789	DD	111 ± 13	Catala et al. (2007)
HD 200775	3608.920	MD	74 ± 63	Alecian et al. (2008a)
<i>Suspected magnetic HAeBe stars</i>				
HD 35929	4884.328	DD	74 ± 19	This paper

continuum and in the N profile, and is detected in multiple observations, we conclude that the star is unambiguously magnetic.

6.2 The magnetic HAeBe stars detected within the survey

Of the 70 stars observed with ESPaDOnS and Narval, 6 show Stokes V Zeeman signatures in their LSD profiles. Four of these stars (V380 Ori, HD 72106, HD 190073, HD 200775) were unambiguously detected for the first time as a result of this study. First results for V380 Ori and HD 72106 were reported by Wade et al. (2005); for HD 190073 by Catala et al. (2007); for HD 200775 by Alecian et al. (2008a). In addition, one HAeBe star for which magnetic field detections were previously reported (HD 36982=Par 1772=LP Ori; Petit et al. 2008) is confirmed to be magnetic. Finally, one new suspected magnetic HAeBe star (HD 35929) is reported here. However as HD 35929 is a δ -Scuti pulsating star (Marconi et al. 2000), more analysis and observations are required to verify that the signature detected in the V profile is of magnetic origin.

In Table 3, for each of the detected program stars, we list the observational details corresponding to the ESPaDOnS/Narval observations from which the presence of a magnetic field was first inferred. In addition, in Fig. 4 we show the positions on the HR diagram of the magnetic HAeBe stars of our sample.

Each of the 5 detected stars has been or will be discussed in detail in a dedicated paper (e.g. HD 190073 by Catala et al. 2007, HD 200775 by Alecian et al. 2008a, HD 72106 by Folsom et al. 2008, V380 Ori by Alecian et al. 2009b). They will not be discussed further here.

Five other magnetic HAeBe stars have been discovered and confirmed during recent years, as part of parallel observational programs with ESPaDOnS, Narval, FORS1 on the Very-Large-Telescope (ESO, Chile), or the Semel Polarimeter (SEM-POL Semel 1989; Semel et al. 1993; Donati et al. 2003) coupled with the spectrograph UCLES on the Anglo-Australian-Telescope (AAT, Australia). The first magnetic detections and their confirmations are reported or are to be reported in other publications : HD 101412 (Wade et al. 2007; Hubrig et al. 2009, Alecian et al. in prep.), HD 104237 (Donati et al. 1997, Alecian et al. in prep.), NGC 6611 601 (Alecian et al. 2008b), NGC 2244 201

(Alecian et al. 2008b), and NGC 6611 83 (Alecian et al. 2009a). We are mentioning them in this paper for the sake of completeness, however they won't be included in the statistical analyses that will be presented in paper II and III as they are not part of the survey presented in this series of papers. They will not be discussed any further here.

6.3 Magnetic analysis of the remaining sample

The polarised spectra of the undetected stars, i.e. displaying no magnetic signatures, contain a valuable information that we want to extract : the upper limits on admissible surface magnetic fields. In this section we first describe the problems that a typical spectrum of Herbig Ae/Be stars can bring in evaluating realistic values of such limits due to the CS contribution to the spectra. Then we propose the method that we adopted to solve the problems : the hybrid method.

6.3.1 The CS contribution to the Stokes I and V spectra

Before discussing the analysis of the stars in which no firm magnetic detections was obtained, it is instructive to consider the formation of the stellar spectrum, beginning in the photosphere of a magnetised HAeBe star. Upon exiting the "top" of the photosphere, the (absorption) lines will be partially circularly polarized due the magnetic field. As the flux propagates into the CS environment, it will undergo absorption or emission contributions due to the CS material. As observed in the spectra of real HAeBe stars, this can strongly modify the Stokes I line profiles. However, we expect that the magnetic field strength will decrease rapidly with distance from the star : as $1/r^3$ for a dipole, and more rapidly for more complex fields. Therefore the contribution of the Zeeman effect to Stokes V in the CS environment should be very small compared to the photospheric contribution. In other words, the CS contribution to the flux is expected to be negligibly circularly polarized. A consequence of this conclusion is that the observed Stokes V/I_c spectrum of a magnetic HAeBe star is expected to be reflective of the *photospheric* spectrum of the star, even if the Stokes I spectrum is strongly modified by the CS environment. An important implication of this conclusion it that CS contamination of spectral lines cannot serve to "hide" the Zeeman signatures produced by a photospheric magnetic field. Note however, because the V spectrum is normalised to the inferred continuum, this conclusion and its implication rely on the assumption that no significant veiling is present (Ghandour et al. 1994; Folsom et al. 2012). Although veiling does not modify the absolute amplitude or shape of the Zeeman signature, it serves to increase the noise, and could therefore render a Zeeman signature undetectable.

The LSD profiles produced for line profile analysis in Sect. 5.2 with the cleaned masks are heavily filtered : many lines have been removed from the line masks in order to reduce the CS contribution and to reveal the photospheric profile. In the case of the Stokes V profile, this results in a relatively high noise level (because of the relatively small number of lines used in the deconvolution) and consequently low sensitivity to magnetic fields (see the SNR in V obtained from both full and cleaned masks in Table 1). However, in contrast to the Stokes I profile, we have concluded that Stokes V is not strongly modified by the CS contribution to the line. Therefore the most sensitive magnetic diagnosis should be obtained by including as many lines as possible in the mask. However, as we have seen in Sect. 5, LSD Stokes I profiles derived from

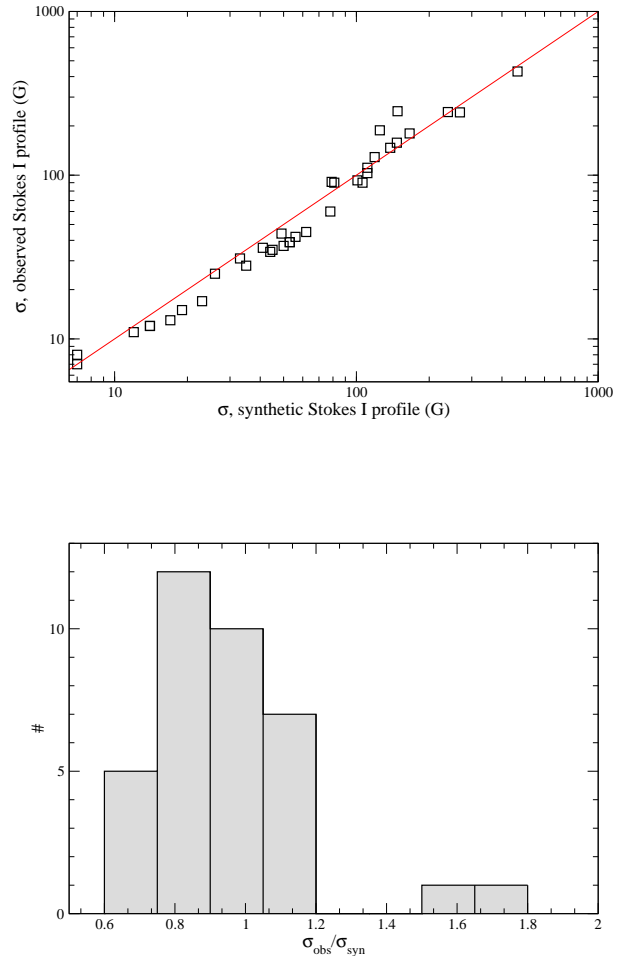


Figure 7. Comparison of longitudinal field error bars for synthetic versus observed Stokes I profiles. *Upper frame* - Scatter plot of longitudinal field error bars computed using synthetic Stokes I versus error bars computed using the observed Stokes I dominated by the photospheric component only. The solid (red) line corresponds to perfect agreement. *Lower frame* - Histogram of the ratio of error bars with synthetic Stokes I to error bars with observed Stokes I , for observations with LSD profiles dominated by the photospheric component.

such masks can be heavily modified by CS contributions. Even if the Stokes V Zeeman signature is not modified significantly, using such contaminated I profiles has two important consequences for our diagnosis of the magnetic field. First, uncertainty is introduced into the appropriate integration range to use to compute the longitudinal magnetic field in Eq. (1), and the reduced χ^2 in Eq. (2). Secondly, the equivalent width of the Stokes I profile (i.e. the denominator of Eq. (1)) is modified. Both of these consequences can change the inferred values of the longitudinal field and its error bar, while the first can influence the derived FAP. Of these, the impact on the longitudinal field is the most severe. For example, CS emission/absorption superimposed with the photospheric spectral lines can reduce/increase the equivalent width of the Stokes I profile significantly, artificially increasing/decreasing the derived longitudinal field and its error. In the absence of a magnetic detection, the longitudinal field error bar is the only important statistical quantity,

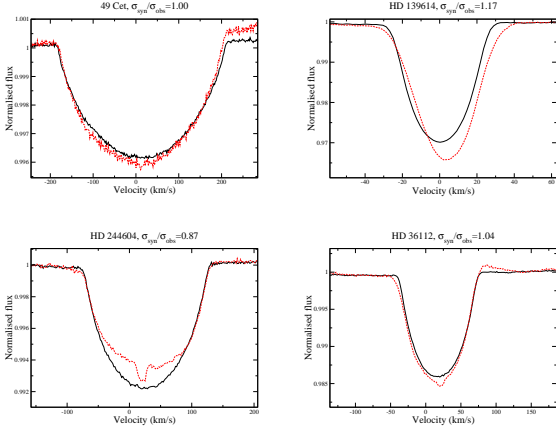


Figure 8. Illustrations of observed versus synthetic LSD Stokes I profiles for stars with profiles dominated by the photospheric component. The black full line is the synthetic, and the red dashed line is observed. Upper left : 49 Cet. Upper right : HD 139614. Lower left : HD 244604. Lower right : HD 36112.

as it provides an estimate of the upper limit on admissible fields. Because it is sensitive to CS contamination of Stokes I , it is important to understand, and potentially limit, the CS contribution to the I profile (even if the V profile is unmodified).

6.3.2 An hybrid approach

With these insights, we approached the problem of obtaining realistic quantitative longitudinal field measurements of the 65 program stars for which no significant magnetic field was detected. Our goal was to obtain measurements of the longitudinal field for which the error bars were simultaneously accurate and precise. The first option considered was to use the cleaned line masks described in Sect. 5. These have the advantage that they reveal, in many cases, the photospheric profile of the star. The disadvantage is that, in many cases, this is accomplished by excluding most of the lines - especially strong lines - that contribute significantly to reducing the Stokes V noise level. The second option was to use the full line masks. This has the advantage of reducing the noise level of Stokes V to the greatest extent, but the disadvantages of a strongly-contaminated I profile (as described above). We considered using masks for which an intermediate level of cleaning had been applied, but it was not obvious to what extent to clean the masks, nor was it clear that we were not simply combining the uncertainties and disadvantages of both options 1 and 2.

In reality, we wished to combined the *advantages* of options 1 and 2, essentially by combining the more nearly photospheric Stokes I profiles obtained from the cleaned masks and the high-SNR Stokes V profiles from the full masks. While such an approach can solve the problem of determination of the integration range, it does not solve the problem of determination of the longitudinal field : the I and V profiles obtained from two different masks correspond to averages of different lines with different weights, and are therefore not directly comparable or quantitatively compatible in Eq. (1).

As a solution to this problem, we decided to take advantage of the atmospheric and spectral parameters determined in Sects. 4 and 5 and to compute the approximate photospheric spectrum of each star using spectrum synthesis. We used the Synth3 LTE spectrum synthesis code (Kochukhov 2007) and effective temperature,

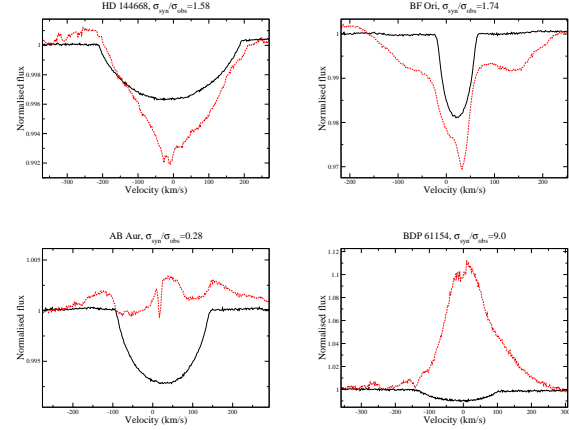


Figure 9. Illustrations of observed versus synthetic LSD Stokes I profiles for stars with profiles dominated by the circumstellar component. The black full line is the synthetic, and the red dashed line is observed. Upper left : HD 144668. Upper right : BF Ori. Lower left : AB Aur. Lower right : BD+61 154.

surface gravity, $v \sin i$ and v_{rad} of each star (reported in Table 2) to compute its photospheric Stokes I spectrum with the same spectral domain and resolution as ESPaDONS/Narval. We assumed solar abundances. To each synthetic spectrum we added synthetic gaussian noise (calculated from the SNR of the spectra) that varied with wavelength in the same manner as in the observed spectrum. For each observed spectrum we then used the full line mask appropriate to the star to extract the Stokes I LSD profile from the synthetic spectrum, and the Stokes V LSD profiles from the observed spectrum. Combining the I and V profiles, this ultimately resulted in "hybrid" LSD profiles consisting of the real, observed Stokes V profiles and a synthetic Stokes I profile, both extracted using the same mask. The advantage of this approach is that we avoid the uncertainty related to CS contributions to the Stokes I profile. On the other hand, we introduce uncertainty related to the compatibility of the synthetic photospheric spectrum with the real stellar photospheric spectrum.

6.3.3 Tests and effectiveness of the hybrid method

Using an integration range equal to the 1.2 times the measured $v \sin i$ of each star symmetric about the measured radial velocity, we evaluated Eqs. (1) and (2) for each of the hybrid LSD profiles. For comparison, we also performed the same measurements, but using the original LSD profiles extracted using the full masks obtained only from the observed spectra. These measurements are listed in Table 4.

Based on the analysis of Sect. 5, we conclude that some of our observations have relatively small CS contamination, and are dominated by the photospheric component. We identified 17 stars (corresponding to 35 observations) for which this was the case ; these stars are underlined in Table 4. We have used these observations as a test of the accuracy of this method by comparing the longitudinal field extracted using the LSD profiles with observed Stokes I profile, and those with the synthetic Stokes I profile. For stars with purely photospheric spectra we expect the longitudinal field error bars to agree. (Because the value of the longitudinal field itself is determined by the details of the noise pattern, we do not expect those values to agree, except that they should have values

compatible with the uncertainties.) The results of this comparison are shown in Fig. 7.

The upper panel of Fig. 7 shows the derived value of the longitudinal field error bar using the synthetic Stokes I profile (σ_{syn} , on the horizontal axis) versus that derived from the real Stokes I profile (σ_{obs} , on the vertical axis) of the stars with mostly photospheric spectra. As can be seen, the correspondence between the error bars is quite close, with most points clustered tightly about the line $x = y$. The detailed agreement is summarised in the lower panel, which shows a histogram of the ratio $\sigma_{\text{syn}}/\sigma_{\text{obs}}$. The median of the distribution is 0.85, the mean is 1.2 and the standard deviation is 0.4. Most of the values of $\sigma_{\text{syn}}/\sigma_{\text{obs}}$ are clustered within ± 0.15 of unity, although two significant outliers (the stars HD 34282 and HD 68695) exist at ~ 1.5 . The dispersion results from (usually) small differences in the equivalent widths of the computed versus observed Stokes I profiles. A comparison of the observed and computed Stokes I profiles for 4 of the stars with mostly photospheric spectra is shown in Fig. 8. The stars are typical of the sample, and illustrate the level of agreement usually achieved. Clearly some of the differences in the Stokes I profiles result from small CS contributions to the real spectrum (e.g. HD 244604, lower left frame). The remainder we attribute mainly to errors in the adopted atmospheric parameters and the detailed chemistry of the star. HD 34282 and HD 68695 are both instructive in this respect : a detailed examination of their spectra reveals underabundances of the Fe peak elements that dominate their spectra, while the abundance of oxygen appears to be solar. This suggests that these two stars represent further examples of HAeBe stars with λ Boo abundance patterns (Cowley et al. 2010; Folsom et al. 2012). In fact, one of these stars (HD 68695) was analysed by Folsom et al, who found it to exhibit clear lambda boo abundance peculiarities. From Fig. 7 we conclude that typically our spectrum synthesis approach is able to determine the expected longitudinal field error bar within $\pm 20\%$, although larger deviations sometimes occur for stars with strongly peculiar chemistry.

Examples of the remaining stars - those with profiles with significant CS contributions - are shown in Fig. 9. In these cases the magnetic diagnosis is highly uncertain, and often no reasonable diagnosis can be performed using the observed Stokes I profile. When we measure the longitudinal fields of the hybrid profiles of these objects, we find that while sometimes the error bars are reduced, sometimes they increase significantly. Examination of individual profiles reveals that often when the error bar derived by our method is significantly larger than that from the observed profile, it is because the observed profile is in strong emission or contains strong CS absorption, artificially increasing the magnitude of the equivalent width (e.g. BDP 61 154, lower right frame of Fig. 9, HD 144668 and BF Ori, upper frames of Fig. 9). On the other hand, partial infilling of the photospheric profile as a result of CS contributions may reduce the equivalent width, thereby increasing the error bar relative to that obtained from a synthetic profile (e.g. AB Aur, lower left frame of Fig. 9). In some extreme cases, the infilling can produce an observed equivalent width very close to zero, resulting in a divergent longitudinal field and error bar (e.g. HD 50083, observed on 03/04/08. Interestingly, the observation obtained on 12/11/07 has much less infilling, and a much more realistic error bar).

The results we obtain from our hybrid analysis are very different from those that we would obtain using the clean masks derived for the profile analysis of Sect. 5.2. To illustrate, in Table 4 there are 44 measurements (corresponding to 19 stars) with "hybrid" error bars smaller than 100 G. In contrast, analysis of the

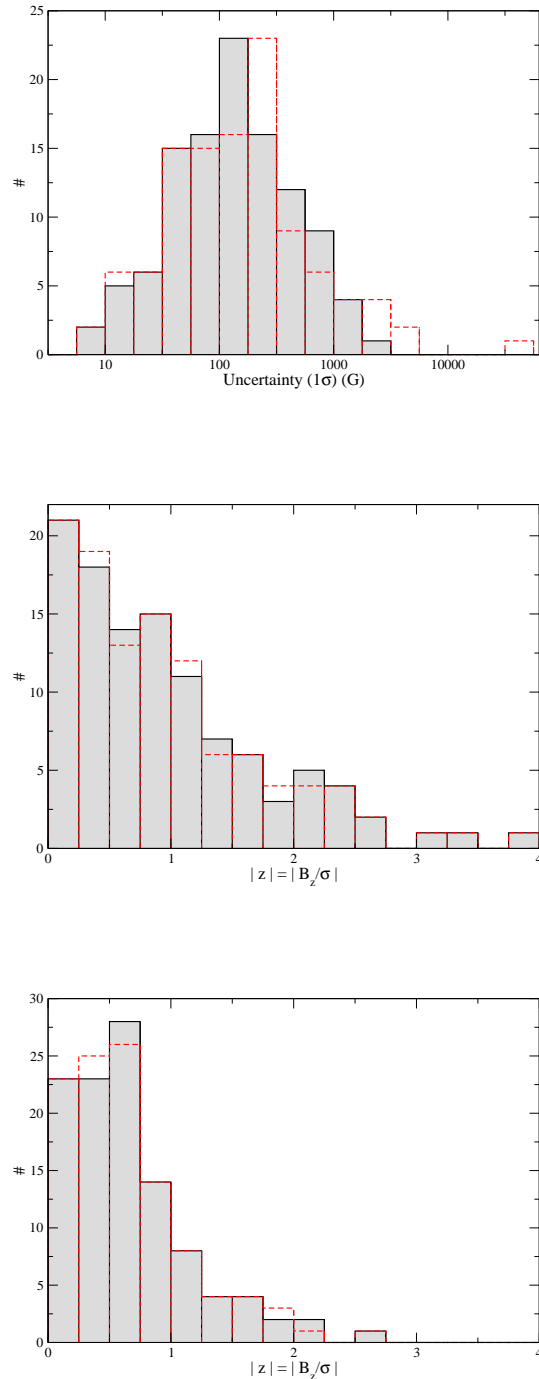


Figure 10. Final results for the longitudinal field uncertainties of the program stars. *Upper panel* - Error bars from the hybrid and original LSD profiles. The black filled histogram corresponds to the hybrid profiles, while the dashed red unfilled histogram corresponds to the original profiles. *Middle panel* - Detection significance $z = |\langle B_z \rangle / \sigma|$. Note that the three detections (i.e. $z \geq 3$) correspond to the magnetic HAeBe star LP Ori and to the suspected magnetic HAeBe star HD 35929. Both are sometimes detected in the V signatures of the LSD profiles and in $\langle B_z \rangle / \sigma$. *Lower panel* - Same as the middle but for the N profiles. Note on one side the absence of detections (i.e. $z \leq 3$), and on the other side, the numerous values with z between 1 and 2, while by definition an N spectrum does not contain any signal.

”clean” profiles results in only 10 measurements smaller than 100 G. For some stars for which the raw and hybrid profiles yield quite good errors (a few 10s of G), the clean profiles produce errors of hundreds of G. This confirms our view that in many cases, the line masks required to obtain a relatively pure photospheric profile for determining e.g. $v \sin i$ are not suitable to obtain profiles yielding the most realistic magnetic diagnosis.

Based on these experiments and examination of individual profiles, we conclude that our hybrid approach provides a useful way of determining the longitudinal magnetic field for a large and diverse sample of HAeBe stars, and that while inherent uncertainties exist in the determination of the longitudinal field using synthetic photospheric Stokes I profiles, those uncertainties (errors in atmospheric parameters, detailed chemistry) are better controlled and understood than the uncertainties associated with the determination of $\langle B_z \rangle$ using the observed Stokes I profiles. We therefore recommend the use of the hybrid determinations of $\langle B_z \rangle$ for characterisation of the magnetic fields of individual stars or samples of stars for which poorly understood contamination of Stokes I by CS environment is a problem.

In order to evaluate the impact of our choices of the masks on the $\langle B_z \rangle$ and their uncertainties, we have computed new LSD profiles of different stars of our sample with various masks of different temperature, gravity and abundance. We have then computed new values of $\langle B_z \rangle$ and compared them to those of Table 4. We selected stars in our sample of various spectral types and rotation velocities, and with small CS contribution. We changed the temperature within the error bars (Table 2), the $\log g$ from 3.5 to 4.5, and the abundance at $\pm 25\%$. We find that the $\langle B_z \rangle$ vary within the error bars in all cases. The uncertainties on the $\langle B_z \rangle$ vary by a factor lower than 1% when the $\log g$ and the abundances are varied. When we change the temperatures, the uncertainties vary from 1% (for large uncertainties of ~ 800 G) to 10% (for uncertainties lower than ~ 100 G).

Of the 70 stars observed in our survey, 65 (93%) show no direct evidence of a magnetic field. The derived characteristics of the longitudinal magnetic fields of the sample are summarised in Table 4. The magnetic geometries of the detected stars, as well as interpretation of the general magnetic properties of the sample from the distributions illustrated in Fig. 10, will be discussed in detail in Paper III.

7 CONCLUSIONS

This paper is the first of a series that presents the results of a high-resolution spectropolarimetric analysis of a sample of 70 Herbig Ae/Be stars. We carried out this analysis in order to address the problems of magnetism, angular momentum evolution and circumstellar environment during the pre-main sequence phase of intermediate-mass stars.

We obtained 132 high-resolution Stokes I and V spectra of 70 HAeBe stars using the instruments ESPaDOnS at CFHT and Narval at TBL. In this paper, we described the sample selection, the observations and their reduction, and the measurements that will comprise the basis of much of our following analysis. We described the determination of fundamental parameters for each target :

- the published effective temperatures have been verified by a visual comparison of observed with synthetic spectra. For some stars, new determinations of T_{eff} are given here. In the case of a few stars with high SNR observations weakly

contaminated by CS material, we have re-determined their T_{eff} with an automatic procedure described here.

- the luminosities have been estimated using the most reliable distance and photometric data that we could find in the literature.
- the radius, mass and age have been determined by comparing the position of the stars in an HR diagram with PMS evolutionary tracks computed with CESAM. The ages have been measured from the birthline of Behrend & Maeder (2001).

We discussed the Least-Squares Deconvolution method that we have applied to each of our spectra, including the careful selection, editing and tuning of the LSD line masks. We described the fitting of the LSD Stokes I profiles using a multi-component model that yields the rotationally-broadened photospheric profile (providing the projected rotational velocity and radial velocity for each observation) as well as circumstellar emission and absorption components. The $v \sin i$ measurements are summarised in Table 2.

Finally, we detail the method that we used to confidently affirm that a star is magnetic. We diagnosed the longitudinal Zeeman effect via the measured circular polarisation inside spectral lines. In this survey, 5 (out of 70) HAeBe stars have been confirmed to be magnetic (V380 Ori and HD 72106 reported by Wade et al. 2005 ; HD 190073 by Catala et al. 2007 ; HD 200775 by Alecian et al. 2008a ; LP Ori by Petit et al. 2008). Four of them have been discovered within this program. One star (HD 35929) is reported here as a new suspected magnetic star. We also present the ”hybrid” method that we have adopted in order to obtain realistic quantitative measurements of the magnetic fields of the 65 non-magnetic stars. The results are reported in Tables 3 and 4.

As an appendix, we have also provided a detailed review of each star observed.

In three forthcoming papers we will present our analysis of the rotational properties of the sample (paper II ; Alecian et al. 2012), the magnetic properties of the sample (paper III ; Wade et al. in prep.), and the properties of the circumstellar environment of the Herbig Ae/Be stars (paper IV ; Alecian et al. in prep.).

ACKNOWLEDGMENTS

We are very grateful to O. Kochukhov, who provided his BINMAG1 code. We thank Nikolai Piskunov, the referee, which led to important improvements in the paper. EA has been supported by the Marie Curie FP6 program, and the Centre National d’Etudes Spatiales (CNES). EA has also been supported by the Ministry of Higher Education and Research (MESR) and the Ministry of Foreign and European Affairs (MAEE), via the Hubert Curien Partnership (PHC) FAST (French-Australian Science & Technology). GAW and JDL acknowledge support from the Natural Science and Engineering Research Council of Canada (NSERC). GAW has also been supported by the DND Academic Research Programme (ARP). This research has made use of the SIMBAD database and the VizieR catalogue access tool, operated at CDS, Strasbourg (France), and of NASA’s Astrophysics Data System. SM and IW have been supported by the Commonwealth of Australia under the International Science Linkages programme.

Références

- Abt H. A., 2009, *AJ*, 138, 28

Table 4. Results of the magnetic analysis of the program HAeBe stars. The data of HD 190073, V380 ori, HD 200775 and HD 72106 have already been published and do not appear here. Columns 1 and 2 give the name of the star and the date of the observation. Columns 3 and 4 give the limits of the integration range. The False Alarm Probability (FAP) of a Zeeman detection in the V profile is indicated in column 5. The magnetic diagnosis (ND, MD or DD) is indicated in column 6. The B_ℓ measurement, its error (σ), and the detection significance (B_ℓ/σ) computed using the hybrid and original profiles are given in the columns 7 to 10. The final column give the ratio of the B_ℓ errors of the hybrid over the observed solutions.

Filename	Date	Start (km/s)	End	FAP	Diagnosis	HYBRID		ORIGINAL		$\sigma_{\text{syn}}/\sigma_{\text{obs}}$
						$B_\ell \pm \sigma$ (G)	B_ℓ/σ	$B_\ell \pm \sigma$ (G)	B_ℓ/σ	
BD-06 1259	12/03/09	-25	69	0.7990	ND	62±87	0.711	37±51	0.711	1.71
	20/02/05	-25	69	0.5826	ND	53±54	0.986	31±31	0.987	1.74
BD-05 1329	23/08/05	-148	205	0.6266	ND	201±396	0.508	144±282	0.508	1.40
<u>BD-05 1324</u>	11/01/06	-59	118	0.3831	ND	-51±111	-0.455	-47±103	-0.455	1.08
<u>BD+41 3731</u>	06/11/07	-428	400	1.0000	ND	2367±1890	1.252	3415±2731	1.250	0.69
	25/08/05	-428	400	0.9987	ND	50±1008	0.049	51±1038	0.049	0.97
BD+46 3471	25/08/05	-242	235	0.6788	ND	-20±526	-0.038	-45±1202	-0.038	0.44
BD+61 154	21/02/05	-151	118	0.6030	ND	146±666	0.219	-16±74	-0.219	9.00
	23/08/05	-151	118	0.2323	ND	985±549	1.796	-177±98	-1.798	5.60
BD+65 1637	10/06/06	-360	308	0.9998	ND	574±1109	0.518	-2045±3955	-0.517	0.28
	24/09/09	-360	308	0.9997	ND	-806±874	-0.923	938±1023	0.917	0.85
BD+72 1031	11/06/06	-59	118	0.9309	ND	-28±118	-0.234	-36±156	-0.234	0.76
	11/11/07	-225	207	0.9810	ND	1072±1122	0.955	412±431	0.956	2.60
<u>HD 9672</u>	24/08/05	-221	247	0.9509	ND	27±111	0.239	27±111	0.239	1.00
<u>HD 17081</u>	19/02/05	-11	37	0.3758	ND	2±7	0.268	2±8	0.268	0.88
	20/02/05	-13	35	0.9972	ND	0±7	0.010	0±7	0.010	1.00
HD 31293	27/11/04	-113	163	0.5567	ND	-112±87	-1.283	393±308	1.274	0.28
	19/02/05	-113	163	0.8017	ND	-27±157	-0.172	31±179	0.172	0.88
	21/02/05	-113	163	0.7151	ND	51±103	0.490	-63±128	-0.490	0.80
HD 31648	21/02/05	-104	130	0.9268	ND	9±65	0.134	10±77	0.134	0.84
	24/08/05	-104	130	0.9687	ND	149±62	2.411	220±92	2.408	0.67
<u>HD 34282</u>	24/08/05	-111	142	0.3744	ND	-223±148	-1.505	-369±246	-1.504	0.60
<u>HD 35187 B</u>	25/08/05	-85	139	0.7977	ND	-94±101	-0.925	-86±93	-0.926	1.09
<u>HD 35929</u>	11/03/09	-53	95	0.9993	ND	-8±35	-0.227	-6±28	-0.227	1.25
	12/11/07	-53	95	0.0091	ND	-59±23	-2.598	-45±17	-2.598	1.35
	13/11/07	-53	95	0.9704	ND	-137±45	-3.007	-106±35	-3.007	1.29
	20/02/09	-53	95	0.0002	MD	33±17	1.957	25±13	1.957	1.31
	21/02/09	-53	95	0.0000	DD	74±19	3.928	57±15	3.928	1.27
<u>HD 36112</u>	29/11/04	-47	83	0.9382	ND	27±26	1.034	26±25	1.034	1.04
	19/02/05	-47	83	0.9395	ND	-35±33	-1.059	-33±31	-1.059	1.06
HD 36910	04/04/08	-81	143	0.9018	ND	-141±85	-1.654	-180±109	-1.653	0.78
HD 36917	08/11/07	-126	179	0.9960	ND	-672±384	-1.748	-978±560	-1.745	0.69
HD 36982	08/11/07	-65	90	0.9402	ND	-307±251	-1.224	-326±267	-1.224	0.94
	09/11/07	-65	90	0.0059	ND	-225±108	-2.090	-227±109	-2.086	0.99
	10/11/07	-65	90	1.0000	ND	-10±79	-0.129	-10±76	-0.129	1.04
	11/11/07	-65	90	0.0009	MD	-248±76	-3.267	-233±71	-3.265	1.07
	24/02/09	-209	271	0.6827	ND	-216±404	-0.535	-196±366	-0.535	1.10
HD 37258	24/02/09	-127	170	0.9917	ND	133±197	0.674	212±315	0.674	0.63
HD 37806	24/08/05	-97	191	0.1909	ND	239±179	1.336	349±261	1.334	0.69
HD 38120	13/03/09	-89	144	0.3659	ND	191±203	0.942	679±723	0.939	0.28
<u>HD 38238</u>	16/03/07	-105	133	0.7370	ND	18±81	0.221	20±90	0.221	0.90
HD 50083	03/04/08	-279	278	0.9978	ND	124±236	0.525	10860±33614	0.323	0.01
	12/11/07	-279	278	1.0000	ND	-229±191	-1.200	-304±254	-1.200	0.75
HD 52721	03/04/08	-237	280	0.9520	ND	222±235	0.943	212±225	0.943	1.04
	06/11/07	-237	280	1.0000	ND	-22±204	-0.107	-24±220	-0.107	0.93
HD 53367	19/02/05	-2	97	0.9606	ND	-19±46	-0.406	-20±48	-0.406	0.96
	20/02/05	-2	97	0.9917	ND	18±29	0.617	19±31	0.617	0.94
<u>HD 68695</u>	21/02/05	-32	73	0.7696	ND	10±125	0.078	15±188	0.078	0.66
HD 76534 A	21/02/05	-58	105	0.9331	ND	-154±151	-1.019	-203±199	-1.019	0.76
HD 98922	20/02/05	-60	60	0.3729	ND	-144±71	-2.015	194±96	2.012	0.74
HD 114981	11/01/06	-335	236	0.9968	ND	-105±203	-0.518	-157±303	-0.518	0.67
	19/02/05	-335	236	0.9875	ND	-117±459	-0.255	-197±775	-0.255	0.59
<u>HD 135344</u>	09/01/06	-98	98	0.9417	ND	-124±138	-0.893	-131±147	-0.893	0.94
<u>HD 139614</u>	19/02/05	-29	29	0.1845	ND	-24±14	-1.760	-22±12	-1.760	1.17
	20/02/05	-29	29	0.8027	ND	-13±14	-0.947	-11±12	-0.947	1.17
	21/02/05	-29	29	0.7707	ND	12±12	0.998	11±11	0.998	1.09
HD 141569	06/03/07	-286	262	0.6638	ND	-73±149	-0.492	-591±1219	-0.485	0.12
	12/02/06	-286	262	0.8590	ND	645±778	0.829	1672±2023	0.826	0.38

Table 4 – *continued*

Filename	Date	Start	End	FAP	Diagnosis	HYBRID		ORIGINAL		$\sigma_{\text{syn}}/\sigma_{\text{obs}}$
						$B_{\ell} \pm \sigma$ (G)	B_{ℓ}/σ	$B_{\ell} \pm \sigma$ (G)	B_{ℓ}/σ	
<u>HD 142666</u>	19/02/05	-85	72	0.9918	ND	28±78	0.359	22±60	0.359	1.30
	21/02/05	-85	72	0.4443	ND	-45±44	-1.009	-34±34	-1.010	1.29
	21/05/05	-85	72	0.8100	ND	16±53	0.298	12±39	0.298	1.36
	21/05/05	-85	72	0.9985	ND	-29±53	-0.543	-21±39	-0.543	1.36
	22/05/05	-85	72	0.6419	ND	54±62	0.873	39±45	0.873	1.38
	23/05/05	-85	72	0.8755	ND	-14±50	-0.282	-11±37	-0.282	1.35
	24/05/05	-85	72	0.5239	ND	-29±56	-0.511	-21±42	-0.511	1.33
	19/02/05	-97	93	0.7430	ND	-113±49	-2.296	-101±44	-2.296	1.11
20/02/05	-97	93	0.8485	ND	-9±41	-0.227	-8±36	-0.227	1.14	
HD 144668	23/08/05	-249	229	0.8869	ND	299±145	2.064	191±92	2.066	1.58
HD 145718	25/08/05	-139	132	0.0961	ND	17±85	0.204	15±72	0.204	1.18
HD 150193	23/08/05	-135	125	0.8757	ND	-194±117	-1.664	-382±230	-1.661	0.51
HD 163296	21/05/05	-164	146	0.8992	ND	41±106	0.387	103±266	0.387	0.40
	22/05/05	-164	146	0.9703	ND	47±141	0.333	59±176	0.333	0.80
	23/05/05	-164	146	0.7855	ND	138±96	1.431	160±112	1.431	0.86
	23/05/05	-164	146	0.8324	ND	0±135	-0.001	0±131	-0.001	1.03
	24/05/05	-164	146	0.6017	ND	109±96	1.134	250±221	1.132	0.43
	24/05/05	-164	146	0.6782	ND	313±136	2.292	523±229	2.285	0.59
	24/08/05	-164	146	0.2564	ND	202±93	2.160	-1835±998	-1.840	0.09
HD 169142	19/02/05	-58	57	0.9872	ND	12±28	0.434	23±52	0.434	0.54
	21/02/05	-58	57	0.1944	ND	51±34	1.521	100±66	1.520	0.52
	21/05/05	-58	57	0.9848	ND	-21±20	-1.038	-40±38	-1.038	0.53
	23/08/05	-58	57	0.9943	ND	28±12	2.215	52±23	2.214	0.52
HD 174571	15/04/08	-249	277	0.9923	ND	-1733±687	-2.521	-1825±724	-2.520	0.95
	16/03/07	-249	277	0.9983	ND	213±544	0.392	220±560	0.392	0.97
<u>HD 176386</u>	24/08/05	-212	208	0.6676	ND	304±239	1.272	309±243	1.271	0.98
HD 179218	03/10/09	-67	98	0.9902	ND	-1±39	-0.026	-1±42	-0.026	0.93
	20/02/05	-67	98	0.3448	ND	-97±114	-0.850	-98±115	-0.849	0.99
	25/08/05	-67	98	0.8626	ND	77±50	1.536	78±51	1.536	0.98
<u>HD 244314</u>	05/11/07	-40	85	0.9511	ND	-46±106	-0.436	-39±90	-0.436	1.18
<u>HD 244604</u>	23/08/05	-91	145	0.8532	ND	-90±79	-1.138	-103±91	-1.137	0.87
HD 245185	19/02/05	-124	157	0.7352	ND	-255±335	-0.760	-1674±2216	-0.755	0.15
HD 249879	05/04/08	-294	316	0.9577	ND	1465±1326	1.104	971±879	1.104	1.51
HD 250550	07/11/07	-117	72	0.0256	ND	-60±249	-0.241	54±225	0.241	1.11
HD 259431	17/03/07	-73	126	0.7920	ND	-117±184	-0.636	75±118	0.636	1.56
	17/03/10	-73	126	0.3502	ND	22±281	0.078	-27±351	-0.078	0.80
	24/02/09	-73	126	0.6835	ND	93±197	0.474	-58±122	-0.474	1.61
	10/12/06	-267	270	0.9871	ND	80±303	0.263	43±163	0.263	1.86
HD 275877	24/09/09	-267	270	0.9182	ND	6±418	0.014	5±346	0.014	1.21
	20/02/05	-82	109	0.8934	ND	74±119	0.627	81±129	0.627	0.92
	20/02/05	-82	109	0.7830	ND	-105±147	-0.717	-113±158	-0.717	0.93
21/02/05	-82	109	0.9398	ND	-62±166	-0.370	-67±180	-0.370	0.92	
<u>HD 287841</u>	20/02/09	-119	159	0.7004	ND	61±268	0.229	55±242	0.229	1.11
HD 290409	06/11/07	-299	301	0.9883	ND	-939±980	-0.958	-4140±4385	-0.944	0.22
<u>HD 290500</u>	21/02/09	-73	131	0.9775	ND	601±464	1.296	557±430	1.295	1.08
HD 290770	24/02/09	-249	324	0.8890	ND	1088±985	1.105	2264±2068	1.095	0.48
HD 293782	10/01/06	-253	277	0.8452	ND	1178±942	1.251	508±406	1.253	2.32
HD 344261	06/11/07	-240	231	0.9608	ND	-817±928	-0.880	-463±526	-0.880	1.76
	23/08/05	-240	231	0.7389	ND	-275±491	-0.561	-162±289	-0.561	1.70
	25/08/05	-100	201	0.9998	ND	1138±485	2.348	561±238	2.355	2.04
VV Ser	25/08/05	-100	201	0.9998	ND	1138±485	2.348	561±238	2.355	2.04
VX Cas	/24/08/05	-199	180	0.9707	ND	-286±994	-0.288	-242±840	-0.288	1.18

Abt H. A., Morrell N. I., 1995, *ApJS*, 99, 135

Acke B., van den Ancker M. E., 2004, *A&A*, 426, 151

Acke B., Waelkens C., 2004b, *A&A*, 427, 1009

Alecian E., Catala C., Wade G. A., Bagnulo S., Böhm T., Bouret J.-C., Donati J.-F., Folsom C., Grunhut J., Landstreet J. D., Marsden S. C., Petit P., Ramirez J., Silvester J., 2009a, in C. Neiner & J.-P. Zahn ed., *EAS Publications Series Vol. 39 of EAS Publications Series, Magnetism in Herbig Ae/Be stars and the link to the Ap/Bp stars*, pp 121–132

Alecian E., Catala C., Wade G. A., Donati J., Petit P., Landstreet J. D., Böhm T., Bouret J., Bagnulo S., Folsom C., Grunhut J., Silvester J., 2008a, *MNRAS*, 385, 391

Alecian E., Wade G. A., Catala C., Bagnulo S., Böhm T., Bohlender D., Bouret J., Donati J., Folsom C. P., Grunhut J., Landstreet J. D., 2008b, *A&A*, 481, L99

Alecian E., Wade G. A., Catala C., Bagnulo S., Böhm T., Bouret J., Donati J., Folsom C. P., Grunhut J., Landstreet J. D., 2009b, *MNRAS*, pp 1250–+

- Alecian E., Wade G. A., Catala C., Grunhut J. H., Landstreet J. D., Böhm T., Bouret J., Flood J., Folsom C., 2012, MNRAS, in press
- Alencar S. H. P., Melo C. H. F., Dullemond C. P., Andersen J., Batalha C., Vaz L. P. R., Mathieu R. D., 2003, A&A, 409, 1037
- Alonso-Albi T., Fuente A., Bachiller R., Neri R., Planesas P., Testi L., Berné O., Joblin C., 2009, A&A, 497, 117
- Andersen J., Lindgren H., Hazen M. L., Mayor M., 1989, A&A, 219, 142
- Artymowicz P., 2000, Space Science Reviews, 92, 69
- Augereau J. C., Lagrange A. M., Mouillet D., Ménard F., 1999, A&A, 350, L51
- Aurière M., Wade G. A., Silvester J., Lignières F., Bagnulo S., Bale K. e. a., 2007, A&A, 475, 1053
- Aveni A. F., Hunter J. H., 1972, AJ, 77, 17
- Beals C. S., 1953, Publications of the Dominion Astrophysical Observatory Victoria, 9, 1
- Behrend R., Maeder A., 2001, A&A, 373, 190
- Belikov A. N., 1995, Bulletin d'Information du Centre de Données Stellaires, 47, 9
- Bernabei S., Ripepi V., Ruoppo A., Marconi M., Monteiro M. J. P. F. G., Rodriguez E., Oswalt T. D., Leccia S., Palla F., Cantanzaro G., Amado P. J., Lopez-Gonzalez M. J., Aceituno F. J., 2009, A&A, 501, 279
- Bernes C., 1977, A&AS, 29, 65
- Beskrovnaya N. G., Pogodin M. A., Miroshnichenko A. S., Thé P. S., Savanov I. S., Shakhovskoy N. M., Rostopchina A. N., Kozlova O. V., Kuratov K. S., 1999, A&A, 343, 163
- Blaauw A., 1964, ARAA, 2, 213
- Boersma C., Peeters E., Martín-Hernández N. L., van der Wolk G., Verhoeff A. P., Tielens A. G. G. M., Waters L. B. F. M., Pel J. W., 2009, A&A, 502, 175
- Böhm T., Catala C., 1994, A&A, 290, 167
- Böhm T., Catala C., 1995, A&A, 301, 155
- Böhm T., Catala C., Balona L., Carter B., 2004, A&A, 427, 907
- Bouret J.-C., Catala C., 1998, A&A, 340, 163
- Bouret J.-C., Catala C., Simon T., 1997, A&A, 328, 606
- Brown A. G. A., de Geus E. J., de Zeeuw P. T., 1994, A&A, 289, 101
- Catala C., Alecian E., Donati J.-F., Wade G. A., Landstreet J. D., Böhm T., Bouret J.-C., Bagnulo S., Folsom C., Silvester J., 2007, A&A, 462, 293
- Catala C., Böhm T., Donati J.-F., Semel M., 1993, A&A, 278, 187
- Catala C., Czarny J., Felenbok P., Praderie F., 1986a, A&A, 154, 103
- Catala C., Donati J. F., Böhm T., Landstreet J., Henrichs H. F., 1999, A&A, 345, 884
- Catala C., Felenbok P., Czarny J., Talavera A., Boesgaard A. M., 1986b, ApJ, 308, 791
- Catala C., Kunasz P. B., 1987, A&A, 174, 158
- Catala C., Simon T., Praderie F., Talavera A., The P. S., Tjin A Djie H. R. E., 1989, A&A, 221, 273
- Chiang E. I., Joungh M. K., Creech-Eakman M. J., Qi C., Kessler J. E., Blake G. A., van Dishoeck E. F., 2001, ApJ, 547, 1077
- Claret A., 2000, A&A, 363, 1081
- Cohen M., 1973, MNRAS, 164, 395
- Corcoran M., Ray T. P., 1998, A&A, 331, 147
- Corporon P., Lagrange A.-M., 1999, A&AS, 136, 429
- Coulson I. M., Walther D. M., Dent W. R. F., 1998, MNRAS, 296, 934
- Cowley C. R., Hubrig S., González J. F., Savanov I., 2010, A&A, 523, A65
- Crawford D. L., Barnes J. V., 1970, AJ, 75, 952
- de Winter D., van den Ancker M. E., Maira A., Thé P. S., Djie H. R. E. T. A., Redondo I., Eiroa C., Molster F. J., 2001, A&A, 380, 609
- de Zeeuw P. T., Hoogerwerf R., de Bruijne J. H. J., Brown A. G. A., Blaauw A., 1999, AJ, 117, 354
- Deleuil M., Bouret J., Catala C., Lecavelier des Etangs A., Vidal-Madjar A., Roberge A., Feldman P. D., Martin C., Ferlet R., 2005, A&A, 429, 247
- Dent W. R. F., Greaves J. S., Coulson I. M., 2005, MNRAS, 359, 663
- Doering R. L., Meixner M., 2009, AJ, 138, 780
- Dolan C. J., Mathieu R. D., 2001, AJ, 121, 2124
- Donati J.-F., Collier Cameron A., Semel M., Hussain G. A. J., Petit P., Carter B. D., Marsden S. C., Mengel M., López Ariste A., Jeffers S. V., Rees D. E., 2003, MNRAS, 345, 1145
- Donati J.-F., Semel M., Carter B. D., Rees D. E., Collier Cameron A., 1997, MNRAS, 291, 658
- Donati J.-F., Semel M., Rees D. E., 1992, A&A, 265, 669
- Doucet C., Pantin E., Lagage P. O., Dullemond C. P., 2006, A&A, 460, 117
- Dunkin S. K., Crawford I. A., 1998, MNRAS, 298, 275
- Eggen O. J., 1986, AJ, 92, 1074
- Eiroa C., Garzón F., Alberdi A., de Winter D., Ferlet R., Grady e. a., 2001, A&A, 365, 110
- Eisner J. A., Graham J. R., Akeson R. L., Najita J., 2009, ApJ, 692, 309
- Eisner J. A., Lane B. F., Hillenbrand L. A., Akeson R. L., Sargent A. I., 2004, ApJ, 613, 1049
- ESA 1997, VizieR Online Data Catalog, 1239, 0
- Fabricius C., Makarov V. V., 2000, A&A, 356, 141
- Fernández D., Figueras F., Torra J., 2008, A&A, 480, 735
- Finkenzeller U., 1985, A&A, 151, 340
- Finkenzeller U., Mundt R., 1984, A&AS, 55, 109
- Folsom C. P., Bagnulo S., Wade G. A., Alecian E., Landstreet J. D., Marsden S. C., Waite I. A., 2012, MNRAS, 422, 2072
- Folsom C. P., Wade G. A., Kochukhov O., Alecian E., Catala C., Bagnulo S., Böhm T., Bouret J., Donati J., Grunhut J., Hanes D. A., Landstreet J. D., 2008, MNRAS, 391, 901
- Fossati L., Ryabchikova T., Bagnulo S., Alecian E., Grunhut J., Kochukhov O., Wade G., 2009, A&A, 503, 945
- Frémat Y., Neiner C., Hubert A., Floquet M., Zorec J., Janot-Pacheco E., Renan de Medeiros J., 2006, A&A, 451, 1053
- Friedemann C., Reimann H., Guertler J., 1992, A&A, 255, 246
- Frink S., Roeser S., Alcalá J. M., Covino E., Brandner W., 1998, A&A, 338, 442
- Getman K. V., Flaccomio E., Broos P. S., Grosso N., Tsujimoto M. e. a., 2005, ApJS, 160, 319
- Ghandour L., Strom S., Edwards S., Hillenbrand L., 1994, in P. S. The, M. R. Perez, & E. P. J. van den Heuvel ed., The Nature and Evolutionary Status of Herbig Ae/Be Stars Vol. 62 of Astronomical Society of the Pacific Conference Series, Spectroscopic diagnostic of disk accretion in Herbig Ae/Be stars. pp 223–+
- Glebocki R., Stawikowski A., 2000, Acta Astronomica, 50, 509
- Grady C. A., Devine D., Woodgate B., Kimble R., Bruhweiler F. C., Boggess A., Linsky J. L., Plait P., Clampin M., Kalas P., 2000a, ApJ, 544, 895
- Grady C. A., Perez M. R., Talavera A., Bjorkman K. S., de Winter D., The P., Molster F. J., van den Ancker M. E., Sitko M. L., Morrison N. D., Beaver M. L., McCollum B., Castelaz M. W., 1996, A&AS, 120, 157
- Grady C. A., Perez M. R., The P. S., 1993, A&A, 274, 847
- Grady C. A., Sitko M. L., Russell R. W., Lynch D. K., Hanner

- M. S., Perez M. R., Bjorkman K. S., de Winter D., 2000b, *Protostars and Planets IV*, pp 613–+
- Gray D. F., 1992, *The observation and analysis of stellar photospheres*. Cambridge Astrophysics Series, Cambridge : Cambridge University Press, 1992, 2nd ed., ISBN 0521403200.
- Gregorio-Hetem J., Lepine J. R. D., Quast G. R., Torres C. A. O., de La Reza R., 1992, *AJ*, 103, 549
- Grinin V. P., Kozlova O. V., Natta A., Ilyin I., Tuominen I., Ros-topchina A. N., Shakhovskoy D. N., 2001, *A&A*, 379, 482
- Guetter H. H., 1976, *AJ*, 81, 537
- Guetter H. H., 1979, *AJ*, 84, 1846
- Guetter H. H., 1981, *AJ*, 86, 1057
- Guimarães M. M., Alencar S. H. P., Corradi W. J. B., Vieira S. L. A., 2006, *A&A*, 457, 581
- Günther H. M., Schmitt J. H. M. M., 2009, *A&A*, 494, 1041
- Harvey P. M., Huard T. L., Jørgensen J. K., Gutermuth R. A., Mamajek E. E., Bourke T. L., Merín B., Cieza L., Brooke T., Chapman N., Alcalá J. M., Allen L. E., Evans II N. J., Di Francesco J., Kirk J. M., 2008, *ApJ*, 680, 495
- Herbig G. H., 1960, *ApJS*, 4, 337
- Herbst W., 1975, *AJ*, 80, 683
- Herbst W., Shevchenko V. S., 1999, *AJ*, 118, 1043
- Herbst W., Warner J. W., Miller D. P., Herzog A., 1982, *AJ*, 87, 98
- Hernández J., Calvet N., Briceño C., Hartmann L., Berlind P., 2004, *AJ*, 127, 1682
- Hernández J., Calvet N., Hartmann L., Briceño C., Sicilia-Aguilar A., Berlind P., 2005, *AJ*, 129, 856
- Hill P. W., 1970, *MNRAS*, 150, 23
- Hillenbrand L. A., Strom S. E., Calvet N., Merrill K. M., Gatley I., Makidon R. B., Meyer M. R., Skrutskie M. F., 1998, *AJ*, 116, 1816
- Hillenbrand L. A., Strom S. E., Vrba F. J., Keene J., 1992, *ApJ*, 397, 613
- Høg E., Fabricius C., Makarov V. V., Urban S., Corbin T., Wycoff G., Bastian U., Schwekendiek P., Wicenec A., 2000, *A&A*, 355, L27
- Høg E., Kuzmin A., Bastian U., Fabricius C., Kuimov K., Lindgren L., Makarov V. V., Roeser S., 1998, *A&A*, 335, L65
- Houk N., 1982, *Michigan Catalogue of Two-dimensional Spectral Types for the HD stars*. Volume 3. Declinations -40 deg to -26 deg.
- Houk N., 1994, *VizieR Online Data Catalog*, 3080, 0
- Hubeny I., 1988, *Comput. Phys. Comm.*, 52, 103
- Hubeny I., Lanz T., 1992, *A&A*, 262, 501
- Hubeny I., Lanz T., 1995, *ApJ*, 439, 875
- Hubrig S., Pogodin M. A., Yudin R. V., Schöller M., Schnerr R. S., 2007, *A&A*, 463, 1039
- Hubrig S., Schöller M., Yudin R. V., 2004, *A&A*, 428, L1
- Hubrig S., Stelzer B., Schöller M., Grady C., Schütz O., Pogodin M. A., Curé M., Hamaguchi K., Yudin R. V., 2009, *A&A*, 502, 283
- Hughes A. M., Wilner D. J., Kamp I., Hogerheijde M. R., 2008, *ApJ*, 681, 626
- Hussain G. A. J., Collier Cameron A., Jardine M. M., Dunstone N., Ramirez Velez J., Stempels H. C., Donati J.-F., Semel M., Aulanier G., Harries T., Bouvier J., Dougados C., Ferreira J., Carter B. D., Lawson W. A., 2009, *MNRAS*, 398, 189
- Jenniskens P., Desert F., 1994, *A&AS*, 106, 39
- Johnson H. M., 1965, *ApJ*, 142, 964
- Jordi C., Trullols E., Galadi-Enriquez D., 1996, *A&A*, 312, 499
- Juhász A., Prusti T., Ábrahám P., Dullemond C. P., 2007, *MNRAS*, 374, 1242
- Jura M., Malkan M., White R., Telesco C., Pina R., Fisher R. S., 1998, *ApJ*, 505, 897
- Kazarovets E. V., Samus N. N., Durlevich O. V., Kireeva N. N., Pastukhova E. N., 2006, *Information Bulletin on Variable Stars*, 5721, 1
- Keller L. D., Sloan G. C., Forrest W. J., Ayala S., D'Alessio P., Shah S., Calvet N., Najita J., Li A., Hartmann L., Sargent B., Watson D. M., Chen C. H., 2008, *ApJ*, 684, 411
- Kenyon S. J., Hartmann L., 1995, *ApJS*, 101, 117
- Kharchenko N. V., Piskunov A. E., Röser S., Schilbach E., Scholz R., 2004, *Astronomische Nachrichten*, 325, 740
- Kharchenko N. V., Piskunov A. E., Röser S., Schilbach E., Scholz R., 2005, *A&A*, 438, 1163
- Kholopov P. N., 1959, *Soviet Astronomy*, 3, 291
- Kochukhov O. P., 2007, in I. I. Romanyuk, D. O. Kudryavtsev, O. M. Neizvestnaya, & V. M. Shapoval ed., *Physics of Magnetic Stars Spectrum synthesis for magnetic, chemically stratified stellar atmospheres*. pp 109–118
- Kovalchuk G. U., Pugach A. F., 1997, *A&A*, 325, 1077
- Kraus S., Preibisch T., Ohnaka K., 2008, *ApJ*, 676, 490
- Kun M., 1998, *ApJS*, 115, 59
- Kun M., Vinkó J., Szabados L., 2000, *MNRAS*, 319, 777
- Kurucz R., 1993, *Opacities for Stellar Atmospheres : [-3.5],[-4.0],[-4.5]*. Kurucz CD-ROM No. 7. Cambridge, Mass. : Smithsonian Astrophysical Observatory, 1993., 7
- Landstreet J. D., 1982, *ApJ*, 258, 639
- Larson R. B., 1972, *MNRAS*, 157, 121
- Levato H., Abt H. A., 1976, *PASP*, 88, 712
- Levreault R. M., 1985, PhD thesis, Texas Univ., Austin.
- Lignieres F., Catala C., Mangeney A., 1996, *A&A*, 314, 465
- Lynds B. T., 1962, *ApJS*, 7, 1
- Magakian T. Y., 2003, *A&A*, 399, 141
- Malfait K., Bogaert E., Waelkens C., 1998, *A&A*, 331, 211
- Mamajek E. E., Lawson W. A., Feigelson E. D., 2000, *ApJ*, 544, 356
- Mannings V., Barlow M. J., 1998, *ApJ*, 497, 330
- Mannings V., Sargent A. I., 1997, *ApJ*, 490, 792
- Manoj P., Maheswar G., Bhatt H. C., 2002, *MNRAS*, 334, 419
- Manset N., Bastien P., Bertout C., 2005, *AJ*, 129, 480
- Marconi M., Ripepi V., Alcalá J. M., Covino E., Palla F., Terrane-gra L., 2000, *A&A*, 355, L35
- Martayan C., Floquet M., Hubert A. M., Neiner C., Frémat Y., Baade D., Fabregat J., 2008, *A&A*, 489, 459
- Mason K. O., Breeveld A., Much R., Carter M., Cordova F. A., Cropper M. S., Fordham J., Huckle H., Ho C., Kawakami H., Kennea J., Kennedy T., Mittaz J., Pandel D., Priedhorsky W. C., Sasseen T., Shirey R., Smith P., Vreux J., 2001, *A&A*, 365, L36
- Mathys G., 1991, *A&AS*, 89, 121
- Merín B., Montesinos B., Eiroa C., Solano E., Mora A., 2004, *A&A*, 419, 301
- Michaud G., 1970, *ApJ*, 160, 641
- Michaud G., Charland Y., Megessier C., 1981, *A&A*, 103, 244
- Miroshnichenko A., Ivezić Ž., Vinković D., Elitzur M., 1999b, *ApJL*, 520, L115
- Miroshnichenko A. S., Bjorkman K. S., Chentsov E. L., Klochkova V. G., Gray R. O., García-Lario P., Perea Calderón J. V., 2001, *A&A*, 377, 854
- Miroshnichenko A. S., Gray R. O., Klochkova V. G., Bjorkman K. S., Kuratov K. S., 2004, *A&A*, 427, 937

- Miroshnichenko A. S., Gray R. O., Vieira S. L. A., Kuratov K. S., Bergner Y. K., 1999a, *A&A*, 347, 137
- Montesinos B., Eiroa C., Mora A., Merín B., 2009, *A&A*, 495, 901
- Mora A., Eiroa C., Natta A., Grady C. A., de Winter D., Davies J. K. e. a., 2004, *A&A*, 419, 225
- Mora A., Merín B., Solano E., Montesinos B., de Winter D. e. a., 2001, *A&A*, 378, 116
- Mora A., Natta A., Eiroa C., Grady C. A., de Winter D., Davies J. K., Ferlet R., Harris A. W., 2002, *A&A*, 393, 259
- Morel P., 1997, *A&AS*, 124, 597
- Müller A., van den Ancker M. E., Launhardt R., Pott J. U., Fedele D., Henning T., 2011, *A&A*, 530, A85
- Murdin P., Penston M. V., 1977, *MNRAS*, 181, 657
- Natta A., Grinin V. P., Mannings V., Ungerechts H., 1997, *ApJ*, 491, 885
- Natta A., Grinin V. P., Tambovtseva L. V., 2000, *ApJ*, 542, 421
- Neiner C., Alecian E., Briquet M., Floquet M., Frémat Y., Martayan C., Thizy O., Mimes Collaboration 2012, *A&A*, 537, A148
- Nesterov V. V., Kuzmin A. V., Ashimbaeva N. T., Volchkov A. A., Röser S., Bastian U., 1995, *A&AS*, 110, 367
- Norberg P., Maeder A., 2000, *A&A*, 359, 1025
- Oliver R. J., Masheder M. R. W., Thaddeus P., 1996, *A&A*, 315, 578
- Oudmaijer R. D., Palacios J., Eiroa C., Davies J. K., de Winter D. e. a., 2001, *A&A*, 379, 564
- Oudmaijer R. D., van der Veen W. E. C. J., Waters L. B. F. M., Trams N. R., Waelkens C., Engelsman E., 1992, *A&AS*, 96, 625
- Palla F., Stahler S. W., 1990, *ApJL*, 360, L47
- Palla F., Stahler S. W., 1991, *ApJ*, 375, 288
- Palla F., Stahler S. W., 1992, *ApJ*, 392, 667
- Palla F., Stahler S. W., 1993, *ApJ*, 418, 414
- Paunzen E., Duffee B., Heiter U., Kuschnig R., Weiss W. W., 2001, *A&A*, 373, 625
- Pérez M. R., Imhoff C. L., Thé P. S., 1991, in *Bulletin of the American Astronomical Society Vol. 23 of Bulletin of the American Astronomical Society, The Unusual 2800 Mg II Profiles of Bright Herbig Ae/Be Stars*. pp 1374+
- Perryman M. A. C., ESA eds, 1997, *The HIPPARCOS and TYCHO catalogues Vol. 1200 of ESA-SP*
- Petit V., Wade G. A., Drissen L., Montmerle T., Alecian E., 2008, *MNRAS*, 387, L23
- Piskunov N. E., 1992, in *Stellar Magnetism SYNTH - a code for rapid spectral synthesis*. pp 92+
- Pontoppidan K. M., Dullemond C. P., Blake G. A., Boogert A. C. A., van Dishoeck E. F., Evans II N. J., Kessler-Silacci J., Lahuis F., 2007, *ApJ*, 656, 980
- Praderie F., Catala C., Simon T., Boesgaard A. M., 1986, *ApJ*, 303, 311
- Preibisch T., Kraus S., Driebe T., van Boekel R., Weigelt G., 2006, *A&A*, 458, 235
- Preibisch T., Mamajek E., 2008, *The Nearest OB Association : Scorpius-Centaurus (Sco OB2)*. p. 235
- Press W. H., Teukolsky S. A., Vetterling W. T., Flannery B. P., 1992, *Numerical recipes in C. The art of scientific computing*
- Prosser C. F., 1992, *AJ*, 103, 488
- Prusti T., Natta A., Palla F., 1994, *A&A*, 292, 593
- Pugach A. F., Kovalchuk G. U., 1986, *Astronomische Nachrichten*, 307, 13
- Reid M. J., Menten K. M., Zheng X. W., Brunthaler A., Moscadelli L., Xu Y., Zhang B., Sato M., Honma M., Hirota T., Hachisuka K., Choi Y. K., Moellenbrock G. A., Bartkiewicz A., 2009, *ApJ*, 700, 137
- Rostopchina A. N., Grinin V. P., Shakhovskoi D. N., Thé P. S., Minikulov N. K., 2000, *Astronomy Reports*, 44, 365
- Royer F., Zorec J., Gómez A. E., 2007, *A&A*, 463, 671
- Saffe C., Gómez M., Pintado O., González E., 2008, *A&A*, 490, 297
- Sahu M. S., Blades J. C., He L., Hartmann D., Barlow M. J., Crawford I. A., 1998, *ApJ*, 504, 522
- Sandqvist A., Lindroos K. P., 1976, *A&A*, 53, 179
- Sartori M. J., Gregorio-Hetem J., Rodrigues C. V., Hetem A., Batalha C., 2010, *AJ*, 139, 27
- Sartori M. J., Lépine J. R. D., Dias W. S., 2003, *A&A*, 404, 913
- Semel M., 1989, *A&A*, 225, 456
- Semel M., Donati J.-F., Rees D. E., 1993, *A&A*, 278, 231
- Shakhovskoi D. N., Rostopchina A. N., Grinin V. P., Minikulov N. K., 2003, *Astronomy Reports*, 47, 301
- Shevchenko V. S., Ezhkova O. V., Ibrahimov M. A., van den Ancker M. E., Tjin A Djie H. R. E., 1999, *MNRAS*, 310, 210
- Shevchenko V. S., Ibragimov M. A., Chenysheva T. L., 1991, *Soviet Astronomy*, 35, 229
- Shevchenko V. S., Yakubov S. D., 1989, *Soviet Astronomy*, 33, 370
- Shorlin S. L. S., Wade G. A., Donati J.-F., Landstreet J. D., Petit P., Sigut T. A. A., Strasser S., 2002, *A&A*, 392, 637
- Shultz M., Wade G. A., Grunhut J. H., Bagnulo S., Landstreet J. D., Neiner C., Alecian E., Hanes D., the MiMeS Collaboration 2011, *ApJ*, submitted
- Silvester J., Neiner C., Henrichs H. F., Wade G. A., Petit V., Alecian E., Huat A.-L., Martayan C., Power J., Thizy O., 2009, *MNRAS*, 398, 1505
- Stepień K., 2000, *A&A*, 353, 227
- Straižys V., Černis K., Bartašiūte S., 1996, *Baltic Astronomy*, 5, 125
- Sylvester R. J., Skinner C. J., Barlow M. J., Mannings V., 1996, *MNRAS*, 279, 915
- Testa P., Huenemoerder D. P., Schulz N. S., Ishibashi K., 2008, *ApJ*, 687, 579
- Thé P. S., Cuypers H., Tjin A Djie H. R. E., Felenbok P., 1985a, *A&A*, 149, 429
- The P. S., de Winter D., Perez M. R., 1994, *A&AS*, 104, 315
- The P. S., Tjin A Djie H. R. E., Catala C., Praderie F., Felenbok P., 1985b, *The Messenger*, 41, 8
- Tian K. P., van Leeuwen F., Zhao J. L., Su C. G., 1996, *A&AS*, 118, 503
- Tjin A Djie H. R. E., The P. S., Andersen J., Nordstrom B., Finkenzeller U., Jankovics I., 1989, *A&AS*, 78, 1
- van den Ancker M. E., de Winter D., Tjin A Djie H. R. E., 1998, *A&A*, 330, 145
- van den Ancker M. E., The P. S., de Winter D., 1996, *A&A*, 309, 809
- van den Ancker M. E., The P. S., Tjin A Djie H. R. E., Catala C., de Winter D., Blondel P. F. C., Waters L. B. F. M., 1997, *A&A*, 324, L33
- van den Bergh S., 1966a, *AJ*, 71, 990
- van den Bergh S., 1966b, *AJ*, 71, 990
- van der Plas G., van den Ancker M. E., Fedele D., Acke B., Dominik C., Waters L. B. F. M., Bouwman J., 2008, *A&A*, 485, 487
- van Leeuwen F., 2007, *A&A*, 474, 653
- Vieira S. L. A., Corradi W. J. B., Alencar S. H. P., Mendes L. T. S., Torres C. A. O., Quast G. R., Guimarães M. M., da Silva L., 2003, *AJ*, 126, 2971

- Wade G. A., Bagnulo S., Drouin D., Landstreet J. D., Monin D., 2007, *MNRAS*, 376, 1145
- Wade G. A., Donati J.-F., Landstreet J. D., Shorlin S. L. S., 2000, *MNRAS*, 313, 851
- Wade G. A., Drouin D., Bagnulo S., Landstreet J. D., Mason E., Silvester J., Alecian E., Böhm T., Bouret J.-C., Catala C., Donati J.-F., 2005, *A&A*, 442, L31
- Wahhaj Z., Koerner D. W., Sargent A. I., 2007, *ApJ*, 661, 368
- Walker M. F., 1959, *ApJ*, 130, 57
- Wang S., Looney L. W., Brandner W., Close L. M., 2008, *ApJ*, 673, 315
- Warren Jr. W. H., Hesser J. E., 1977, *ApJS*, 34, 115
- Warren Jr. W. H., Hesser J. E., 1978, *ApJS*, 36, 497
- Weinberger A. J., Becklin E. E., Schneider G., Smith B. A., Lovrance P. J., Silverstone M. D., Zuckerman B., Terriile R. J., 1999, *ApJL*, 525, L53
- Weinberger A. J., Rich R. M., Becklin E. E., Zuckerman B., Matthews K., 2000, *ApJ*, 544, 937
- Wheelwright H. E., Oudmaijer R. D., Goodwin S. P., 2010, *MNRAS*, 401, 1199
- Wolff S. C., Strom S. E., Hillenbrand L. A., 2004, *ApJ*, 601, 979
- Wood D. O. S., Myers P. C., Daugherty D. A., 1994, *ApJS*, 95, 457

APPENDIX A: ANALYSIS OF INDIVIDUAL STARS

This appendix describes the approach that has been followed in order to determine the $v \sin i$ of all the stars of our sample, and the fundamental parameters (luminosity, effective temperature and surface gravity) required to estimate the masses and ages of the stars, that will be used in the statistical analysis described in paper II. The basic procedure we have followed has been to first check that the effective temperature found in the literature corresponds to our data, and modify it if necessary. Then we have computed the LSD profiles for most of the data, using masks of appropriate temperature and gravity for each star, and fit them (see Section 5). Sometimes it was necessary to add one or more Gaussian functions to the photospheric rotational velocity broadening function in order to obtain a better fit, and hence a more accurate value of the $v \sin i$. This paper does not aim to propose a physical origin of these Gaussian functions. Most of them are assumed to have a circumstellar (CS) origin. However, a more detailed analysis of the non-photospheric spectral features observed in the spectra (and in the LSD profiles) of our sample will be presented in a forthcoming paper. This appendix summarises only the information required to fully understand the method that we applied to determine the $v \sin i$ of the stars.

For each of the stars we compared the observed normalised spectra with a grid of synthetic spectra, in order to check the published values and estimate new ones if required. As described above, these spectra assume solar chemical composition. In most cases the effective temperature could be estimated from this comparison, but not the surface gravity, due to imperfect continuum normalisation of individual echelle orders and/or circumstellar contamination. Therefore, unless specified, we used by default a surface gravity $\log g = 4.0$ (cgs) (see Sc. 4.1). In order to better understand the shape of the LSD profiles and the choice of the adopted mask, a description of the non-photospheric features has been added for each star. In these descriptions, the Balmer profiles emission types that are sometimes mentioned have been classified according to the system of Beals (1953).

For each one of the stars, a short discussion has also been added to support their PMS nature, and therefore to justify their membership to our sample. The references of the photometric data and the distances used to derive the luminosity are also detailed. In the cases of stars members of the Orion OB 1 association, the distance adopted is the weighted mean of the distances of the six sub-groups described by Brown et al. (1994).

Finally, apart from LP Ori, for which we obtained more data since its magnetic detection reported in Petit et al. (2008), this appendix concerns only the stars that have not been detected as magnetic. For the magnetic stars we refer the reader to the following papers : Catala et al. (2007); Alecian et al. (2008a); Folsom et al. (2008); Alecian et al. (2009b), Alecian et al. in prep.

A1 BD-06 1259 (= BF Ori)

BF Ori is a member of the subgroup c of the Ori OB 1 association (Warren & Hesser 1978), at a distance of 375 pc (Brown et al. 1994). It belongs to the UXOR sub-class of HAeBe objects (UXOR stars, hereinafter, Mora et al. 2004), whose the prototype is UX Ori (see Sec. A61). These stars are strong photometric variables. For the same reasons as for UX Ori, we used the Hipparcos photometric data (Perryman & ESA 1997) at maximum brightness ($V_T = 7.81$ mag, $B_T = 7.85$ mag, in the Tycho system), and converted them to the Johnson system (see the method in Sec. A61). We find $V = 7.85$ mag and $(B - V) = -0.028$ mag, values that have been adopted to derive the luminosity of the star. BF Ori displays strong near-IR excess, very likely due to the presence of an optically thick circumstellar accretion disk (Hillenbrand et al. 1992).

The spectrum of BF Ori is very complex, highly variable, and similar to other UXOR stars. In the February 2005 spectrum, we can distinguish two classes of spectral lines among the metals. The first class consists of strong and broad CS absorption features at the positions of the predicted strong photospheric lines. These lines are still observed in the March 2009 spectrum, with different shapes and increased depth. The second class of lines concerns the predicted weak lines of the spectrum, which show a photospheric component on which is superimposed a narrower circumstellar absorption. In our 2009 spectrum these lines show only photospheric components. As with other UXOR stars, these transient absorption features are assumed to come from gaseous clouds in the disk of the star (see Sec. A61).

The Balmer lines from $H\delta$ to $H\beta$ show strong absorption components superimposed on the cores of the photospheric lines, with weak emission in the wings of the absorption component. The amplitudes of these features increase with wavelength, and their shape has changed between our two observations. $H\alpha$ is in emission with a double-peaked profile of type VI and a strong central absorption that goes below the continuum. The amplitude of the emission doubled between 2005 and 2009. The Ca II K line, the He I lines at 5875 Å, 6678 Å, and 7065 Å, and the OI 7775 Å and O I 8446 Å triplets display very strong (stronger than predicted) absorption profiles. The three IR Ca II lines at 8498 Å, 8542 Å, and 8662 Å (hereinafter the Ca II IR triplet) show strong and broad emission profiles superimposed on the three photospheric absorption lines. The Paschen lines seem also to be slightly contaminated with circumstellar emission.

The wings of the Balmer lines are consistent with the temperature and surface gravity determination of Mora et al. (2004, $T_{\text{eff}} = 8750 \pm 250$ K, $\log g = 4.0 \pm 0.5$). We have cleaned the Kurucz mask by rejecting as many contaminated lines as possible. The resulting LSD profile for 2009 shows only a photospheric component.

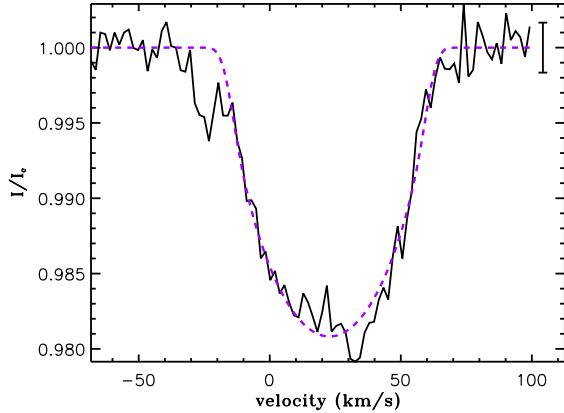


Figure A1. The LSD I profile of the March 2009 observation of BD-06 1259 = BF Ori (black full line), superimposed with its best fit (purple dashed-line).

However the 2005 profile still shows a photospheric line with a superimposed circumstellar absorption component. We first tried to fit both observations simultaneously using the following model : a photospheric profile + a Gaussian function in absorption for the 2005 profile, and only a photospheric profile for the 2009 observation. However, we found that fitting the 2009 profile only resulted in a more accurate value of $v \sin i$. We therefore adopted this value. The resulting fit is shown in Fig. A1.

A2 BD-05 1329 (= T Ori)

T Ori is part of the Ori OB1d cluster situated at a distance of 375 pc from the Sun (Brown et al. 1994). We used the photometric data of Herbst & Shevchenko (1999) to derive the luminosity of the star. T Ori displays a near-IR excess that could be attributed to an accretion disk (Hillenbrand et al. 1998).

The spectrum of T Ori is consistent with the temperature and surface gravity determination of Folsom et al. (2012, $T_{\text{eff}} = 8500 \pm 300$ K, $\log g = 4.2 \pm 0.3$). The spectrum shows strong circumstellar features : the Ca II K line and the O I 777 nm triplet display redshifted absorption. From H η to H γ a redshifted absorption is superimposed on the core of the line. A similar, but deeper, absorption is present in the core of H β , as well as emission in the blue wing of the CS absorption component. H α displays a double-peaked emission profile with a redshifted absorption component that goes below the continuum. The He I lines at 5875 Å, 6678 Å, and 7065 Å, and the O I 8446 Å triplet show inverse P Cygni profiles. Faint emission is observed in the cores of the Paschen lines. The Ca II K and metallic lines, as well as the Ca II IR-triplet, do not display any CS features.

We have cleaned the Kurucz mask in order to reject all the lines contaminated with circumstellar or interstellar features. The resulting LSD I profile displays a photospheric shape slightly contaminated with CS emission. We first tried to fit the profile with a photospheric function and two emission Gaussian function. Then we fit the profile by rejecting, into the fitting procedure, the data points of the profile contaminated with emission. The last option gives a more accurate $v \sin i$ value. The result is shown in Fig. A2.

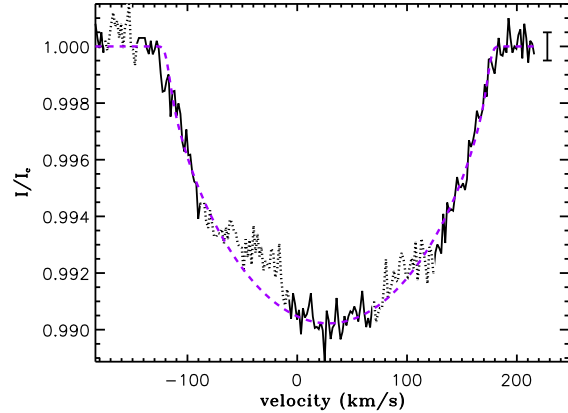


Figure A2. As Fig. A1 for BD-05 1329 (= T Ori). The dotted part of the observed profile has not been included in the fitting procedure.

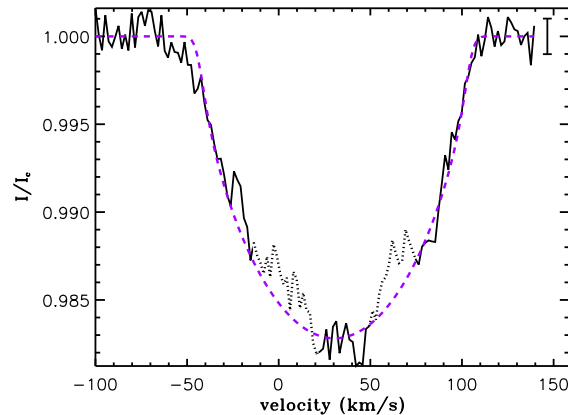


Figure A3. As Fig. A2 for BD-05 1324 (= NV Ori).

A3 BD-05 1324 (= NV Ori)

NV Ori is part of the Ori OB 1 association (Warren & Hesser 1977), situated at a distance of 375 pc from the Sun (Brown et al. 1994). We used the photometric data (V and $(B - V)$) from Herbst & Shevchenko (1999), to compute the luminosity of the star. It does not seem to display infrared (IR) excess, but emission lines in its spectrum, as well as its membership to the Ori OB 1 star forming region, are good indications that the star is very young.

The spectrum of NV Ori is consistent with a $T_{\text{eff}} = 6350 \pm 250$ K, corresponding to the spectral type determination of Mora et al. (2001). It shows circumstellar emission in the core of H β , H γ , and H δ . H α displays a strong and complex emission profile, while the O I 777 nm and Ca II IR triplets show strong absorptions with emissions in the blue wings. The O I 8446 Å absorption profile is stronger than predicted, while the He I D3 line (at 5875 Å) displays a broad absorption profile. The Ca II K, metallic and Paschen lines do not display any special features.

The LSD I profile shows a photospheric shape with broad wings, as well as a narrow and deep blueshifted CS absorption component. In order to improve the profile, we have calculated new masks by varying the cut-off of the intrinsic depths (d_i) or excitation potential (χ_{exc}) of the lines. The best profile that we found has been computed with a mask containing only lines with $\chi_{\text{exc}} > 5$ eV. The

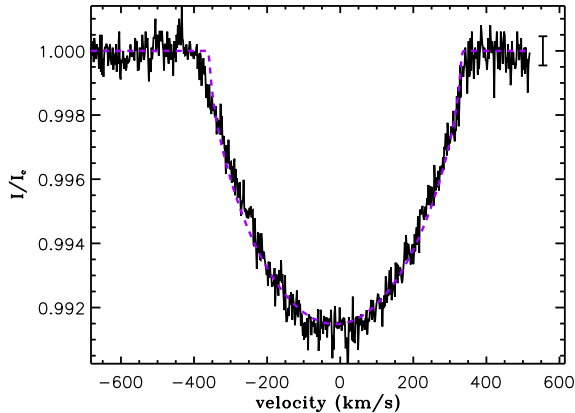


Figure A4. As Fig. A2 for the August 2005 observation of BD+41 3731.

resulting I profile is slightly distorted in the core, which might be due to circumstellar emission. We therefore excluded the contaminated data points from the fit, and fit the profile with a photospheric function. The result is shown in Fig. A3.

A4 BD+41 3731

BD+41 3731 is associated with the star forming region 2 Cyg and the young cluster NGC 6910 at a distance of 980 pc (Shevchenko et al. 1991). We used the photometric data from the Hipparcos catalogue (Perryman & ESA 1997) to compute the luminosity. This star does not seem to display a strong IR excess, and shows a spectral energy distribution similar to classical Be stars. However, its association with a star forming region, as well as to a young cluster, suggests that it is a young intermediate mass star lacking an accretion disk (Hillenbrand et al. 1992).

The most recent spectroscopic determination of the effective temperature and $v \sin i$ is found in Finkenzeller (1985). He assigns a spectral type of B2 (i.e. $T_{\text{eff}} \sim 22000$ K), and $v \sin i \sim 300 \text{ km.s}^{-1}$. Our spectra are very well fit with a non-LTE TLUSTY synthetic spectrum of $T_{\text{eff}} = 17000 \pm 1000$ K and a $v \sin i \sim 345 \text{ km.s}^{-1}$. The difference in temperature might be due to non-LTE effects that have been taken into account in our analysis. Faint circumstellar emission is visible in the cores of the O I 777 nm and Ca II IR triplets. The S II lines (S II 5201 Å, S II 5212 Å, S II 5346 Å, and S II 5429 Å) are very weak compared to synthetic lines computed using solar abundance. They might be filled with circumstellar emission, or an indication that our adopted T_{eff} is too high. No other circumstellar features are observed in the spectrum. Many diffuse interstellar bands (DIB) are present and can be identified with the 1997 version⁴ of the DIB catalogue (Jenniskens & Desert 1994).

The Kurucz mask has been cleaned by keeping lines with excitation potential greater than 1 eV, by rejecting lines contaminated with circumstellar emission, and by keeping only parts of the spectrum with high SNR and not contaminated with telluric lines. Two observations were obtained, one with ESPaDOnS in August 2005, and one with Narval in November 2007. We tried to fit both profiles separately and simultaneously, with a photospheric profile for each one of the observations. Because of its relatively low SNR

(see Table 1), the Nov. 2007 observation does not improve the precision of the fitted parameters when both profiles are fitted simultaneously. Therefore the $v \sin i$ and v_{rad} values have been obtained from the fit of the Aug. 2005 profile only (Fig. A4).

A5 BD+46 3471

BD+46 3471 is associated with the young cluster IC 5146 (Walker 1959) situated at a distance of 950 pc (Harvey et al. 2008). The luminosity has been obtained using this distance and the Hipparcos photometric data (Perryman & ESA 1997). Hillenbrand et al. (1992) reports strong near-IR excess suggesting the presence of an optically thick circumstellar accretion disk.

The spectrum of BD+46 3471 is strongly contaminated with circumstellar absorption and emission lines. A blueshifted absorption and a redshifted emission are superimposed on the core of the Balmer lines from H ζ to H β , while H α displays a single-peaked emission line of type III with a weak absorption in the blue wing. Many metallic lines show narrow emission in the cores of their photospheric profiles. The O I 8446 Å and Ca II IR triplets show strong and redshifted single-peaked emission profiles. Narrow emission is detected in the cores of the Paschen lines. The Ca II K line has the central emission peak of other metal lines superimposed on the photospheric line, with a narrow, probably interstellar, absorption in the centre of the emission. The He I D3 line and the O I 777 nm triplet display very strong absorption profiles, stronger than predicted, but the weaker O I lines at 615 nm have about the correct strength for solar O abundance. The few lines not contaminated with CS features are consistent with the temperature determination of Hernández et al. (2004, $T_{\text{eff}} = 9500 \pm 1000$ K).

We tried many variations of the Kurucz mask, by doing a selection on the excitation potential and the central depth of the lines. We varied the lower value of χ_{exc} between 0.5 and 10 eV, and the maximum value of the central depth between 0.5 and 0.15. In each cases the LSD profiles have the same shape and are still contaminated with emission. We therefore conclude that emission is present in all the lines of the spectrum, and we adopted a mask that has been calculated by rejecting by hand the lines visibly strongly contaminated with emission. The result gives a profile that is not strongly contaminated with emission, but that still contains few emission features. We fit the profile using a photospheric and three Gaussian functions, which reproduces perfectly the LSD I profile. The resulting fit is plotted in Fig. A5.

A6 BD+61 154 (= V594 Cas)

BD+61 154 is often associated with the cluster NGC 225, because its position in the sky coincides with the centre of the cluster. However Kharchenko et al. (2004) determined the membership probability from the proper motions and the photometry of the star, and find both values below 3%, leading to the conclusion that this star is not member of NGC 225 and may be isolated. The Hipparcos parallax (van Leeuwen 2007) and photometric data (Perryman & ESA 1997) have therefore been used to determine the luminosity. BD+61 154 possesses strong near-IR excess that has been attributed by Hillenbrand et al. (1992) to a circumstellar accretion disk.

The spectrum of BD+61 154 is strongly contaminated with circumstellar emission leaving only very few CS-free photospheric lines in the spectrum. The Ca II K line shows a double-peaked emission profile. From H η to H ϵ , narrow emission is superimposed with

⁴ <http://leonid.arc.nasa.gov/DIBcatalog.html>

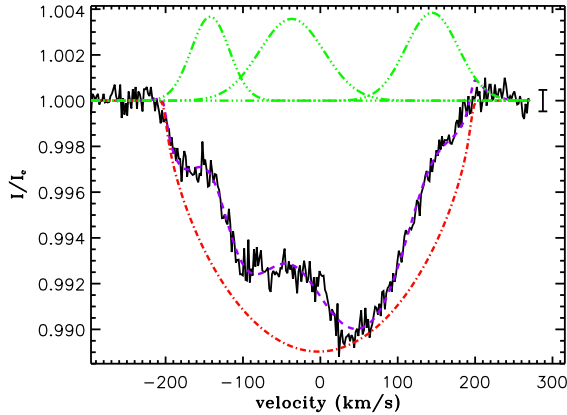


Figure A5. As Fig. A2 for BD+46 3471. The photospheric and Gaussian parts of the best fit are represented in dot-dashed and dot-dot-dot-dashed lines, respectively.

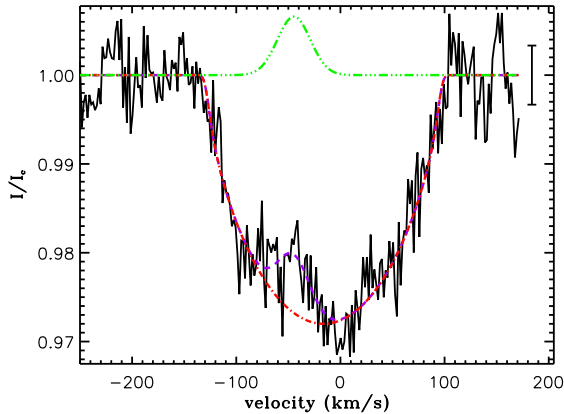


Figure A6. As Fig. A5 for the August 2005 observation of BD+61 154 (= V594 Cas).

the core of the photospheric profile, while P Cygni profiles of type II are observed from $H\delta$ to $H\beta$. $H\alpha$ displays a P Cygni profile of type III. The $O\text{ I } 777\text{ nm}$, $O\text{ I } 8446\text{ \AA}$ and Ca II IR triplets, as well as the Paschen lines, show single-peaked emission profiles. The He I lines at 5875 \AA , 6678 \AA and 7065 \AA display broad and asymmetric emission profiles, but $\text{He I } 4471$ and 4713 appear in absorption with about the normal strength for the photospheric temperature. Finally, many metallic lines show single-peaked emission profiles with a P Cygni blueshifted absorption component in the strongest emission lines, but a few high-excitation lines such as the Si II lines at 5040 and 5056 \AA have nearly photospheric profiles.

By comparing the wings of the $H\gamma$, $H\delta$, and $H\epsilon$ ($H\alpha$ and $H\beta$ are too strongly contaminated with CS features) with synthetic spectra, we find an effective temperature of $T_{\text{eff}} = 13000 \pm 500\text{ K}$, slightly larger than the temperature reported in Alonso-Albi et al. (2009).

We have cleaned the mask in order to reduce as much as possible the contribution of emission. The result gives a photospheric, but noisy profile with only a very faint residual emission. We fit the profile of August 2005 with a rotation function for the photospheric part, and a Gaussian function modeling the emission.

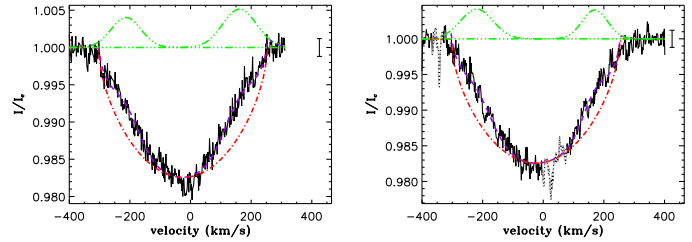


Figure A7. As Fig. A5 for the June 2006 (left) and September 2009 (right) observations of BD+65 1637 (= V361 Cep).

We find $v \sin i = 112 \pm 24\text{ km.s}^{-1}$. The LSD profile of February 2005 is much noisier than the later one. Fitting this profile gives a $v \sin i$ consistent with our previous determination, but with extremely large error bars, which do not improve the precision of $v \sin i$. We therefore did not include it in this determination. The result of the fit of the Aug. 2005 profile is plotted in Fig. A6.

A7 BD+65 1637 (= V361 Cep)

BD+65 1637 is associated with the reflection nebula NGC 7129 that envelops a young and compact cluster (Aveni & Hunter 1972). The luminosity has been estimated from the Hipparcos photometric data (Perryman & ESA 1997) and the photometric determination of the distance of NGC 7129 by Shevchenko & Yakubov (1989). It displays faint near-IR excess similar to classical Be stars (Hillenbrand et al. 1992). However its association with a reflection nebula and a young cluster suggests that the star is very young, and might be at the end of its PMS phase.

The spectrum of BD+65 1637 fits well with a non-LTE TLUSTY spectrum of $T_{\text{eff}} = 18000 \pm 1000\text{ K}$, slightly larger than the determination of Hernandez et al. (2004), but consistent with the work of Finkenzeller (1985). Many iron lines appear in emission with two peaks of different amplitude, the red one being higher than the blue one. These iron emission lines contaminate some helium lines. The other strongest He lines show a V-shape that could be the result of circumstellar contamination. The cores of the Balmer lines from $H\zeta$ to $H\beta$ show double-peaked emission lines, and $H\alpha$ is in emission with a double-peaked profile, all with a red peak higher than the blue one. The Ca II IR , $O\text{ I } 777\text{ nm}$, and $O\text{ I } 8446\text{ \AA}$ triplets, as well as the Paschen lines, also display strong double-peaked emission profiles.

We have cleaned the mask to avoid as much as possible lines contaminated with emission. The inferred LSD I profiles of both observations are in absorption, but have V-shapes, consistent with the lines of the spectrum. Taking into account the shapes of the emission features observed in the spectrum, the best and most reliable fit of the LSD I profiles has been obtained with a photospheric plus two Gaussian functions. We performed a simultaneous fit of both profiles, by forcing the photospheric depth, $v \sin i$, and v_{rad} to be the same for both observations. The result is shown in Fig. A7.

A8 BD+72 1031 (= SV Cep)

SV Cep is associated with L1235, one of the dark clouds of the Cepheus region situated at a distance of 400 pc (Kun 1998). SV Cep is an UXOR star, and displays strong IR excess, both suggesting that a circumstellar accretion disk is present around

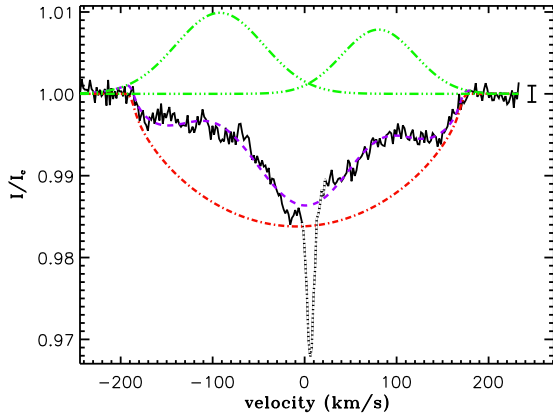


Figure A8. As Fig. A5 for the June 2006 observation of BD+72 1031 (= SV Cep).

this star (Friedemann et al. 1992; Acke & van den Ancker 2004; Juhász et al. 2007). No Hipparcos data are available for this star, however Rostopchina et al. (2000) obtained UBVR photopolarimetric observations of the star. We used these data at the brightest magnitude ($V = 10.48$, $(B - V) = 0.344$) to derive the luminosity.

Like other UXOR stars, SV Cep shows many redshifted or blueshifted transient absorption features in its spectrum that changed in shape and depth from June 2006 to November 2007. From $H\delta$ to $H\beta$ a strong circumstellar absorption is superimposed with the core of the Balmer lines, and in $H\beta$, emission appears in the wings of the CS absorption. The 2007 absorption components are redshifted relative to 2006. $H\alpha$ shows a strong double-peaked emission profile with both red and blue peaks of equal amplitude in 2006, while in 2007 the blue peak is stronger than the red one, and the central absorption is broader, deeper, and redshifted. Strong CS absorptions are also observed in the Ca II IR- and OI 8446 Å triplets, and in the Ca II K line, as well as in many metallic lines. While these absorption features have only a single component in 2006, in 2007 they display two separate components, both redshifted compared to 2006. The He I lines at 5875 Å, 6678 Å, and 7065 Å lines, and the O I 777 nm triplet display inverse P-Cygni profiles, with the absorption component being redshifted from 2006 to 2007. While the Paschen lines do not seem to be contaminated with CS features in 2006, in 2007 they display single and small emission components in the cores. The portions of the spectrum not contaminated with CS absorption is consistent with the temperature determination of Hernández et al. (2004, $T_{\text{eff}} = 9500 \pm 2000$ K).

We tried to clean the Kurucz mask by rejecting the lines obviously contaminated with CS features. However the resulting profiles still display CS features superimposed with the photospheric profile, and could not be improved. We fitted the Jun. 2006 profile with a photospheric profile and two Gaussians modeling the emission, and by rejecting CS absorption in the core. We also fit the Nov. 2007 profile, but because of its lower SNR, the values of the fitted parameters, while consistent with the first fit, have larger error bars, and don't better constrain the model. Therefore we adopted the $v \sin i$ and v_{rad} from the fit of Jun. 2006 only (Fig. A8).

A9 HD 9672 (= 49 Cet)

49 Cet is a β Pictoris-type star having infrared excess emission attributed to circumstellar dust, but being distinguished from a

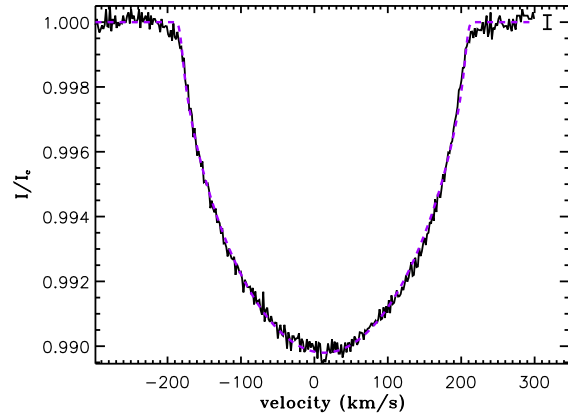


Figure A9. As Fig. A5 for HD 9672 (= 49 Cet)

Vega-type star by a much higher IR to bolometric luminosity ratio (Jura et al. 1998). Such a star would represent a transitional object between Herbig Ae and Vega-like stars (Wahhaj et al. 2007), as is confirmed by the detection of molecular gas in its close environment (Hughes et al. 2008). While this star cannot totally be considered to be a Herbig Ae star, we kept it in our sample because it represents an interesting and rare stellar evolutionary phase between star birth and the MS.

49 Cet is the closest star of our sample, with a distance of 61 pc (Hipparcos, van Leeuwen 2007). Combining both the Hipparcos distance and photometric data we derive a luminosity $\log(L/L_{\odot}) = 1.32$.

With our automatic procedure (see Section 4.1) we find an effective temperature of 8900 ± 200 K and $\log g = 4.5$, consistent with the work of Montesinos et al. (2009). It does not show any circumstellar features, therefore no special cleaning has been applied to the Kurucz mask. The LSD Stokes I profile shows a clean photospheric profile, well reproduced using a photospheric function. The result of the fit is plotted in Fig. A9.

A10 HD 17081 (= π Cet)

HD 17081 does not seem to be associated with a nebula or a star forming region. Based on its IR excess, Malfait et al. (1998) has classified HD 17081 as a Vega-type star, occupying an evolutionary stage subsequent to the Herbig Ae/Be stars, but still very young, and therefore constituting an interesting object to explore in the framework of our study of rotational evolution during the PMS phase. The Hipparcos parallax (van Leeuwen 2007) and photometric data (Perryman & ESA 1997) have been taken for the luminosity determination.

The spectrum of HD 17081 is consistent with the effective temperature and $\log g$ determination of Fossati et al. (2009, 12800 ± 200 K, $\log g = 3.77 \pm 0.15$). No emission is clearly observed, however, the shapes of the line profiles are distorted, possibly due to circumstellar emission or absorption, or possibly to abundance patches at the surface of the star as proposed by Fossati et al. (2009). The presence of abundance anomalies of a few elements detected in the spectrum (Fossati et al. 2009) would support the second explanation.

The LSD profiles have been calculated with the Kurucz mask and have both been modeled simultaneously with a photospheric profile only. We tried with various techniques to model the distort-

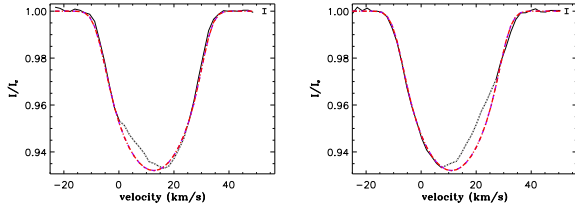


Figure A10. As Fig. A5 for the Feb. 20th (left) and Feb. 21st (right) 2005 observations of HD 17081.

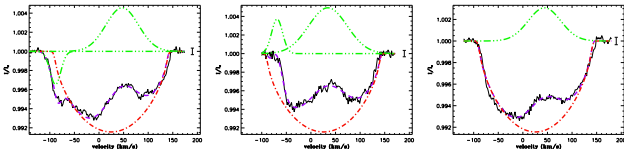


Figure A11. As Fig. A5 for the Nov. 2004 (left), Feb. 20th (middle) and Feb. 22nd (right) 2005 observations of HD 31293 (= AB Aur).

tion of the profiles but we could not find a solution giving consistent photospheric depths and $v \sin i$ for both observations, as well as a better constrained value of $v \sin i$. We therefore choose to ignore the distorted points into the fitting procedure. In this fit, the depth and the $v \sin i$ of the photospheric profiles have been forced to be the same for both observations. We also tried to force the v_{rad} to be the same, but the fit was significantly less good, meaning that the radial velocity has slightly but significantly changed from the 19th ($12.7 \pm 0.8 \text{ km.s}^{-1}$) to the 20th ($11.0 \pm 0.7 \text{ km.s}^{-1}$) February 2005. The result of the fit is shown in Fig. A10.

A11 HD 31293 (= AB Aur)

AB Aur, situated in the Taurus region at a distance of 139 pc (Hipparcos, van Leeuwen 2007), is associated with the dark cloud Lynds 1517, and is clearly surrounded with a bright nebula (van den Ancker et al. 1998). Hipparcos photometric data have been used for its luminosity determination. AB Aur displays near-IR excess interpreted as the presence of a circumstellar accretion disk surrounding the star (Hillenbrand et al. 1992; Malfait et al. 1998)

AB Aur is one of the best studied Herbig Ae stars with strong emission and variability in its spectrum. Rotational modulation has been detected by Praderie et al. (1986) and Catala et al. (1986b, 1993, 1999) in various UV and optical non-photospheric lines that are very likely formed in the wind. $H\alpha$ is strongly variable going from a double-peaked emission profile to a P Cygni of Type IV (Catala et al. 1999). In our 3 observations, $H\alpha$ displays a P Cygni profile. From $H\zeta$ to $H\gamma$ a blueshifted absorption as well as a roughly centered emission component are superimposed on the core of the Balmer lines, with increasing amplitudes with wavelength, for both absorption and emission components. A P Cygni profile of type IV is superimposed with the core of $H\beta$. Some Fe II lines, including those of multiplet 42, also show P Cygni profiles, but most weaker metal lines show largely photospheric profiles, and a few, such as the O I lines at 615 nm are completely photospheric. The Ca II K line is contaminated with emission, while the Ca II IR-, and O I 8446 Å triplets, and the Paschen lines display single-peaked emission profiles. The He I 5878 Å, He I 6678 Å, He I 7065 Å, and the O I 777 nm triplet show complex and variable emission profiles.

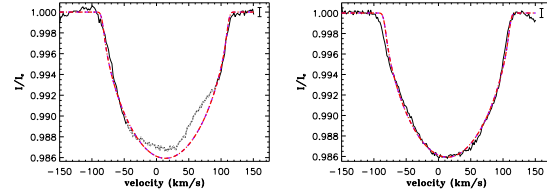


Figure A12. As Fig. A5 for the Feb. (left) and Aug. (right) 2005 observations of HD 31648.

The wings of the Balmer lines are consistent with the effective temperature and $\log g$ determination of Folsom et al. (2012, $T_{\text{eff}} = 9800 \pm 700 \text{ K}$, $\log g = 3.9 \pm 0.3$). Most of the metallic lines are shallower than predicted, suggesting that they are filled with emission. The Kurucz mask has been cleaned by keeping only lines showing similar shapes and being only slightly contaminated with CS emission. The three resulting profiles show a photospheric absorption line superimposed with a slightly redshifted and variable emission component, consistent with the photospheric profiles of the spectrum. The three profiles have been fitted simultaneously with a photospheric function and one or two Gaussians modeling the CS emission and absorption in the 2004 profile. In this fitting procedure the depth, $v \sin i$, and v_{rad} of the photospheric profiles have been forced to be the same for the three observations. The result is shown in Fig. A11.

A12 HD 31648 (= MWC 480)

HD 31648 lies in the star forming Taurus-Aurigae region at a distance of 137 pc (Hipparcos, van Leeuwen 2007). It does not show evidence of association with bright nebulae but high-resolution millimeter-wave images of continuum and molecular-line emission from dust and gas in its neighborhood revealed the presence of a proto-planetary disk (Mannings & Sargent 1997). The high IR excess due to warm dust in its close environment confirms the Herbig Ae/Be status of the star (Malfait et al. 1998). We used the Hipparcos photometric data to determine its luminosity.

In the spectrum of HD 31648, the cores of the Balmer lines from $H\zeta$ to $H\gamma$ are superimposed with a blueshifted circumstellar absorption component with amplitude increasing with wavelength. A similar but stronger absorption component is superimposed on the Ca II K line. $H\beta$ displays a strong blueshifted absorption component and a slightly redshifted emission in the core. $H\alpha$ has the shape of a type III P Cygni profile. Circumstellar emission and absorption are present in a few metallic lines, including the lines of multiplet 42 of Fe II. The He I lines at 5875 Å, 6678 Å, and 7065 Å lines display complex inverse P-Cygni profiles. The O I 777 nm triplet shows a strong (stronger than predicted), roughly centered, absorption profile with wing emissions, but the weaker O I lines at 615 nm are in absorption and well fit with a normal photospheric profile. The O I 8446 Å triplet shows a complex emission profile, and the Ca II IR-triplet displays single-peaked emission profiles, superimposed with a faint blueshifted absorption. The Paschen lines are filled with emission. Using our automatic procedure, we find that the portions of the spectrum that are free of CS features are well reproduced with $T_{\text{eff}} = 8200 \pm 300 \text{ K}$ and $\log g = 4.0$, consistent with the work of Vieira et al. (2003).

We have cleaned the Kurucz mask keeping only lines not contaminated with CS features. The resulting profiles are slightly

distorted, revealing some residual contamination by CS emission, but could not be improved. We fitted both profiles simultaneously with a photospheric function, by forcing the depth, $v \sin i$, and v_{rad} of the photospheric profile to be the same for both observations, and by rejecting the distorted data points in the core of the February 2005 observation. We also tried to include a few Gaussian functions for modelling the distorted data points, instead of rejecting them, but this did not improve the fit. The result is plotted in Fig. A12.

A13 HD 34282

Merín et al. (2004) carried out a thorough spectroscopic and photometric study of HD 34282 motivated by the fact that previous work placed the star below the ZAMS in the HR diagram. This star shows strong IR excess consistent with a circumstellar disk (van den Ancker et al. 1998), as well as PAH emission lines (Keller et al. 2008), confirming its PMS status, and meaning that this star should be situated well above the ZAMS. Their spectroscopic analysis led to an effective temperature and gravity of $T_{\text{eff}} = 8625 \pm 200$ K and $\log g = 4.20 \pm 0.20$ (cgs). They also derived a sub-solar metallicity of $\text{Fe}/\text{H} = -0.8 \pm 0.1$. The Balmer lines of our spectrum fits well with $T_{\text{eff}} = 8750$ K and $\log g = 4.0$ consistent with their work. However using a solar metallicity, all the metallic lines are clearly underabundant as observed by Merín et al. (2004).

Merín et al. (2004) compared the position of HD 34282 with PMS evolutionary tracks of sub-solar metallicity ($Z = 0.004$) in the $\log g - \log T_{\text{eff}}$ diagram, and derived the mass, age, luminosity and distance of the star that we adopted in this study.

In our data, the core of $\text{H}\alpha$ is contaminated with a double-peaked emission profile with a deep central absorption, while $\text{H}\beta$ and $\text{H}\gamma$ show a deep CS absorption centered in the core. Except for stronger absorption than predicted in the He I D3 line and the O I 777 nm triplet, no other CS manifestation is observed in the spectrum.

If we use a solar metallicity and an effective temperature of 10 000 K we are able to accurately reproduce the depth of the metallic lines of the spectrum. We therefore choose the Kurucz mask of effective temperature 10 000 K instead of a temperature closer to the one determined by Merín et al. (2004), simply to determine the rotation velocity. The result is a simple photospheric profile that has been fitted with a single photospheric function, and is shown in Fig. A13.

A14 HD 35187 B

HD 35187 is a binary system situated at a distance of 114 pc (Hipparcos, van Leeuwen 2007) in the Taurus Auriga star forming region with a separation of 1.39 arcsec (Perryman & ESA 1997). Hipparcos resolved the system and the Hipparcos Catalogue Double and Multiple Systems Annex (DMSA) assigned the identifier ‘B’ to the brighter component, i.e. to the more northerly component at the time of Hipparcos observations. We will follow the Hipparcos nomenclature in order to avoid confusion. Spatially resolved optical spectroscopy performed by Dunkin & Crawford (1998) revealed that HD 35187 B has a stronger $\text{H}\alpha$ emission than the HD 35187 A and displays a narrow circumstellar absorption line in the Ca II K line, that is absent in the spectrum of HD 35187 A. Dunkin & Crawford (1998) derived effective temperatures of 8990 K and 7800 K for the components B and A, respectively, and suggest that only HD 35187 B is surrounded with a

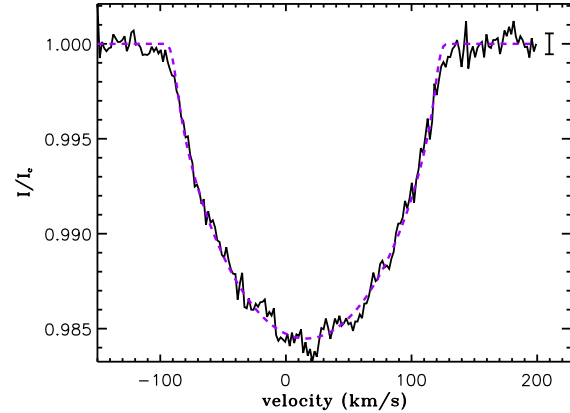


Figure A13. As Fig. A5 for HD 34282

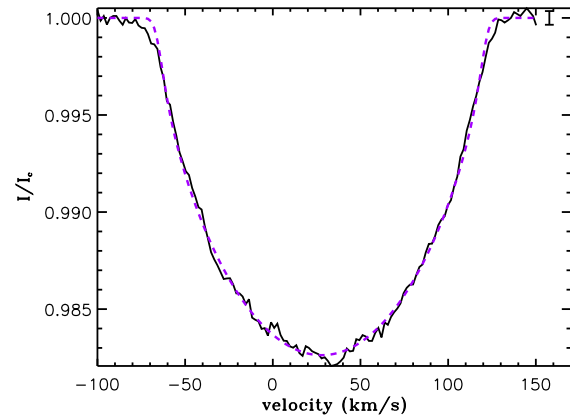


Figure A14. As Fig. A5 for HD 35187 B

circumstellar disk. The spectral energy distribution analysis reveals the presence of a geometrically-flat disk, but is not able to distinguish between a circumstellar or a circumbinary disk.

On the night of August 25th 2005, the seeing was around 0.45 arcsec, allowing us to observe both components separately. However the observation of component B only is of good quality, and has been analysed. With our automatic procedure (see Section 4.1) we find an effective temperature of 8900 ± 200 K and $\log g = 4.0$. It shows faint emissions in the core of $\text{H}\beta$ and $\text{H}\gamma$ roughly centred and not enough strong to fill the core. The emission profile of $\text{H}\alpha$ is of complex structure with a single emission superimposed with two faint absorption components. Apart from the He I D3 line, which displays stronger absorption than predicted, no other CS features are observed in the spectrum.

The LSD I profile fits very well with a single photospheric function. The result is shown in Fig. A14.

A15 HD 35929

HD 35929 belongs to the Ori OB 1c association (van den Ancker et al. 1998) situated at a distance of 375 pc (Brown et al. 1994). δ Scuti-type pulsations have been detected in the star by Marconi et al. (2000). Based on pulsation and also optical and IR properties, these authors conclude that HD 35929 is

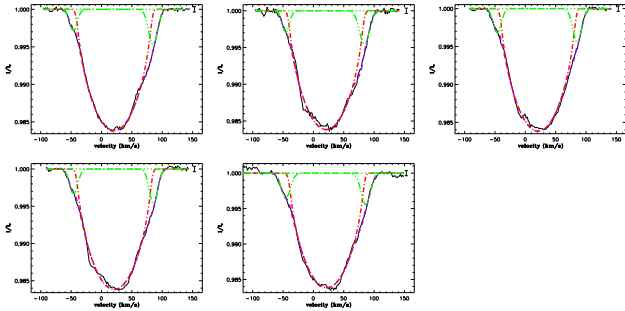


Figure A15. As Fig. A5 for the Nov. 13th, Nov. 14th 2007, Feb. 20th, Feb. 21st, and Mar. 11th 2009 (from top left to bottom right) observations of HD 35929.

probably in the PMS evolutionary stage rather than in the post-MS stage. We used the Hipparcos photometric data (Perryman & ESA 1997) to derive the luminosity.

The spectrum of HD 35929 is consistent with the effective temperature and gravity determination of Miroshnichenko et al. (2004, $T_{\text{eff}} = 6800 \pm 100$ K, $\log g = 3.3 \pm 0.1$). It displays a strong and narrow single-peaked emission profile in $H\alpha$, as well as emissions with central absorption in the Ca II IR-triplet. Emission also seems to be present in the core of $H\beta$ and the Ca II K line, while the O I 777 nm is stronger than predicted. No other CS feature is observed in the spectrum.

We first used the Kurucz mask to compute the LSD profiles of the 5 observations. The results show I profiles in absorption with broad wings. In order to get rid of these broad wings we have calculated a new mask by keeping only lines with intrinsic depth smaller than 0.5. The result shows wings without severe broadening, but now a slight distortion is detected in the profiles that could not be seen directly in the individual lines of the spectrum because of the lower SNR. We fit all the observations simultaneously with a photospheric and two Gaussian functions in absorption in both sides of each profile, by assuming that the distortions are due to CS contamination. In this fitting procedure we forced the depth, $v \sin i$, and v_{rad} of the photospheric profile to be the same for the five observations. The result, shown in Fig. A15 is satisfying. We should note however that all the Gaussians are found to be similar from one observation to another, while we would expect them to vary with time, as is observed in other HAeBe stars.

A16 HD 36112 (= MWC 758)

HD 36112 is part of the Taurus-Aurigae star forming region situated at a distance of ~ 279 pc (Hipparcos, van Leeuwen 2007). Strong IR excess is observed in the direction of the star that could be explained by the presence of a disk that has been directly detected with IR-interferometric data by Eisner et al. (2004). We have used the Hipparcos photometric data to compute the luminosity.

Beskrvnaya et al. (1999) describe the features and variability observed in the spectrum of HD 36112. These are similar to those observed in our spectra. The $H\alpha$ profile shows a P Cygni shape with temporal variations in the amplitudes of the absorption and emission components. The Na D doublet also shows P Cygni profiles. Emission is detected in the He I lines at 5875 Å, 6078 Å, and 7065 Å. Faint emission is observed in the core of $H\delta$, $H\gamma$, and $H\beta$ with amplitude increasing with wavelength. The O I 777 nm triplet is also strongly variable, sometimes showing emission, sometimes absorption, while the O I 8446 Å and Ca II IR triplets show single-

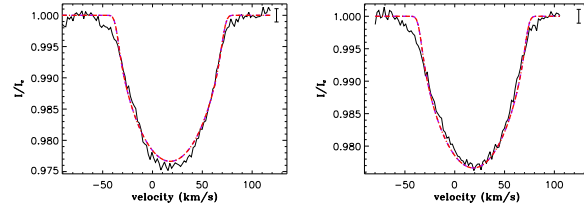


Figure A16. As Fig. A5 for the Nov. 2004 (left) and Feb. 2005 (right) observations of HD 36112.

peaked emission profiles with intensity increasing from 2004 to 2005. Using our automatic procedure, we find that the portions of the spectrum that are free of CS features are well reproduced with $T_{\text{eff}} = 7800 \pm 150$ K and $\log g = 4.0$, consistent with the work of Beskrvnaya et al. (1999).

We have cleaned the Kurucz mask by rejecting the lines strongly contaminated with emission, and used the edited mask to compute the LSD profiles. The resulting I profiles show photospheric absorption lines. The core of the 2004 LSD profile is contaminated with a faint and narrow emission feature which we are not able to distinguish in the spectrum itself because of the lower SNR. We therefore tried to calculate various masks by making a selection on the intrinsic depth or excitation potential of the lines. No matter what selection is made on the intrinsic depth, the emission component is still present. However, with a mask containing only lines with $\chi_{\text{exc}} > 6$ eV, the emission component disappears. We therefore chose this mask to analyse the LSD profiles. A simultaneous fit of both observations with photospheric functions of identical depth, $v \sin i$, and v_{rad} gives a satisfactory result (Fig. A16).

A17 HD 36910 (= CQ Tau)

HD 36910 seems to be part of the T-association Tau 4 (Kholopov 1959) at a distance of 113 pc (Hipparcos, van Leeuwen 2007). This star is strongly variable with amplitude variations greater than 1 mag, and belongs to the UXOR sub-class (Grinin et al. 2001). We therefore used the Hipparcos photometric data at maximum brightness ($V_T = 9.97$ mag, $B_T = 8.87$ mag, in the Tycho system), and converted them into the Johnson system with the calibration formula 1.3.20 of the Hipparcos and Tycho catalogues (Perryman & ESA 1997, p. 57). We find $V = 8.77$ mag and $(B - V) = 0.94$ mag. The derived luminosity is $\log L/L_{\odot} = 1.58$. Strong IR excess as well as mid-IR imaging reveal the presence of a dusty disk surrounding the star (Miroshnichenko et al. 1999b; Doucet et al. 2006).

The spectrum is consistent with the effective temperature determination of Hernández et al. (2004, $T_{\text{eff}} = 6750 \pm 300$ K). A redshifted absorption component is observed in the core of the Balmer lines from $H\epsilon$ to $H\beta$. In addition, $H\beta$ shows emission in the wings of the absorption component. $H\alpha$ displays a complex emission profile with a few redshifted absorption components. The He I D3 line displays an emission profile with a superimposed redshifted absorption. The O I 777 nm triplet is stronger than predicted, with emission in the wings, while the O I 8446 Å line displays a complex emission profile. The Ca II IR-triplet seems to be contaminated with emission on the blue side of the line, and the cores of the Paschen lines are filled with emission. A faint blueshifted emission is observed in the core of the Ca II K line. The metallic lines of the spectrum seem stronger than predicted and are contaminated with CS features.

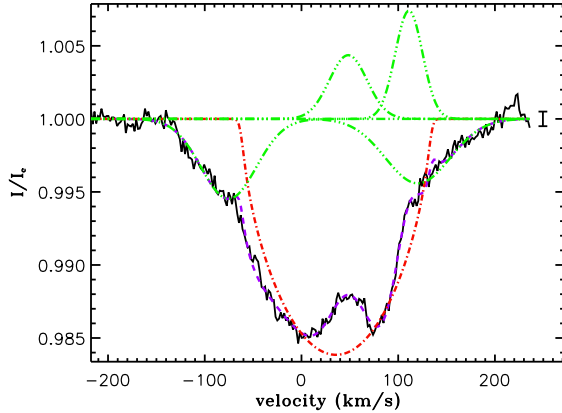


Figure A17. As Fig. A5 for HD 36910 (= CQ Tau)

We first calculated the LSD profiles without performing a special cleaning to the Kurucz mask. The result showed a very complex profile with very broad wings. We therefore tried to clean the mask by suppressing the distorted lines from the profiles, but the result was the same. We also tried to make a selection on the intrinsic line depth or on the excitation potential, but none of the different masks calculated were able to improve the LSD profile, meaning that all the lines of the spectrum are contaminated with circumstellar features. We therefore choose a mask including only lines with $\chi_{\text{exc}} > 4$, because the different CS features are more easily identifiable in the resulting LSD I profile. We fit the profile with a single photospheric function superimposed with four Gaussian functions modelling the CS emission and absorption components. The result is shown in Fig. A17. While the LSD I profile seems to be dominated by CS features, the blue part (from -70 to 0 km.s^{-1}) of the profile can only be reproduced with a photospheric function, which increases our confidence in the interpretation of this profile.

A18 HD 36917 (= V372 Ori)

HD 36917 is part of the Ori OB Id association (Wolff et al. 2004) situated at a distance of 375 pc (Brown et al. 1994). The photometric data of Wolff et al. (2004) have been used for the luminosity determination. The strong far-IR excess and the absence of strong near-IR excess place this object at an intermediate evolutionary state between Herbig Ae/Be and Vega-like stars (Manoj et al. 2002). As explained above, this object still constitutes an interesting target for our study and has been kept in the survey.

According to Levato & Abt (1976) HD 36917 is a double-lined spectroscopic binary, which we do not confirm with our observations. The spectrum of HD 36917 is consistent with a single star of effective temperature $T_{\text{eff}} = 10000 \pm 500$ K, in agreement with the spectral type determination of Johnson (1965). Many CS features are observed in its spectrum. $H\alpha$ displays a strong and narrow emission in the core. Very faint and narrow emissions, slightly blueshifted, are detected in the core of $H\beta$ and $H\gamma$. Faint emission is also present in the core of the O I 8446 Å triplet, while the He I D3 line and the O I 777 nm triplet display stronger absorption than predicted. A few metallic lines seem to be distorted, certainly due to CS features. The Ca II IR-triplet shows strong double-peaked emission profiles, and the Ca II K line displays a V-shape that could be an effect of CS gas. The Paschen lines do not seem to be contaminated with CS features.

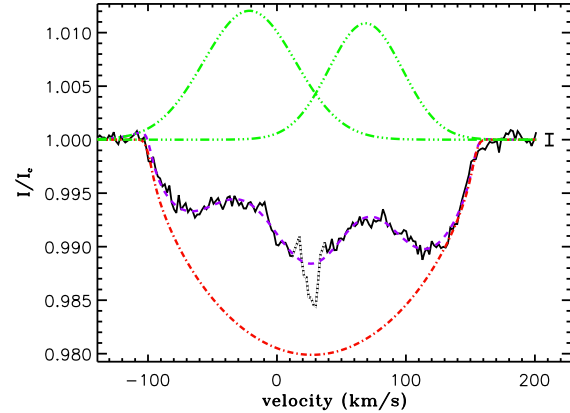


Figure A18. As Fig. A5 for HD 36917

We first calculated the LSD profiles without performing a special cleaning to the Kurucz mask. The result gives an LSD I profile contaminated with CS emission. In order to avoid emission in the I profile we computed various masks by making a selection on the excitation potential of the lines. We find that if all the lines of the mask have $\chi_{\text{exc}} > 3$ eV, then the LSD profile is no longer contaminated with emission. We then fitted both the LSD I profiles computed with the two different masks : the one resulting in a contaminated I profile, and the one giving a profile free from emission. The former has been fit with a photospheric function plus two Gaussians, modeling the emission, and the latter has been fit with a single photospheric function. Both results give consistent $v \sin i$ (127.1 ± 4.6 and 125 ± 20 km.s^{-1} , respectively). The profile free from emission is noisier than the contaminated one because of the smaller number of lines taken into account in the LSD procedure, which explains the larger error bar in $v \sin i$. The contaminated profile, despite the CS contribution, gives a better constrained value of $v \sin i$, and has therefore been adopted for the determination of the final value of $v \sin i$. The fit of this profile is plotted in Fig. A18.

A19 HD 36982 (= LP Ori)

LP Ori is part of the Ori OB Id association at a distance of 375 pc from the Sun (Brown et al. 1994). As with HD 36917, Manoj et al. (2002) reports a strong far-IR excess and the absence of strong near-IR excess, suggesting that this star is at an intermediate evolutionary state between Herbig Ae/Be and Vega-like stars, so that this star is still an interesting target for our study. We used the photometric data of Wolff et al. (2004) to derive the luminosity of the star.

LP Ori was detected as an X-ray source by the Chandra Orion Ultradeep Project (COUP, Getman et al. 2005). A magnetic field has also been detected at the surface of the star by Petit et al. (2008) using ESPaDOnS. Petit et al. (2008) performed a preliminary analysis of the magnetic properties of the star. We obtained additional Narval observations of this star in Nov. 2007. We only present here the intensity spectra obtained during that run, while a full analysis of the polarised spectra will be published in a forthcoming paper (Petit et al. in prep.).

The spectrum is well fit with a TLUSTY non-LTE spectrum of effective temperature $T_{\text{eff}} = 20000 \pm 1000$ K, consistent with the work of Wolff et al. (2004). The only CS manifestations observed in the spectrum are single-peaked CS emission components in the

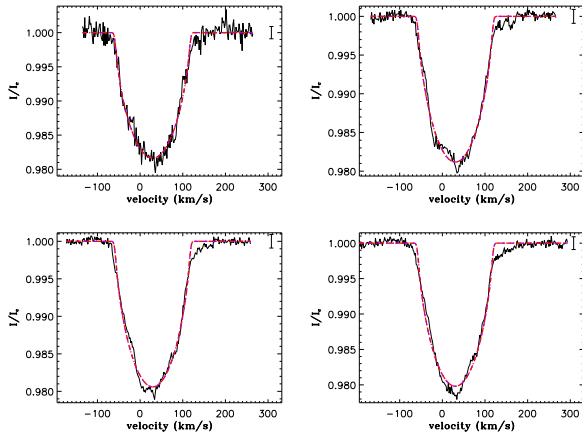


Figure A19. As Fig. A5 for the Nov. 9th, 10th, 11th and 12th 2007 (from top left to bottom right) observations of HD 36982 (= LP Ori).

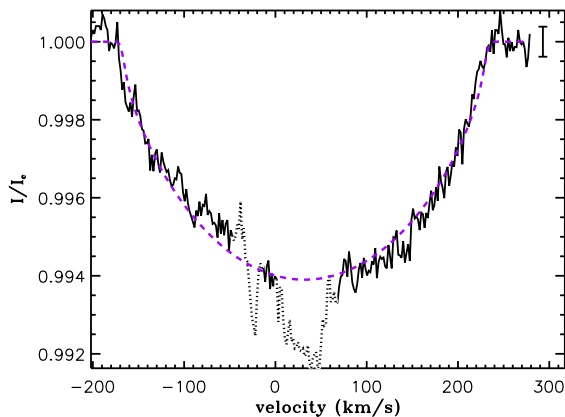


Figure A20. As Fig. A5 for HD 37258 (= V586 Ori)

core of the Balmer lines, a double-peaked emission profile in the core of the O I 8446 Å triplet, and faint distortions in the cores of the He I lines at 5875 Å, 6678 Å, and 7065 Å, and of the O I 777 nm triplet.

We have cleaned the Kurucz mask, by rejecting the strongest lines of the spectrum, as well as the lines clearly contaminated with emission. The result is a photospheric profile slightly distorted in the core, perhaps due to CS emission. We fit the four profiles simultaneously with photospheric functions only, by forcing the $v \sin i$ and v_{rad} to be identical for the four profiles. The depth was left free to vary from one profile to another, because of the distortions in the core. The results of the fit are plotted in Fig. A19.

A20 HD 37258 (= V586 Ori)

HD 37258 belongs to the Ori OB Id association (Tian et al. 1996), at a distance of 375 pc (Brown et al. 1994). Photometric observations of this star revealed strong variability, with changes in brightness of up to 2 mag. These variations are assumed to be caused by circumstellar dust appearing sporadically in the line of sight (Pugach & Kovalchuk 1986); this dust certainly belongs to the circumstellar disk revealed by the strong IR excess (Malfait et al. 1998). We will therefore assume that the brightest observed ma-

gnitude is close to the real magnitude of the star. We used the photometric data of de Winter et al. (2001) at the brightest magnitude ($V = 9.64$, $(B - V) = 0.140$) to compute the luminosity of the star.

The spectrum of HD 37258 is well fit with $T_{\text{eff}} = 9500 \pm 500$ K, in agreement with the temperature determination of Kovalchuk & Pugach (1997). The main characteristic of the spectrum is a strong contamination with redshifted CS absorption in many metallic lines, but also in the Ca II K line, in the core of the Balmer lines from H ζ to H β , in the O I 8446 Å and Ca II IR triplets. Emission is also present in the wings of the CS absorption in H β , and in the O I 8446 Å and Ca II IR triplets. H α displays a strong double-peaked emission with a strong central absorption that goes below the continuum. While HD 37258 has never been classified as an UXOR star, its spectral characteristics, as well as its strong photometric variability, are similar to the UXOR stars. In addition to the UXOR-type spectral features, an inverse P-Cygni profile is observed in the He I lines at 5875 Å and 6678 Å. The Paschen lines might be contaminated with circumstellar features as well.

We have cleaned the Kurucz mask to eliminate as far as possible the CS contamination. The result gives a photospheric profile, with a small residual contamination due to CS absorption, which we could not eliminate. We fit the LSD I profile with a photospheric function and excluded from the fit the data points contaminated with CS features. The result is shown in Fig. A20.

A21 HD 37357

HD 37357 belongs to the Ori OB Ic association situated at a distance of 375 pc (Brown et al. 1994). We used the photometric data of Vieira et al. (2003) to compute the luminosity of the star. The spectral energy distribution of HD 37357 displays an IR excess that is well reproduced with a double dust disk model, suggesting the presence of a protoplanetary disk surrounding the star in which the process of planet formation has already started (Malfait et al. 1998).

The spectrum of HD 37357 is consistent with the temperature determination of Vieira et al. (2003, $T_{\text{eff}} = 9250 \pm 500$ K). Blue-shifted CS absorption features are detected in a few Fe II lines, as well as in the Ca II K line and in the Balmer lines from H δ to H β , the latter also showing emission in the red wing of the CS absorption feature. These CS spectral features are typical of UXOR stars, although in this object they are observed in a smaller number of lines, and with smaller depths. However, because of the absence of strong photometric variability (Herbst & Shevchenko 1999), we cannot class the star as an UXOR-type. These characteristics are also similar to β Pic-like objects (e.g. Artymowicz 2000). HD 37357 could therefore be in a transitional phase from UXOR-type activity to a β Pic-type star. H α displays a P Cygni profile of Type III. Faint emission are detected in the core of the Paschen lines. The Ca II IR triplet shows single-peaked emission profiles, while the O I 8446 Å triplet is filled with emission. The He I D3 line displays a broad double-peaked emission profile.

We have cleaned the Kurucz mask K9000.40, rejecting all the lines contaminated with CS features. The result is a photospheric profile only slightly contaminated with CS absorption features, that is well fit by a photospheric function, if we exclude the contaminated data points. The profile and its best fit are plotted in Fig. A21.

A22 HD 37806 (= MWC 120)

HD 37806 is part of the Ori OB Ib association (Warren & Hesser 1978), situated at a distance of 375 pc

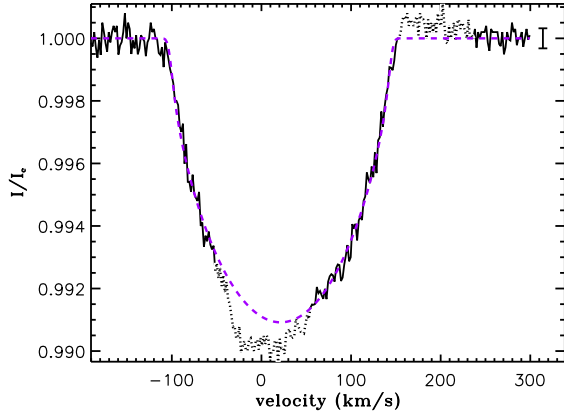


Figure A21. As Fig. A5 for HD 37357

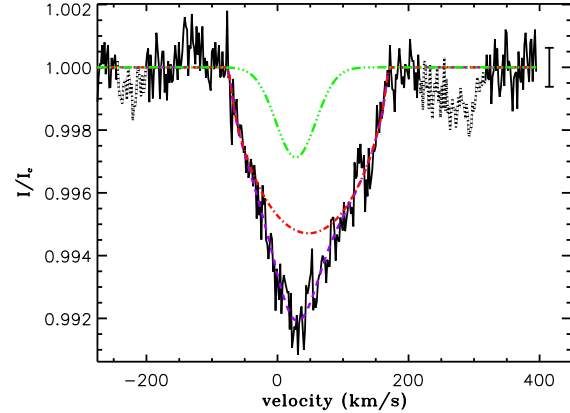


Figure A22. As Fig. A5 for HD 37806 (=MWC 120)

(Brown et al. 1994). We used the Hipparcos photometric data (Perryman & ESA 1997) to derive the luminosity of the star. Like HD 37357, the spectral energy distribution of HD 37806 displays near-and far-IR excess, and reveals the presence of a circumstellar disk with a gap, where planet formation could have started (Malfait et al. 1998).

The spectrum is well fit with $T_{\text{eff}} = 11000 \pm 500$ K, which is equivalent to a spectral type B8 (Kenyon & Hartmann 1995). This value is inconsistent with the spectral type determination of Guetter (1981), but in agreement with the estimation of Grady et al. (1996).

Strong blueshifted circumstellar absorption, often superimposed with still farther blueshifted emission, is present in numerous lines of the spectrum, including the strongest metallic lines, the Ca II K line, and the Balmer lines from H θ to H β . H α displays a strong double-peaked emission with a blueshifted central absorption. The He lines at 5875 Å, 6678 Å, 7065 Å, and the O I 777 nm triplet display strong inverse P-Cygni profiles. The O I 8446 Å triplet shows a single-peaked emission, while the Ca II IR-triplet show double-peaked emissions. Single-peaked emission is superimposed with the cores of the Paschen lines. Some high-excitation lines such as Si II 5040 and 5056 Å and O I 6156 Å are largely or completely free of circumstellar features.

We have cleaned the Kurucz mask by keeping only lines that do not seem to be contaminated with CS features. The result is a photospheric profile still contaminated with a blueshifted CS absorption, which is well fit by a photospheric plus a Gaussian function. The result is plotted in Fig. A22.

A23 HD 38120

HD 38120 belongs to the Ori OB Ic association at a distance of 375 pc (Brown et al. 1994). The IR and submillimetric properties of this star suggest that it could be a less-evolved object than the Vega-type stars, and is therefore very interesting for our study (Coulson et al. 1998). We used the Hipparcos photometric data (Perryman & ESA 1997) to derive the luminosity.

The intensity spectrum of HD 38120 is well fit with an effective temperature of 11000 ± 500 K, in agreement with the work of Vieira et al. (2003). The metallic lines are very faint compared to a solar metallicity spectrum. Faint single emission is observable in the core of a few metallic lines, including the Ca II K line and the Ca II IR-triplet. Broad emission is observed in the He I lines at 5875 Å, 6678 Å, 7065 Å, and in the O I 777 nm triplet. All Bal-

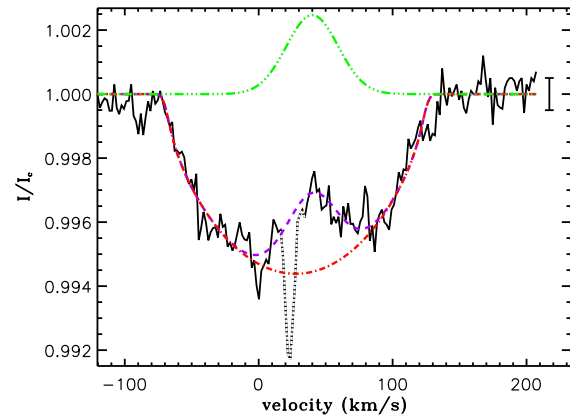


Figure A23. As Fig. A5 for HD 38120

mer lines visible in the spectrum (from H α to H θ) have a narrow emission in the core, with strength increasing with wavelength. The Paschen lines also display narrow emission features in their cores, and the O I 8446 Å triplet appears in emission.

We have calculated the LSD profiles without performing a special cleaning to the Kurucz mask. The resulting I profile shows an emission component in the core, reflecting what is observed in the metallic lines. We fitted the profile with a photospheric function and a Gaussian function modeling the emission. The result is shown in Fig. A23.

A24 HD 38238 (= V351 Ori)

HD 38238 is an irregular variable star, part of the Ori OB Id association, which is situated at a distance of 375 pc (Brown et al. 1994). It changes its photometric behaviour from that of a Herbig Ae star with strong photometric variations, due to extinction by circumstellar dust clouds, to that of an almost non-variable star, suggesting that HD 38238 is in the process of transition from a Herbig Ae star with strong photometric variations to a non-variable one (van den Ancker et al. 1996). We used the Hipparcos photometric data (Perryman & ESA 1997) to derive the luminosity. The IR excess observed in HD 38238 can be explained with an extended disk or dust-shell around the star (van den Ancker et al. 1996).

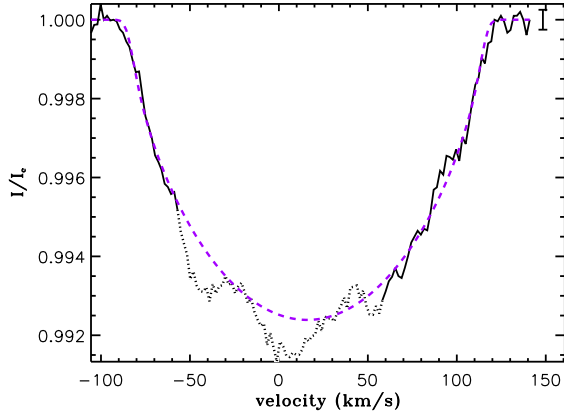


Figure A24. As Fig. A5 for HD 38238 (= V351 Ori)

The spectrum of HD 38238 is well reproduced with $T_{\text{eff}} = 7750 \pm 250$ K, consistent with the spectral type determination of van den Ancker et al. (1996) (A6-A7). No CS features are observed in the spectrum, except an inverse P Cygni of type III in the core of $H\alpha$, and perhaps faint emission in the Paschen lines.

We first calculated the LSD profiles without performing a special cleaning to the Kurucz mask. The resulting I profile show broad wings. In order to avoid this, we have calculated various masks by making a selection on the intrinsic depth and excitation potential of the lines, and we find that a mask containing only lines with $d < 0.6$ gives a profile with normal photospheric wings, consistent with the individual lines of the spectrum itself. The resulting LSD I profile reveals distortion in the core that could be due to CS contamination. We therefore fitted the profile with a photospheric function, but excluding the contaminated data points in the core. The result is shown in Fig. A24.

A25 HD 50083 (= V742 Mon)

HD 50083 is a candidate Herbig Ae/Be star (Vieira et al. 2003) studied in detail by Frémat et al. (2006). Using high-resolution spectroscopy, they determined the effective temperature and the surface gravity of the star ($T_{\text{eff}} = 20000 \pm 1000$ K and $\log g = 3.43 \pm 0.15$ (cgs)). The Hipparcos parallax (van Leeuwen 2007) is too uncertain to be used for a distance estimation. We therefore placed the star in the $T_{\text{eff}} - \log g$ diagram and compared its position with CESAM PMS evolutionary tracks to derive the mass, radius and age. We also derive a luminosity of $\log(L/L_{\odot}) = 4.15 \pm 0.12$, and using the photometric data of Vieira et al. (2003), we estimate the distance of the star to be around 1000 ± 100 pc, consistent with the new determination of the Hipparcos parallax by van Leeuwen (2007). The spectral energy distribution of HD 50083 displays a weak IR excess, similar to classical Be stars (Sartori et al. 2010). However it might be associated with the dark nebulae LDN 1639 (Lynds 1962), indicating that the star is young.

The spectrum of HD 50083 is strongly contaminated with variable circumstellar features. From $H\zeta$ to $H\gamma$ double-peaked emission profiles are observed in the core of the Balmer lines, with increasing amplitude with wavelength. $H\beta$ and $H\alpha$ display single peaked emission profiles superimposed with many absorption features. Many double-peaked emission are observed in Fe II lines, as well as in the Paschen lines, in the O I 8446 Å and Ca II IR triplets. In the He I lines at 5875 Å and 6678 Å, we observe small emission

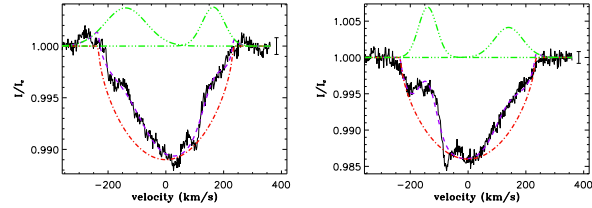


Figure A25. As Fig. A5 for the Nov. 2007 (left) and Apr. 2008 (right) observations of HD 50083.

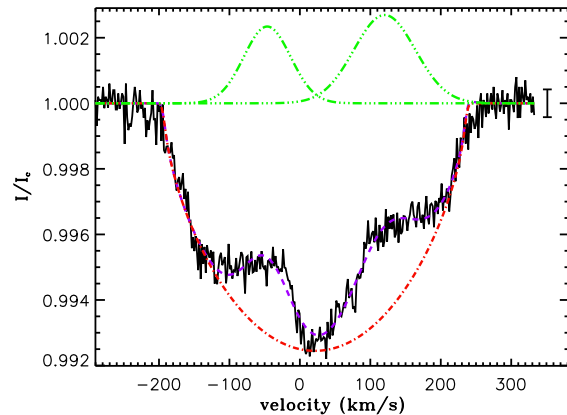


Figure A26. As Fig. A5 for the Apr. 2008 observation of HD 52721 (=GU CMa).

features in each side of the photospheric profile. A strong and narrow interstellar feature is only observed in the Ca II K line. The O I 777 nm triplet displays a strong and complex emission profile.

Those spectral lines that are not contaminated with emission are well fit with a non-LTE TLUSTY model of $T_{\text{eff}} = 24000$ K. This is slightly different from the determination of Frémat et al. (2006), which can be explained by our inability to estimate $\log g$ with our data. We have cleaned the Kurucz mask by rejecting all spectral lines contaminated with CS features. The result is the two photospheric profiles displayed, which are still contaminated with CS emission. We fitted both profiles simultaneously with a photospheric and four Gaussian functions, by forcing the $v \sin i$ and v_{rad} to be the same for both observations. We were unable to find consistent results if we require the photospheric depths of both profiles to be identical. This means that the depth of the LSD profile has changed between the two observations, and therefore that additional CS features (not taken into account in our fit) may contaminate the cores of the profiles. The result of the fitting procedure is shown in Fig. A25.

A26 HD 52721 (=GU CMa)

HD 52721 has been carefully studied by Frémat et al. (2006), who determined the effective temperature and the surface gravity of the star ($T_{\text{eff}} = 22500 \pm 2000$ K and $\log g = 3.99 \pm 0.20$ (cgs)). No star forming region is known to be associated with this star, and the Hipparcos parallax (van Leeuwen 2007) is too uncertain to be used for a distance estimate. We therefore placed the star in the $T_{\text{eff}} - \log g$ diagram and compared its position with CESAM PMS evolutionary tracks to derive the mass, radius and age.

We also derive a luminosity $\log(L/L_{\odot}) = 3.77^{+0.35}_{-0.31}$, and using the photometric data of Shevchenko et al. (1999), we estimate the distance of the star to be about 670^{+140}_{-110} pc. Its spectral energy distribution displays a weak IR excess, similar to classical Be stars (Hillenbrand et al. 1992). HD 52721 illuminates the reflection nebula VdB 88 (van den Bergh 1966a), indicating that the star must be very young.

The spectrum of HD 52721 is strongly contaminated with variable CS emission. From H δ to H β the cores of the Balmer lines are superimposed with double-peaked emission profiles. H α displays a single-peaked emission line superimposed with various faint and narrow absorption. Double-peaked emission is observed in many Fe II lines, as well as in the Paschen lines, in the O I 8446 Å and Ca II IR triplets. We observe two small emission features in the He I 5875 Å line, one on each side of the photospheric profile. A strong and narrow interstellar feature is only observed in the Ca II K line. The O I 777 nm triplet displays an emission profile superimposed with three absorption features.

The spectral lines that do not appear contaminated with CS features fit well with a non-LTE TLUSTY spectrum of $T_{\text{eff}} = 26000$ K and $\log g = 4.0$, slightly different from the temperature derived by Frémat et al. (2006), a difference that could be due to the NLTE effect not taken into account in the Shevchenko et al. (1999) analysis. We have cleaned the Kurucz mask, rejecting the lines contaminated with circumstellar features. The result gives profiles still contaminated with emission. Both observations fit well with a photospheric function plus two Gaussian functions, and give consistent results when fitted separately. However, the SNR of the Nov. 2007 profile is significantly lower than the SNR of the Apr. 2008 profile, so that the former observation does not help to better constraint the fitting parameters. Only the Apr. 2008 profile has been taken into account in the fitting procedure. The result is shown in Fig. A26.

A27 HD 53367

HD 53367 is a candidate Herbig Be star (Vieira et al. 2003), and illuminates the reflection nebula VdB 93 (van den Bergh 1966a). We used the Hipparcos parallax (van Leeuwen 2007) and the photometric data of Shevchenko et al. (1999) to derive the luminosity of the star. Its spectral energy distribution is very similar to HD 52721, and for the same reasons we can argue that the star is still very young.

The spectrum of HD 53367 does not show any obvious emission in any of the Balmer lines. Hints of emission are visible in the blue side of H α and He lines. The spectrum is well fitted with a non-LTE TLUSTY synthetic spectrum of $T_{\text{eff}} = 29000 \pm 2000$ K, consistent with the temperature determination of Shevchenko et al. (1999). The strongest lines of the spectrum do not have the shape of a photospheric function, and the fainter lines show flattened cores.

We have cleaned the Kurucz mask by rejecting the strongest lines of the spectrum, in order to obtain an LSD I profile as close as possible to a photospheric profile. The result is noisy but satisfying. We fitted both observations simultaneously with a single photospheric function (see Fig. A27).

A28 HD 68695

HD 68695 is part of the Vela star cloud situated at a distance of 570 pc (Eggen 1986). We used the photometric data of Vieira et al. (2003) to derive the luminosity. No spectral energy distribution has

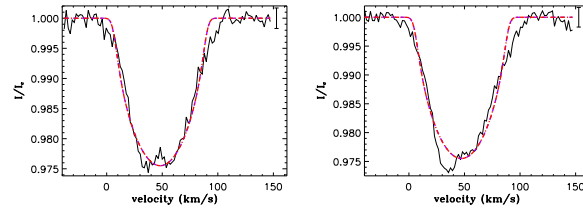


Figure A27. As Fig. A5 for the Feb. 20th (left) and 21st (right) 2005 observations of HD 53367.

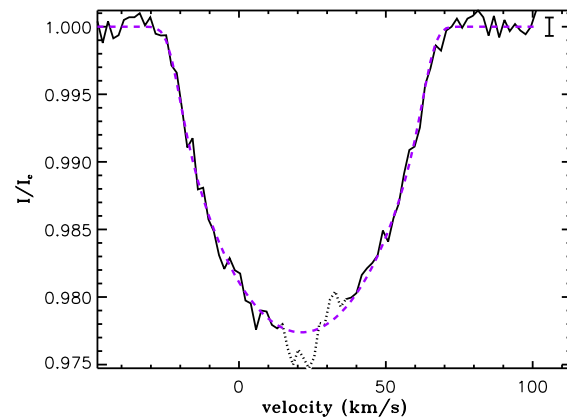


Figure A28. As Fig. A5 for HD 68695

been published until now, however Vieira et al. (2003) reports visible and near-IR photometry of the star. By comparing the near-IR colour excesses to that of HD 38120, a Herbig Ae star of the same temperature, we find similar values, leading to the conclusion that HD 68695 may also be a less-evolved Vega-type star.

The spectrum is consistent with the temperature and gravity determination of Folsom et al. (2012, $T_{\text{eff}} = 9500$ K, $\log g = 4.3 \pm 0.3$). The cores of the Balmer lines from H δ to H α are superimposed with a single-peaked emission line, with amplitude increasing with wavelength. Except for broad emission observed at the He I lines at 5875 Å, 6678 Å and 7065 Å, and emission in the blue wing of the O I 777 nm triplet, no other CS contribution is observed in the spectrum. The abundance of C appears to be higher than the solar value, O appears approximately solar, and Ti, Cr and Fe all seem to have somewhat lower than solar abundance. This may be a young λ Boo star as proposed by Folsom et al. (2012).

We have cleaned the Kurucz mask by rejecting the lines with CS contribution. The result gives a profile in absorption, well fitted with a single photospheric function, and is plotted in Fig. A28

A29 HD 76534 A

HD 76534 illuminates the reflection nebula VdB 24 (van den Bergh 1966a), and is member of the Vela R2 association situated at a distance of 870 pc (Herbst 1975). It is a visual binary star resolved by Hipparcos with a separation of 2.1 arcsec (Perryman & ESA 1997). We observed the brighter component labeled A in the Hipparcos catalogue. We used the Hipparcos Double and Multiple System Annex (DMSA) photometric data of the component A to derive the luminosity of the star. In order to convert the magnitudes from the Tycho to the Johnson system,

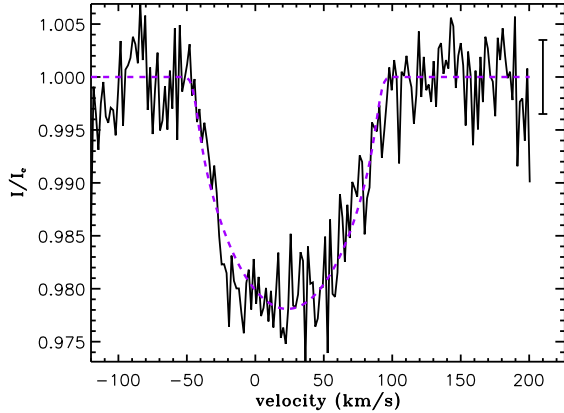


Figure A29. As Fig. A5 for HD 76534 A

we used the calibration formula 1.3.20 of the Hipparcos catalogue (Perryman & ESA 1997, p.57), and we find $V = 8.35$ mag and $(B - V) = 0.107$ mag. Its spectral energy distribution is very similar to HD 52721, and for the same reasons we argue that the star is still very young.

The spectrum is well reproduced by a non-LTE TLUSTY synthetic spectrum of $T_{\text{eff}} = 18000 \pm 2000$ K, consistent with the temperature determination of Thé et al. (1985a). The cores of the Balmer lines from H δ to H β are contaminated with double-peaked emission lines, while H α is totally dominated with a double-peaked emission profile. Slight emission is observed in the wings of the He I lines at 5875 Å, 6678 Å and 7065 Å. The O I 777 nm and O I 8446 Å triplets, and the Paschen lines display double-peaked emission profiles. The Ca II IR-triplet does not seem to contribute to the emission observed in the Paschen lines. The Ca II K line is only contaminated with a narrow interstellar absorption. The strongest metallic lines of the spectrum show broad wings and asymmetric shapes.

We have cleaned the Kurucz mask by selecting only faint lines, with relatively symmetric shapes. The result is satisfactory, but very noisy and slightly asymmetric. It is reasonably well fit with a single photospheric function (Fig. A29).

A30 HD 98922

HD 98922 is a Herbig Be star that does not seem to be associated with any bright nebula or star-forming region. However the large near- and far-IR excess leaves no doubt that the star is young and still surrounded with dust (Malfait et al. 1998). We used the Hipparcos photometric data (Perryman & ESA 1997) and the new Hipparcos parallax (van Leeuwen 2007) to compute the luminosity of the star. The resulting position of the star in the HR diagram is situated well above the birthline (see Fig. 4), which can be the result of either an inaccurate parallax, or an unusual star with an atypical history. The models that we use to compute the mass, radius and age could be inappropriate for this star, and have therefore not been estimated in this paper.

The spectrum is consistent with the temperature determination of Vieira et al. (2003, $T_{\text{eff}} = 10500 \pm 500$ K). Circumstellar absorption and emission lines are present in the whole spectrum. Single peaked emission lines are observed in the core of H δ and H γ , while P Cygni profiles are superimposed with the core of the H β and H α lines. Single-peaked emission lines are also ob-

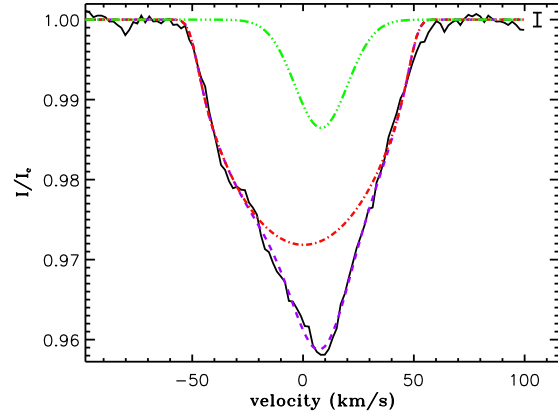


Figure A30. As Fig. A5 for HD 98922

served in the core of the Paschen lines from P17 to P10. The O I 8446 Å and Ca II IR triplets display single-peaked emission profiles. The O I 777 nm triplet displays a triple-peaked emission profile. The He I 5875 Å photospheric profile might be slightly distorted by CS features. The Ca II K line, while very noisy, does not seem to be contaminated with CS features. Many metallic lines display double-peaked emission profiles. The lines of multiplet 42 of Fe II display single-peaked emission profiles.

We have cleaned the Kurucz mask by rejecting all lines showing obvious circumstellar contamination. The resulting LSD I profile still contains a circumstellar absorption contribution, which could not be eliminated. From a more careful analysis of the spectrum, we find that the photospheric lines that are not obviously contaminated with CS emission still seem to be superimposed with a narrow CS absorption, consistent with the LSD profile. We fit the LSD profile with a single photospheric function superimposed with a circumstellar Gaussian. The result is shown in Fig. A30.

A31 HD 114981 (= V958 Cen)

HD 114981 is a B-type star with IR excess typical of Vega-like stars (Mannings & Barlow 1998). We used the Hipparcos photometric data (Perryman & ESA 1997) and the new Hipparcos parallax (van Leeuwen 2007) to compute the luminosity of the star (van Leeuwen 2007).

The spectrum of HD 114981 is well reproduced with a non-LTE TLUSTY synthetic spectrum of $T_{\text{eff}} = 17000 \pm 2000$ K, inconsistent with previous work (Hill 1970; Vieira et al. 2003). This disagreement is certainly due to the lack of high-resolution spectra or to low SNR data in the earlier studies. Our T_{eff} is consistent with the spectral type quoted in the Michigan Catalogue of HD stars, vol. 3 (Houk 1982, 1994). The star displays variable circumstellar contamination. Double-peaked emission lines are observed in the cores of Balmer lines from H δ to H β . H α , the Paschen and Ca II K lines, and the O I 777 nm and O I 8446 Å triplets display double-peaked emission profiles. The Ca II IR-triplet does not seem to contribute to the emission observed in the Paschen lines. The He I D3 line is not contaminated with CS features. Many Fe II lines show double-peaked emission lines.

We have cleaned the Kurucz mask, by rejecting lines contaminated with emission. The resulting LSD I profile is still slightly contaminated with emission, but could not be improved. We performed a simultaneous fit of both observed I profiles with a single

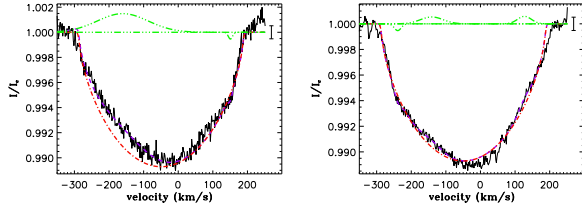


Figure A31. As Fig. A5 for the Feb. 2005 (left) and Jan. 2006 (right) observations of HD114981.

photospheric function, plus circumstellar Gaussians modelling the CS features, by forcing the depth, $v \sin i$ and v_{rad} of the photospheric profiles to be the same for both observations. The result is shown in Fig. A31.

A32 HD 135344

HD 134344 is an F4 type star with strong near and far-IR excesses that are similar to HD 31293, and that can be well reproduced with a two-temperature dust disk model (Malfait et al. 1998), confirming the Herbig Ae nature of the star. It is associated with the Upper Centaurus-Lupus star forming region (de Zeeuw et al. 1999), situated at a distance of 142 pc (Müller et al. 2011). We used the photometric data of Oudmaijer et al. (1992) to derive the luminosity.

The spectrum of HD 135344 is well fit with $T_{\text{eff}} = 6750 \pm 250$ K, consistent with the temperature determination of Saffe et al. (2008). The core of H β is superimposed with faint emission and a strong blueshifted absorption, while H α displays a P Cygni profile of type III. The cores of H γ and H δ are also slightly contaminated with circumstellar emission. The wings of the O τ 777 nm and O τ 8446 Å triplets are contaminated with emission, and the Paschen lines are filled with circumstellar emission. A broad and faint emission is observed in the He τ D3 line. The Ca II K line does not seem to be contaminated with CS features, while other metallic lines seem to be slightly distorted due to CS emission.

We have calculated the LSD profiles without performing a special cleaning to the Kurucz mask. The resulting LSD I profile displays a photospheric profile slightly contaminated with emission, but could not be improved. We fit the profile with a single photospheric function plus a Gaussian. The result is shown in Fig. A32.

A33 HD 139614

HD 139614 is associated with the Upper Centaurus Lupus star forming region (de Zeeuw et al. 1999), situated at a distance of 142 pc (Müller et al. 2011). We used the photometric data of Vieira et al. (2003) to derive the luminosity of the star. Its spectral energy distribution is well reproduced with a two-temperature dust disk model (Malfait et al. 1998), confirming the Herbig Ae nature of the star.

The spectrum is consistent with the temperature and gravity determination of Folsom et al. (2012, $T_{\text{eff}} = 7600 \pm 300$ K, $\log g = 3.9 \pm 0.3$). This temperature does not lead to a very exact fit to the observed metallic line spectrum, which may be due to chemical peculiarities in the atmosphere (see Folsom et al. 2012). The spectrum is slightly contaminated with variable CS features : faint emission is observed in the core of H β , while the core of H α is superimposed with a strong, narrow, single-peaked emission. The

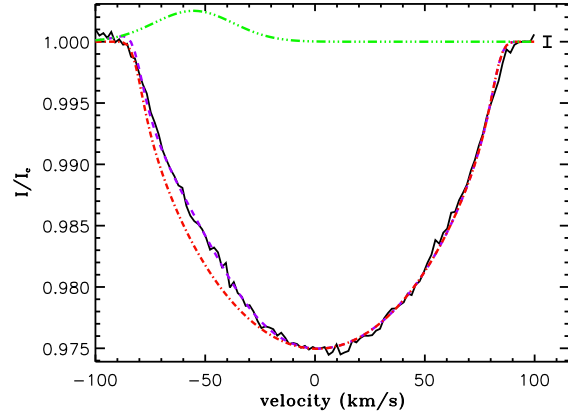


Figure A32. As Fig. A5 for HD 135344

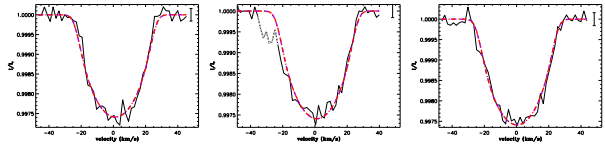


Figure A33. As Fig. A5 for the Feb. 20th (left), 21st (middle), and 22nd (right) 2005 observations of HD 139614

He τ D3 line displays a faint but broad emission profile. A hint of broad emission is also observed at 6878 Å and 7065 Å. The photospheric profile of the O τ 777 nm triplet might also be superimposed with faint emission. No other CS contribution is observed in the spectrum.

We first calculated the LSD profiles without performing a special cleaning to the Kurucz mask. The resulting LSD I profile appears in absorption, but with very large wings, of which the origin is unknown. We therefore choose to compute new masks from K8250.40 by making a selection on the central depth and the excitation potential of the lines. A mask containing lines with central depths below 0.08 provides us with LSD I profiles displaying photospheric shapes. We performed a simultaneous fit of the three observations with a photospheric function, by forcing the depth, $v \sin i$, and v_{rad} to be identical for the three profiles. In the profile of Feb. 20th 2005, we exclude from the fit the few points in the blue wing of the I profile that suggest a small absorption component with an unknown origin. The result of the fit is shown in Fig. A33

A34 HD 141569

HD 141569 is an isolated β Pictoris-like star (Malfait et al. 1998; Sahu et al. 1998), situated at a distance of 116 pc (Hipparcos, van Leeuwen 2007). It is the primary member of a triple system with two late-type companions orbiting at ~ 8 arcsec (Weinberger et al. 2000). The disk of the primary star has been directly observed using coronagraphic observations (Weinberger et al. 1999; Augereau et al. 1999). We used the Hipparcos photometric data to derive the luminosity of the primary.

The spectrum of HD 141569 is consistent with the temperature and gravity determination of Folsom et al. (2012, $T_{\text{eff}} = 9800 \pm 500$ K, $\log g = 4.2 \pm 0.4$). It is only very slightly contaminated with CS features. A faint double-peaked emission is present

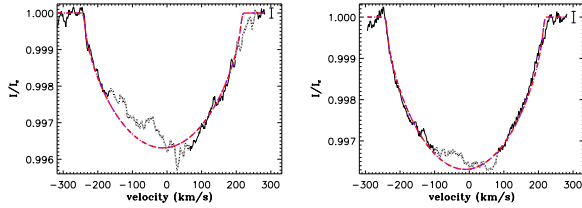


Figure A34. As Fig. A5 for the Feb. 2006 (left) and Mar. 2007 (right) observations of HD 141569. The data have been smoothed with a width equal to 4 pixels.

in the core of $H\beta$, and a strong double-peaked emission is superimposed on the core of $H\alpha$. Some of the metallic lines appear less deep than predicted, which could be due to CS contamination. Except for a double-peaked emission profile in the O I 777 nm and O I 8446 Å triplets, and in a few Fe II lines of the IR part of the spectrum, no other CS contribution is observed.

We first calculated the LSD profiles without performing a special cleaning to the Kurucz mask. The resulting LSD I profiles display photospheric profiles contaminated with emission. In order to reduce the contamination, we have cleaned the mask by rejecting, as far as possible, lines that seem to be contaminated with emission. The resulting I profiles look better but are still slightly contaminated. We therefore choose to fit both profiles simultaneously with a single photospheric function, by rejecting the data points contaminated with CS emission, and by forcing the photospheric depth, $v \sin i$, and v_{rad} to be the same for both observations. The result is shown in Fig. A34.

A35 HD 142666 (= V1026 Sco)

HD 142666 could be associated with the Upper Scorpius star forming region at a distance of 145 pc (Preibisch & Mamajek 2008). We used the photometric data of Vieira et al. (2003) to derive the luminosity. Its spectral energy distribution is well reproduced with a two-temperature dust disk model (Malfait et al. 1998), confirming the Herbig Ae nature of the star.

Using our automatic procedure, we find that the spectrum of HD 142666 is well reproduced with $T_{\text{eff}} = 7900 \pm 200$ K and $\log g = 4.0$, consistent with the work of Vieira et al. (2003). The spectrum is contaminated with variable CS features. Redshifted circumstellar absorption components are observed in the core of the Ca II K and Balmer lines from $H\zeta$ to $H\beta$. In addition, emission is present in the wings of the CS absorption component in $H\beta$. The core of $H\alpha$ is superimposed with an inverse P Cygni profile. The He I D3 line displays a strong and broad absorption component, while the O I 777 nm triplet is stronger than predicted. No other circumstellar features are observed in the spectrum.

We first calculated the LSD profiles without performing a special cleaning to the Kurucz mask. The resulting LSD I profiles display broad wings that could not be correctly reproduced with a photospheric function. We therefore computed various other masks by making a selection on the central depth and excitation potential of the individual lines in the mask K8000.40. The mask including only lines with central depths of less than 0.5 gives profiles with photospheric-like shapes. The profiles of Feb 21st, May 21st, and May 23rd 2005 display asymmetric shapes. We first fit all the observations simultaneously with a single photospheric function, but the result was not satisfactory. We then fit simultaneously the sym-

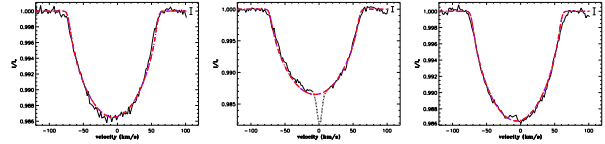


Figure A35. As Fig. A5 for the Feb. 20th (left), May 23rd 07:50 (middle) and May 25th (right) 2005 observations of HD 142666

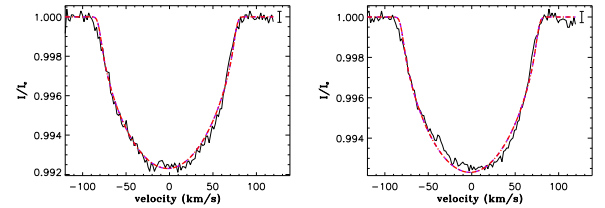


Figure A36. As Fig. A5 for the Feb. 20th (left) and 21st (right) observations of HD 144432.

metric profiles of Feb. 19th, May 22nd, and May 24th 2005 only, leading to a better solution. The result is shown in Fig. A35.

A36 HD 144432

Combining the new Hipparcos data reduction (van Leeuwen 2007) and the membership criteria of (de Zeeuw et al. 1999), we find that HD 144432 is a member of the Upper Scorpius OB association, situated at a distance of 145 pc (Preibisch & Mamajek 2008). We used the Hipparcos photometric data (Perryman & ESA 1997) to derive the luminosity of the star. The spectral energy distribution, as well as the the optical photometric and spectroscopic properties of HD 144432 strongly suggest that it is surrounded by a disk, confirming the Herbig Ae nature of the star.

Using our automatic procedure, we find that the spectrum of HD 144432 is well reproduced with $T_{\text{eff}} = 7500 \pm 300$ K and $\log g = 3.5$, consistent with the work of Vieira et al. (2003). Its spectrum is slightly contaminated with variable CS features. Blueshifted circumstellar absorption components are observed in the core of the Balmer lines from $H\delta$ to $H\beta$. In addition, emission is observed in the wings of the CS absorption component of $H\beta$. $H\alpha$ displays a complex P Cygni profile, with two blueshifted absorption components. Faint emission is observed in the core of the Ca II K line. The He I D3 line displays a faint and broad emission profile. Emission is observed in the blue wing of the O I 777 nm triplet, as well as in the blue and red wings of the O I 8446 Å line. The Ca II IR-triplet displays double-peaked emission profiles. No other CS features are observed in the spectrum.

We first calculated the LSD profiles without performing a special cleaning to the Kurucz mask. The resulting LSD I profile displays an absorption profile with broad wings, not well reproduced by a photospheric function. We have therefore calculated many masks from K7500.40 by making a selection on the central depth or excitation potential of the lines. We find that a mask containing lines with central depths of less than 0.4 leads to photospheric profiles. We fit both observations simultaneously, by forcing the photospheric depths, $v \sin i$ and v_{rad} to be identical for both observations. The result is shown in Fig. A36

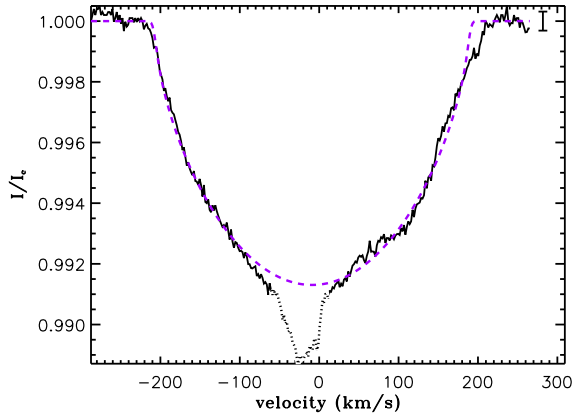


Figure A37. As Fig. A5 for HD 144668

A37 HD 144668 (= HR 5999)

Combining the Hipparcos data reduction (Perryman & ESA 1997) and the membership criteria of (de Zeeuw et al. 1999), we find that HD 144668 is part of the Upper Centaurus Lupus OB association, situated at a distance of 142 pc (Müller et al. 2011). This distance is consistent with the Hipparcos parallax, and will be used in the following. HD 144668 illuminates the reflection nebula B149 (Bernes 1977; Magakian 2003) situated in the molecular cloud SL 14 (Sandqvist & Lindroos 1976). We used the Hipparcos photometric data (Perryman & ESA 1997) to derive the luminosity of the star. Its spectral energy distribution is well reproduced with a two-temperature dust disk model (Malfait et al. 1998), a disk that has also been detected by Preibisch et al. (2006) using mid-infrared long-baseline interferometry.

Using our automatic procedure, we find that the spectrum of HD 144668 is well reproduced with $T_{\text{eff}} = 8200 \pm 200$ K and $\log g = 3.5$, consistent with the work of Tjin A Djie et al. (1989). The Balmer lines from $H\zeta$ to $H\beta$ are superimposed with a centered CS absorption. In addition, emission is observed in the wings of the CS absorption of $H\beta$. $H\alpha$ displays a double-peaked emission profile. Strong circumstellar absorption is also observed in some Fe II lines and in the Ca II K line, as well as in the O I 8446 Å, and in Ca II IR triplets. Emission is also observed in the wings of the Ca II IR lines. The O I 777 nm triplet displays a very deep absorption profile with weak emission in the blue wing. The He I 5875 Å line shows an inverse P Cygni profile. The Paschen lines do not seem to be contaminated with CS features.

We first cleaned the Kurucz mask by rejecting lines contaminated with CS features. The resulting LSD I profile displays broad wings and a small CS contamination in the core. In order to improve this profile we have calculated various masks from the cleaned mask, by making a selection on the central depth or the excitation potential of the lines. The best result was obtained with a mask containing lines with central depths of less than 0.7. The result still shows weak CS contamination but could not be improved. It is well fit with a photospheric function, by excluding from the fit the data points contaminated with CS features. The result is shown in Fig. A37.

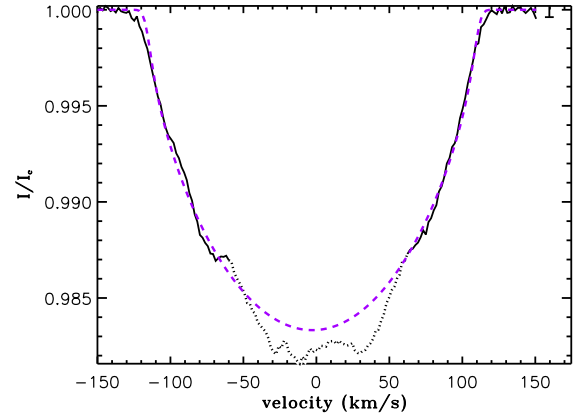


Figure A38. As Fig. A5 for HD 145718

A38 HD 145718 (V718 Sco)

HD 145718 is part of the Upper Scorpius OB association, situated at a distance of 145 pc (Preibisch & Mamajek 2008). This distance is consistent with the new Hipparcos parallax determination of van Leeuwen (2007), and will be used in the following. We used the Hipparcos photometric data (Perryman & ESA 1997) to derive the luminosity. IR, optical and submillimetric observations strongly suggest the presence of a circumstellar disk around the star (Dent et al. 2005; Guimarães et al. 2006).

Using our automatic procedure, we find that the spectrum of HD 145718 is well reproduced with $T_{\text{eff}} = 8100 \pm 200$ K and $\log g = 4.0$, consistent with the work of Vieira et al. (2003). The core of the Balmer lines, from $H\delta$ to $H\beta$, are superimposed on redshifted CS absorption. Emission is present in the wings of the CS absorption component of $H\beta$. The core of $H\alpha$ is superimposed on an inverse P Cygni profile with two redshifted absorption components (instead of one). The He I D3 line displays a broad and asymmetric absorption profile. Due to strong non-LTE effects, the O I 777 nm triplet is stronger than predicted. The cores of a few metal lines seem to be distorted due to CS features. No other CS contribution is observed.

We first calculated the LSD profiles without performing a special cleaning to the Kurucz mask. The resulting I profile displays a photospheric shape with a slight distortion in the core due to CS contribution. We tried to improve the fit by calculating new masks by making a selection on the central depth and the excitation potential of the lines. We find that a mask containing only lines with an excitation potential greater than 8 eV does not show CS contamination, but is much noisier than the first computed I profile. We fit both computed profiles with a single photospheric function. We excluded from the fit the data points contaminated with CS features in the first LSD I profile that we computed. Both results give consistent $v \sin i$, but the second profile, due to a lower SNR, is less accurate. We therefore determined $v \sin i$ from the first profile that we computed. The result of the fitting is shown in Fig. A38.

A39 HD 150193 (V2307 Oph)

HD 150193 is part of the Upper Scorpius OB association situated at a distance of 145 pc (Preibisch & Mamajek 2008). This distance is consistent with the new Hipparcos parallax determination of (van Leeuwen 2007), and will be used in the follo-

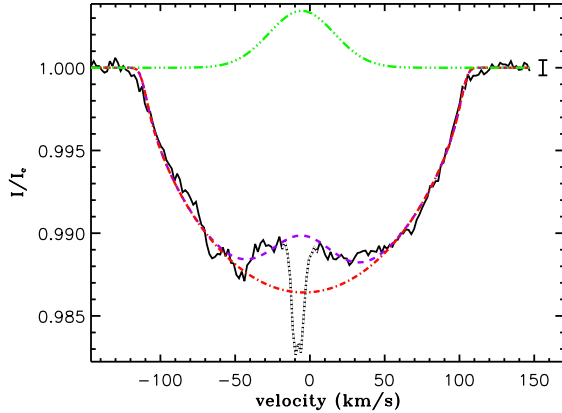


Figure A39. As Fig. A5 for HD 150193

wing. We used the Hipparcos photometric data (Perryman & ESA 1997) to derive the luminosity. Its IR spectral energy distribution is well reproduced with a two-temperature dust disk model (Malfait et al. 1998), describing a disk that has been spatially resolved by (Eisner et al. 2009) using near-IR interferometry.

The stellar spectrum is well reproduced with an effective temperature of $T_{\text{eff}} = 9500 \pm 500$ K, consistent with the work of Hernández et al. (2005). Blueshifted CS absorption components are superimposed on the core of the Balmer lines from H ζ to H β , with increasing depth with wavelength. Emission is observed in the wings of the CS absorption of H β . H α displays a P Cygni profile of type III. A strong absorption component with emission in the wings is also observed in the Ca II K line. The He I lines at 5875 Å, 6678 Å and 7065 Å display broad emission profiles. The lines of the multiplet 42 of Fe II have blueshifted CS absorption superimposed on centered emission profiles. The O I 777 nm triplet shows emission in the blue wing. The O I 8446 Å triplet is filled with emission, while the Ca II IR-triplet displays single-peaked lines. The core of the Paschen lines seem to be filled with emission. The cores of a few other metallic lines might be superimposed on a faint emission component.

We have calculated the LSD profiles without performing a special cleaning to the Kurucz mask. The resulting I profile displays a photospheric profile still slightly contaminated with CS features, but could not be improved. It is well fit with a single photospheric profile together with a Gaussian that models the emission. The small absorption component in the core has been rejected from the fit. The result is shown in Fig. A39.

A40 HD 152404 (= AK Sco)

HD 152404 is a binary system, part of the the Upper Centaurus Lupus OB association, situated at a distance of 103 pc (van Leeuwen 2007, Hipparcos,). A strong IR excess is recorded in the direction of the system, confirming its PMS nature (Andersen et al. 1989).

Our observations confirm the SB2 nature of the system, with two components of similar temperature. We use a modified version of the BINMAG1 code of O. Kochukhov (private communication), which computes the composite spectrum of a binary star, to fit the observed spectrum. This code takes as input two synthetic spectra of different effective temperatures and gravities, each corresponding to one of the two components. The code convolves

the synthetic spectra with instrumental, turbulent and rotational broadening profiles and combines them according to the radii ratio of the components specified by the user, and the flux ratio at the considered wavelength given by the atmosphere models, to produce the spectrum of the binary star. The individual synthetic spectra have been calculated in the local thermodynamic equilibrium (LTE) approximation, using the code SYNTH of Piskunov (1992). SYNTH requires, as input, atmosphere models obtained using the ATLAS 9 code (Kurucz 1993) and a list of spectral line data obtained from the VALD database⁵ (Vienna Atomic Line Data base). Our observations are consistent with an effective temperature of 6500 ± 100 K for both components (Alencar et al. 2003) and a ratio of radii $R_p/R_s = 1.3 \pm 0.15$. We used the new Hipparcos parallaxes (van Leeuwen 2007) and the photometric data (Perryman & ESA 1997) to compute the luminosity of the system, then we derived the luminosity of the two components : $L_p/L_\odot = 0.94 \pm 0.21$, and $L_s/L_\odot = 0.71 \pm 0.21$.

A redshifted CS absorption component is superimposed on the core of the Balmer lines from H ϵ to H β . H α displays an inverse P Cygni profile of type III. Faint emission is observed in the core of the Ca II K line. Strong CS absorption components are observed in the He I lines at 5875 Å, 6678 Å and 7065 Å, as well as in the O I 777 nm triplet. No other CS feature is observed.

We first calculated the LSD profiles without performing a special cleaning to the Kurucz mask. The result shows the photospheric composite profile of the binary with very broad wings. We have therefore calculated various masks by making a selection on the central depth and excitation potential of the lines. We find that a mask containing only lines with central depths of less than 0.30 gives a satisfactory result : an LSD profile with photospheric wings. In order to determine the $v \sin i$ and v_{rad} of the two components, we performed a least-square fit to the composite I profile of the binary. Each profile is fitted with the normalised sum of two photospheric functions. We adopted an isotropic macroturbulent velocity of 2 km.s^{-1} in order to fit the wings of the LSD I profiles. The free parameters of the fitting procedure are the centroids, depths and $v \sin i$ of both components. The result is shown in Fig. A40. As both stars have the same temperature, the ratio of the equivalent widths of the two components measured on the LSD profile is equal to the luminosity ratio L_p/L_s (Alecian et al. 2008a). From our fit to the composite profile we derive a luminosity ratio $L_p/L_s = 1.7$, consistent with our radii ratio determined above from the fit of the spectrum ($R_p/R_s = 1.3 \pm 0.15$).

A41 HD 163296

HD 163296 is an isolated Herbig Ae star situated at a distance of 119 pc (van Leeuwen 2007), not associated with any star forming regions, and not illuminating a bright nebulosity. However the star is associated with Herbig-Haro objects (Grady et al. 2000a). It displays a large IR excess well reproduced with a two-temperature disk, perhaps reflecting the presence of a gap inside the accretion disk (Malfait et al. 1998). The presence and the geometry of the disk has been confirmed by Grady et al. (2000a) using coronagraphic imaging with the Space Telescope Imaging Spectrograph (STIS) on board the Hubble Space Telescope (HST). All these characteristics leave no doubt that HD 163296 belongs to the Herbig Ae/Be class of objects. We used the Hipparcos photometric data to compute the luminosity of the star.

⁵ <http://ams.astro.univie.ac.at/~vald/>

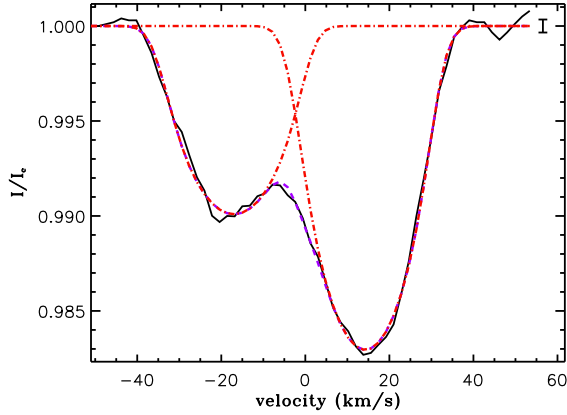


Figure A40. As Fig. A5 for AK Sco

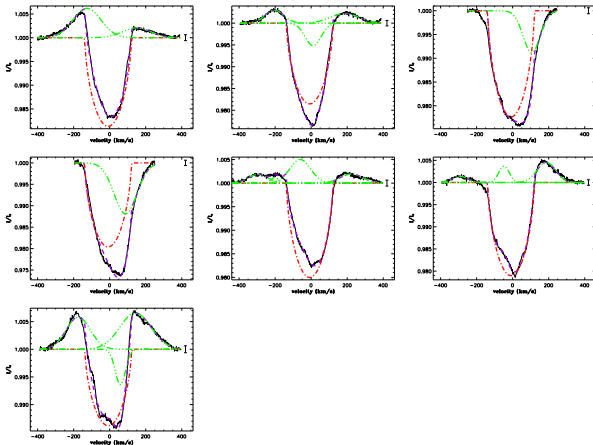


Figure A41. As Fig. A5 for the May 22nd, 23rd, 24th 09 :49, 24th 14 :48, 25th 09 :52, 25th 14 :53, and Aug. 25th 2005 observations (from top left to bottom right) of HD 163296.

HD 163296 displays circumstellar activity that could be of magnetic origin, such as rotational modulation in non-photospheric lines (Catala et al. 1989), X-ray emission (Günther & Schmitt 2009), and emission lines of highly ionised species (Deleuil et al. 2005, e.g. O VI,). The spectrum displays strong circumstellar emission. $H\alpha$ is strongly variable, going from a double-peaked emission line profile to a P Cygni of type IV profile (Thé et al. 1985a; Catala et al. 1989). In our spectra of May 2005, $H\alpha$ appears single-peaked with variable blueshifted absorption components, while in August 2005, a strong P Cygni of type IV profile is observed, confirming the high variability of $H\alpha$. $H\beta$ displays variable emission and blueshifted absorption components. Faint emission is observed in the cores of $H\gamma$ and $H\delta$. Fe II lines, including those of multiplet 42, the O I 8446 Å and Ca II IR triplets display single-peaked emission profiles. Faint blueshifted emission is also present in the core of the Paschen lines. The Ca II K line displays a strong and complex absorption profile. The He I lines at 5875 Å, 6678 Å, and 7065 Å show very broad double-peaked emission profiles, with a stronger blue peak with respect to the red one. The portions of the spectrum not contaminated with CS features is consistent with temperature and gravity determination of Folsom et al. (2012, $T_{\text{eff}} = 9200 \pm 300$ K, $\log g = 4.2 \pm 0.3$).

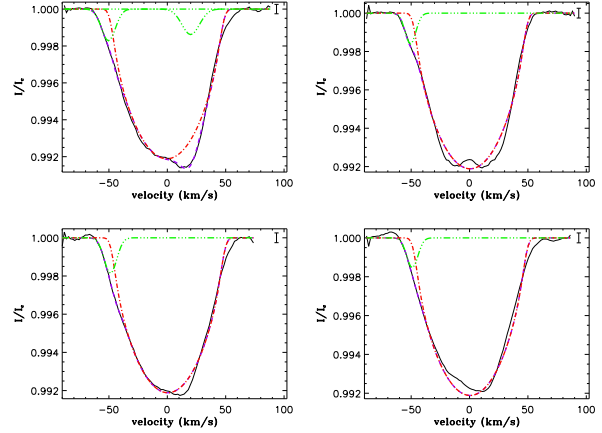


Figure A42. As Fig. A5 for the Feb. 20th, 22nd, May 22nd, and Aug. 24th 2005 observations (from top left to bottom right) of HD 169142

We first cleaned the mask in order to reject the lines contaminated with CS features. The resulting LSD I profiles still show contamination. We therefore tried to make a selection on the central depth of the lines and the excitation potential, but we could not improve the profiles. We therefore fit the 7 observations at once, with single photospheric functions superimposed with Gaussians modelling the emission or absorption features where necessary, and by forcing the $v \sin i$ and v_{rad} to be identical for all the observations. The photospheric depths of the profiles can vary from one observation to the other, because of the variable CS contamination. The result is shown in Fig. A41.

A42 HD 169142

HD 169142 is an isolated Herbig Ae star not associated with a star forming region, nor illuminating a bright nebulosity. No Hipparcos data has been obtained, which makes a precise determination of its distance from the Sun very difficult. We therefore used the photometric distance derived by Sylvester et al. (1996), and the photometric data of Vieira et al. (2003) to compute the luminosity. The spectral energy distribution in the near- and far-IR can be well reproduced with a two-temperature dust disk model, like many other Herbig Ae stars (Malfait et al. 1998).

The spectrum of HD 169142 is consistent with the temperature and gravity determination of Folsom et al. (2012, $T_{\text{eff}} = 7500 \pm 200$ K). It displays few CS features. Faint emission is observed in the core of $H\beta$. $H\alpha$ displays a single-peaked emission profile. The He I D3 line shows a double-peaked emission profile. The O I 777 nm triplet is slightly stronger than predicted, with weak emission in the blue wing. No other CS contribution is observed in the spectrum.

We first calculated the LSD profiles without performing a special cleaning to the Kurucz mask. The resulting LSD I profiles are absorption profiles slightly distorted due to circumstellar contribution, and have broad wings, not easy to fit with a photospheric function. Therefore we have calculated various masks from by making a selection on the depth and excitation potential. We find that a mask containing lines with central depths of less than 0.6 gives a good compromise between the SNR of the resulting I profile and its shape. The I profiles are still slightly contaminated with CS features, but could not be improved. We fit the four observations simultaneously, with a single photospheric function and se-

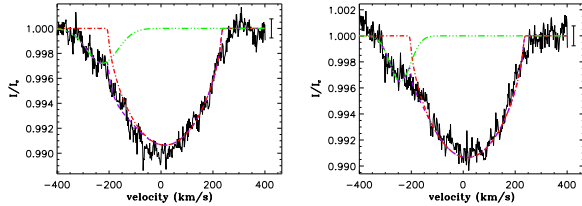


Figure A43. As Fig. A5 for the Mar 2007 (left) and Apr. 2008 (right) observations of HD 174571

veral Gaussians modelling the CS contribution. In this fit we force the photospheric depth, $v \sin i$, and v_{rad} to be the same for the four observations. The result is shown in Fig. A42.

A43 HD 174571 (=MWC 610)

HD 174571 is often classified as a classical Be star. However its near-IR excess is large and more similar to those observed among the Herbig Ae/Be class of objects (Vieira et al. 2003). No star forming regions or nebulosity are known to be associated with the star, and the Hipparcos parallax (Perryman & ESA 1997) is too uncertain to constrain the distance of the star. We therefore could not estimate the luminosity directly using photometric data. Instead, we used the well-constrained effective temperature and surface gravity of Frémat et al. (2006, $T_{\text{eff}} = 21000 \pm 1500$ K and $\log g = 4.00 \pm 0.10$ (cgs)) to place the star in the $T_{\text{eff}} - \log g$ diagram and derive the mass, radius, and age. We then derived a luminosity $\log L/L_{\odot} = 3.58 \pm 0.21$, and using the photometric data of Vieira et al. (2003), we estimated the distance of the star at 540^{+80}_{-70} pc.

The spectrum of HD 174571 is well reproduced with a non-LTE synthetic spectrum of effective temperature $T_{\text{eff}} = 22000$ K, consistent with the work of Frémat et al. (2006). Variable CS contributions are observed in the spectra. Double-peaked emission features are superimposed on the core of the Balmer lines from H δ to H β with increasing strength with wavelength. H α displays a double-peaked emission profile. The strongest He lines of the spectrum are slightly distorted, which could be due to CS material. Many double-peaked emission profiles are observed in the spectrum, which could come from CS Fe II. The O I 777 nm triplet presents emission in the wings. The O I 8446 Å triplet displays a double-peaked emission profile. Double-peaked emission is also observed in the cores of the Paschen lines. While the Ca II K line is only contaminated with a strong and narrow interstellar (IS) absorption component, the Ca II IR triplet seems to display single-peaked emission.

We have cleaned the Kurucz mask in order to eliminate the CS contribution. The resulting LSD I profiles do not look like photospheric profiles, certainly due to CS contamination, and could not be improved. We fit both observations simultaneously, with a single photospheric function, and Gaussians modelling the CS features. The result is shown in Fig. A43.

A44 HD 176386

HD 176386 is located in the R Coronae Australis star-forming region (Fernández et al. 2008), at ~ 1 arcminute from TY CrA. We used the new Hipparcos parallax (van Leeuwen 2007) and photometric data (Perryman & ESA 1997) to derive the luminosity of the

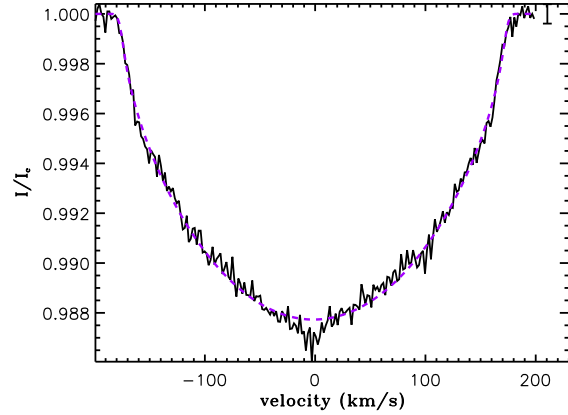


Figure A44. As Fig. A5 for HD 176386

star. HD 176386 lacks strong near-IR emission; however its mid-IR energy distribution reveals the presence of an extended emission region and a large-scale structure, as well as silicate emission distributed in a disk (Prusti et al. 1994; Boersma et al. 2009). Ongoing accretion has been reported (Grady et al. 1993). This star is therefore very probably still in the PMS phase of stellar evolution.

Using our automatic procedure, we find that the spectrum of HD 176386 is well reproduced with $T_{\text{eff}} = 11500 \pm 350$ K and $\log g = 4.5$, consistent with the work of Paunzen et al. (2001). The He I lines at 5875 Å and 6678 Å display V-shaped profiles that could be due to CS emission. The O I 777 nm triplet is stronger than predicted. No other CS manifestation is observed in the spectrum.

We have calculated the LSD profiles without performing a special cleaning to the Kurucz mask. The resulting LSD I profile displays a photospheric shape well fitted with a single photospheric function. The result is plotted in Fig. A44

A45 HD 179218

HD 179218 is an isolated Herbig Ae star displaying strong IR excess that is well reproduced with a two-temperature dust-disk model (Malfait et al. 1998). We used the new Hipparcos parallax (van Leeuwen 2007) and photometric data (Perryman & ESA 1997) to derive the luminosity of the star.

The spectrum of HD 179218 is consistent with the temperature and gravity determination of Folsom et al. (2012, $T_{\text{eff}} = 10500$ K, $\log g = 3.9 \pm 0.2$). The observed Fe II lines seem systematically fainter than the computed lines, revealing possible circumstellar contamination. Faint emission is observed in the core of the Balmer lines from H δ to H β , while H α displays a strong single-peaked emission superimposed on the core of the photospheric profile. The Ca II K line, and the O I 777 nm and O I 8446 Å triplets display absorption profiles that are stronger than predicted. The Paschen lines and the Ca II IR triplet do not seem to be contaminated with circumstellar features. The He I lines at 5875 Å and 6678 Å display inverse P-Cygni profiles.

We have cleaned the Kurucz mask by removing the lines obviously contaminated with CS features, then calculated the LSD profiles for the three observations. The three profiles display photospheric shapes. We fit them simultaneously with photospheric functions, by forcing the photospheric parameters (depth, $v \sin i$, v_{rad}) to be the same for each one of the observations. The resulting fit is plotted in Fig. A45.

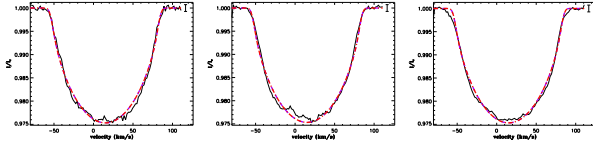


Figure A45. As Fig. A5 for the Feb. 2005 (left), Aug. (middle) 2005, and Oct. 2009 (right) observations of HD 179218.

A46 HD 203024

HD 203024 is a Herbig Ae star belonging to the Cepheus R2 association, situated at a distance of 420 pc (Kun et al. 2000). The spectral energy distribution shows a slope in the IRAS wavelength region that is typical of optically thick disks surrounding Herbig Ae/Be stars (Kun et al. 2000).

Corporon & Lagrange (1999) reports the detection of the Li I line at 6707 Å, and conclude that a low-mass star companion might be present close to the Herbig star. In our spectra we detect the spectral lines of a secondary star at almost the same radial velocity as the primary. The primary is a fast rotator, with $v \sin i = 162 \text{ km.s}^{-1}$; the secondary rotates more slowly with $v \sin i = 57 \text{ km.s}^{-1}$. We used the same method as for HD 152404 (= AK Sco) to compute the synthetic composite spectrum of this binary star. We find that our spectra are well reproduced with effective temperatures of 9250 K and 6500 K for the primary (P) and secondary (S), respectively, with a ratio of radii R_P/R_S equal to 1.5. We also estimate the ratio of the luminosity to be $L_P/L_S = 9.2$. We used the SIMBAD photometric data to derive the luminosity of the system: $\log(L/L_\odot) = 1.93$, and then the luminosity of each component: $\log(L_P/L_\odot) = 1.88$ and $\log(L_S/L_\odot) = 0.93$.

The temperature that we derive for the secondary is too high to display a detectable Li I line at 6707 Å in the spectrum. We confirm the presence of a line at about 6708 Å but it is not clear whether it is of photospheric origin. As the spectra that we obtained are relatively noisy compared to the depth of the lines from the secondary, we tried to change the effective temperature of the secondary. A temperature as low as 5000 K could still fit the spectrum reasonably well, but even at this temperature we do not fit the feature observed at 6708 Å. The feature observed at 6708 Å does not appear to belong to the secondary component that we detect, and its origin is therefore not understood.

The spectrum displays little circumstellar contamination. The blue part of the Ca II K line is superimposed on a strong and complex CS absorption, while the O I 777 nm and Ca II IR triplets are stronger than predicted by the synthetic spectrum. Faint emission is superimposed on the blue side of the core of H α . A faint absorption is visible in the He I D3 line, while no photospheric feature is predicted by the synthetic spectrum. No other evidence of CS material is observed in the spectrum.

We have cleaned the mask in order to reject the lines contaminated with CS features to compute the synthetic profiles of the binary star. The resulting LSD profiles show both components of the system at almost the same radial velocity. While the secondary radial velocity changed slightly from August 2005 to November 2007, that of the primary did not change. Due to the different temperatures of the stars, and the fact that the LSD profiles have been computed with a line list appropriate for the primary, the ratio of the LSD profiles of both components cannot be used to derive the luminosity ratio (as in HD 200775, e.g., Alecian et al. 2008). However the fit of the combined profile can give us the radial velocities and the $v \sin i$ of both stars. We used the same method as for AK Sco to

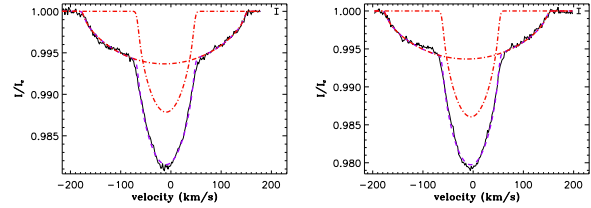


Figure A46. As Fig. A5 for the Aug. 2005 (left) and Nov. 2007 (right) observations of HD 203024.

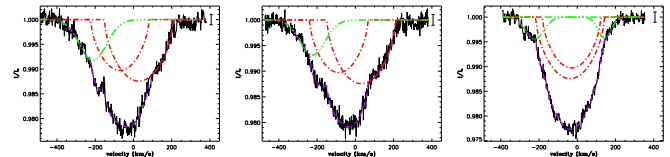


Figure A47. As Fig. A5 for the Jun. 2006 (left), Dec. 2006 (middle), and Nov. 2007 (right) observations of HD 216629 (= IL Cep).

the fit the LSD profiles of both observations, by fixing a macroturbulent velocity of 2 km.s^{-1} , and by forcing the $v \sin i$ of both components, as well as the photospheric depth and the radial velocity of the primary to be identical for both observations. We could not find a satisfactory fit of both profiles by forcing the photospheric depth of the secondary to be identical for both observations, which means that its depth has varied, but this is not yet understood. The result is presented in Fig. A46.

A47 HD 216629 (=IL Cep)

Jordi et al. (1996) re-analysed the membership of the Cepheus OB3 association, and found that IL Cep is part of the youngest subgroup (b) of the region. The Hipparcos parallax (Perryman & ESA 1997) is not well enough constrained to be useful. We therefore used the Crawford & Barnes (1970) distance modulus determination ($d = 720^{190}_{-150}$ pc) and the Hipparcos photometric data to derive the luminosity of the star. The resulting position of the star in the HR diagram is well below the ZAMS, which may mean that the luminosity determination is wrong, and therefore IL Cep is not a member of Cep OB3.

The spectrum of IL Cep is well fit with an effective temperature $T_{\text{eff}} = 19000 \text{ K}$, consistent with the work of Finkenzeller (1985). Wheelwright et al. (2010) find that IL Cep is a double-lined spectroscopic binary, using spectroastrometric methods. They attempted a separation of the unresolved spectrum into two composite spectra, and find that the secondary has a spectral type B4, while the primary is a B3 star. Indications of binarity can be found in our spectra, as explained below. As both stars have different temperatures they should have different luminosity. The quality of our spectra is not sufficient to attempt a determination of the luminosity ratio. For this reason, and also because the position of the binary in the HR diagram is well below the ZAMS (see Fig. 4), no mass, radius, nor age of the components have been estimated.

Circumstellar features are observed in the spectrum, and vary from one observation to the other. The cores of H γ and H δ are filled with CS emission. A double-peaked emission line is superimposed on the core of H β , while H α displays a single-peaked emission profile. Many Fe II lines (including those of multiplet 42), the Paschen lines, and the O I 777 nm, O I 8446 Å, and Ca II IR triplets

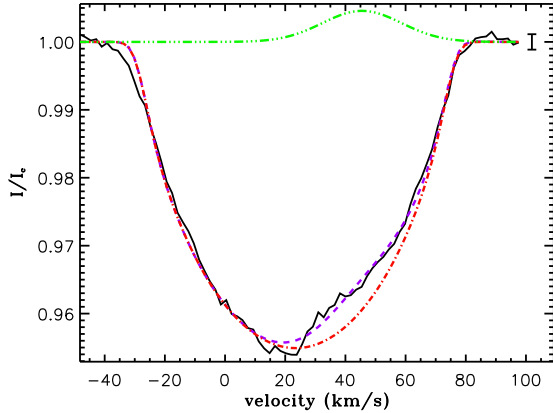


Figure A48. As Fig. A5 for HD 244314

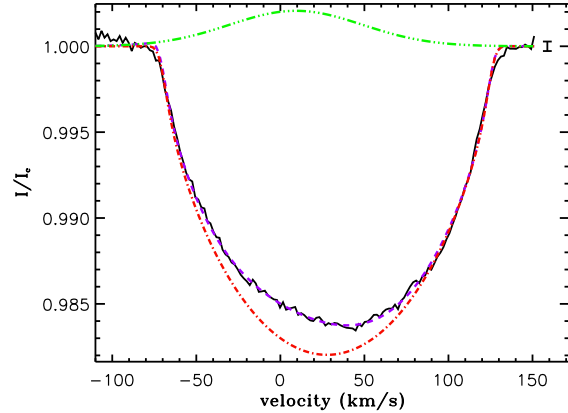


Figure A49. As Fig. A5 for HD 244604

display double-peaked emission profiles. A narrow and deep absorption line is observed in the Ca II K line. The broadening and the depth of the He I lines vary from one observation to another, which may be due to the spectroscopic companion mentioned by Wheelwright et al. (2010).

We have cleaned the mask in order to reject the lines contaminated with CS features to compute the synthetic profiles of the binary star. The profiles of June and December 2006 look similar, revealing a broad and complex photospheric profile, that could be formed by an SB2, superimposed with a broad blue wing. The profile of November 2007 is different showing a single photospheric profile, with slightly less broad wings, and with a photospheric depth much deeper than in 2006. This observation could have been obtained during a spectroscopic conjunction, so that the observed profile could be the result of the superposition of the two components at a similar radial velocity, and therefore consistent with an SB2 profile. We fit the three observations simultaneously with the photospheric function of a double star (as in HD 152404 = AK Sco), and many Gaussian functions to reproduce the wings. In this fitting procedure the photospheric depths and $v \sin i$ of both components were forced to be identical for both observations, while the v_{rad} were free to vary from one observation to another. The radial velocities of the two components are not significantly different between June 2006 and Dec. 2006, suggesting that both observations may have been obtained at a similar orbital phase, while they are definitely different in 2007. The resulting fit is shown in Fig. A47.

The success of this fitting procedure, the fact that in 2007 both radial velocities are found to be very similar, and that the depth of the combined profile is much larger than in the other observations, confirm the SB2 nature of IL Cep. The combination of large $v \sin i$ for both components (180 and 150 km.s⁻¹), the small velocity separation between the two components of the spectral lines, and the relatively low SNR of our data, explain our inability to detect the SB2 nature of IL Cep within the spectrum itself, and illustrate the capability of the LSD procedure to provide more information on the object than the analysis of the individual spectral lines.

A48 HD 244314 (=V1409 Ori)

HD 244314 is part of the Orion star forming region situated at a distance of 375 pc (Brown et al. 1994). We used the

Miroshnichenko et al. (1999a) photometric data (V_0 and $E(B - V)$) to derive the luminosity of the star. Miroshnichenko et al. (1999a) detected near-IR excess, and classified the star as a PMS candidate.

The spectrum of HD 244314 is consistent with the effective temperature determination of Vieira et al. (2003, $T_{\text{eff}} = 9250 \pm 500$ K), and displays little CS contamination. The cores of H γ and H δ are filled with emission and superimposed on a narrow blueshifted CS absorption line. The core of H β is superimposed on a P Cygni profile. H α displays a P Cygni profile of type II. The core of the Ca II K photospheric line is filled with emission and superimposed on a narrow and deep IS absorption line. The wings of the Fe II multiplet 42 lines are in emission. The He I lines at 5875 Å, 6678 Å and 7065 Å show broad and double-peaked emission profiles. The wings of the O I 777 nm and O I 8446 triplets are in emission. The core of the Paschen lines are filled with emission, and the Ca II IR-triplet displays single-peaked emission lines.

We have calculated the LSD profiles without performing a special cleaning to the Kurucz mask. The result shows a photospheric profile slightly distorted, which we believe to be due to circumstellar contamination. We fit the profile with a photospheric function and one Gaussian function. The result is shown in Fig. A48.

A49 HD 244604 (=V1410 Ori)

HD 244604 is part of the Orion star forming region situated at a distance of 375 pc (Brown et al. 1994). We used the photometric data of de Winter et al. (2001) to derive the luminosity of the star. The spectral energy distribution displays an IR excess well reproduced using a model of a two-temperature dust disk, as is the case for most HAeBe stars (Malfait et al. 1998).

Using our automatic procedure, we find that the spectrum of HD 244604 is well reproduced with $T_{\text{eff}} = 8200 \pm 200$ K and $\log g = 4.0$, consistent with the work of Miroshnichenko et al. (1999a). The cores of the Balmer lines from H ζ to H γ are filled with emission. The core of the H β profile is superimposed on a single-peaked, slightly redshifted, emission, as well as a blueshifted absorption. H α displays a P Cygni profile of type II. A narrow, faint and blueshifted CS absorption line is superimposed on the photospheric profile of the Ca II K line. Faint emission is observed in the core of the photospheric profiles of the lines of multiplet 42 of Fe II, and in the O I 8446 Å triplet. Broad and faint emission are observed in the He I lines 5875 Å, 6678 Å and 7065 Å, where nei-

ther absorption nor emission is predicted by the synthetic spectrum. Faint emission is observed in the wings of the O I 777 nm triplet. The cores of the Paschen lines are filled with emission, and the Ca II IR-triplet displays strong and single-peaked emission profiles.

We have cleaned the mask in order to reject the lines contaminated with CS features, to compute the LSD profiles. The result shows a slightly distorted single photospheric profile, certainly due to CS contamination, but could not be improved. We fit the profile with a photospheric function and a Gaussian function. The result is shown in Fig. A49.

A50 HD 245185 (=V1271 Ori)

HD 245185 is part of the λ Ori star-forming region (Murdin & Penston 1977) situated at a distance of 450 pc (Dolan & Mathieu 2001). We used the Tycho-2 photometric data (Høg et al. 2000), and converted them into the Johnson system using the calibration formula 1.3.20 of the Hipparcos and Tycho catalogues (Perryman & ESA 1997, p. 57), to derive the luminosity of the star. The spectral energy distribution displays IR excess that is well reproduced using a two-temperature dust disk model, similar to most HAeBe stars (Miroshnichenko et al. 1999b).

The spectrum is consistent with the temperature and gravity determination of Folsom et al. (2012, $T_{\text{eff}} = 9500 \pm 750$ K). All the metallic lines of the spectrum, except the O I and Si II lines between 6000 and 6500 Å, are much weaker than predicted by the synthetic spectrum. This might be due to CS extinction, but it could also be due chemical peculiarities consistent with the work of Folsom et al. (2012) that report λ Boo peculiarities. Many circumstellar features are observed in the spectrum. The cores of the metallic lines, including Ca II K, are superimposed on narrow emission features. The cores of the Balmer lines from H ζ to H β are also superimposed on emission lines, of increasing amplitude with wavelength. H α displays a double-peaked emission line. The He I lines at 5875 Å, 6678 Å, and 7065 Å show broad and double-peaked emission profiles. The cores of the Paschen lines are filled with emission, and the O I 8446 and Ca II IR-triplets show small P Cygni profiles. The wings of the O I 777 nm triplet are in emission.

We tried to clean the the Kurucz mask, but could not get rid of the emission in the core of the LSD profile. We therefore decided to use the full mask to obtain a more accurate value of the $v \sin i$, and fit the LSD profile with a photospheric function and a Gaussian. The result is shown in Fig. A50

A51 HD 249879

Vieira et al. (2003) proposes that HD 249879 is part of the Gemini OB1 star association, situated at a distance 2000 pc (Vieira et al. 2003). We used the photometric data of Vieira et al. (2003) to derive the luminosity of the star. No spectral energy distribution has yet been published, but the strong IR excess, as well as the presence of H α emission led Gregorio-Hetem et al. (1992) to classify the star as an Herbig Ae/Be.

The metallic lines and the Balmer lines of the spectrum are well fit with an effective temperature $T_{\text{eff}} = 9000 \pm 1000$ K, which is inconsistent with the unique temperature determination available in the literature of 12000 K (Vieira et al. 2003). We suggest that the combination of a large $v \sin i$ (~ 250 km.s $^{-1}$) Vieira et al. (2003) and their low SNR (~ 80) meant that they were not able to resolve the metallic lines. In contrast, we can easily detect and resolve the metallic lines with our higher SNR spectrum (~ 550), and therefore

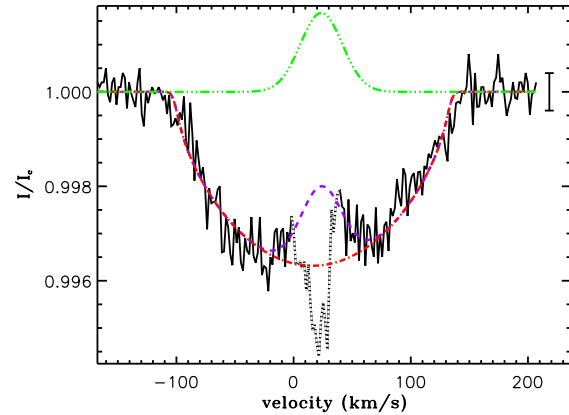


Figure A50. As Fig. A5 for HD 245185

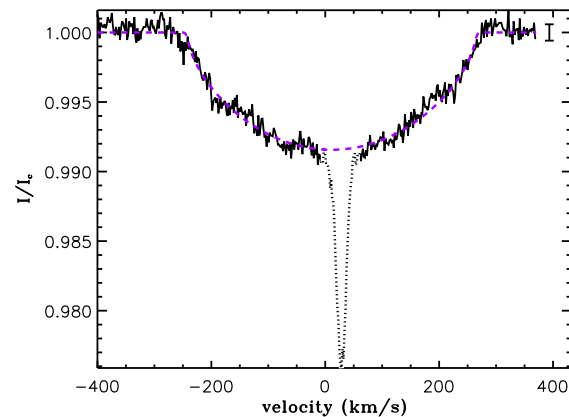


Figure A51. As Fig. A5 for HD 249879

get a better estimate of the effective temperature of the star. The spectrum shows only a few CS features. The Ca II K line is much stronger than predicted. Weak emission is observed in the cores of H α , the O I 777 nm triplet, and the Paschen line P12. The O I 8446 Å triplet seems to show double-peaked emission, while the Ca II IR triplet might display an inverse P Cygni profile.

We have cleaned the mask in order to reject the lines contaminated with CS features, to compute the LSD profiles. The result is a photospheric profile with a strong and narrow absorption line superimposed on the core. Its origin is unknown, but a careful examination of the spectrum confirms that the metallic lines are indeed superimposed on narrow absorption. We therefore decided to ignore this absorption in the fitting procedure, using only a photospheric function. The result is shown in Fig. A51.

A52 HD 250550

HD 250550 is located centrally in a small obscuring cloud, and is also the central object of a bright arc of nebulosity (Herbig 1960). No reliable distance or parallax determination were obtained for this star. We are therefore unable to determine its luminosity. Based on its spectral energy distribution, HD 250550 has been classified as a group I object by Hillenbrand et al. (1992); these are objects that are surrounded with flat optically thick accretion disks.

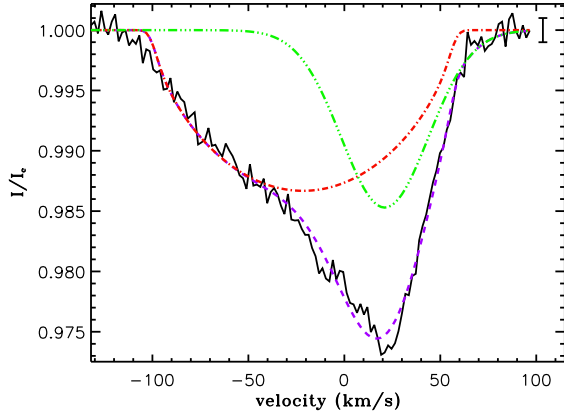


Figure A52. As Fig. A5 for HD 250550

The spectrum of HD 250550 is highly contaminated with CS features, which makes temperature determination difficult. The few portions of the spectrum not contaminated with CS features is well fit with $T_{\text{eff}} = 12000 \pm 1500$ K, consistent with the work of Hernández et al. (2004). The strongest metallic lines show emission profiles, sometimes with a P Cygni absorption component. When no emission is observed in these lines, a strong redshifted CS absorption is superimposed on the photospheric profiles. A strong blueshifted CS absorption is superimposed on the core of the Balmer lines, from H θ to H γ , of increasing strength with wavelength. In H γ and H δ , a redshifted emission is also observed in the core of the lines. The core of H β is superimposed on a P Cygni profile with a saturated blueshifted absorption. H α displays a P Cygni profile of type IV. The Ca II K line shows a strong highly blueshifted absorption line, as well as centered IS absorption, and emission in the red wing of the profile. The He I lines at 5875 Å, 6678 Å, and 7064 Å are much stronger than predicted, and display V-like shapes. The O I 777 nm triplet shows a P Cygni profile. The core of the Paschen lines are superimposed on emission, while the O I 8446 Å and Ca II IR triplets show very strong single-peaked emission profiles.

We have cleaned the mask in order to reject the lines contaminated with CS features. The resulting LSD I profile shows a photospheric profile superimposed to a CS redshifted absorption line, but could not be improved. We therefore fit the LSD I profile with a photospheric function and a Gaussian function. The result is shown in Fig. A52.

A53 HD 259431 (=V700 Mon)

HD 259431 is associated with the reflection nebula VdB 82, a member of the association of reflection nebulae Mon R1 (van den Bergh 1966b). Mon R1 is part of the same cloud complex as NGC 2264 (Herbst et al. 1982), situated at a distance of 660 pc (Kharchenko et al. 2005), which disagrees with the Hipparcos parallax of HD 259431 ($\pi = 3.45 \pm 1.41$, Perryman & ESA 1997). The new Hipparcos parallax of van Leeuwen (2007) ($\pi = 5.78 \pm 1.22$) is even larger than the previous determination, and still inconsistent with an association of this star with Mon R1. Furthermore this recent determination of the parallax is also inconsistent with our temperature determination for the star; in the HR diagram, the star falls well below the ZAMS. Because of the reflection nebulaosity, we suspect that the Hipparcos data might not be suitable for parallax determination, and we adopt a distance of 660 pc. We used

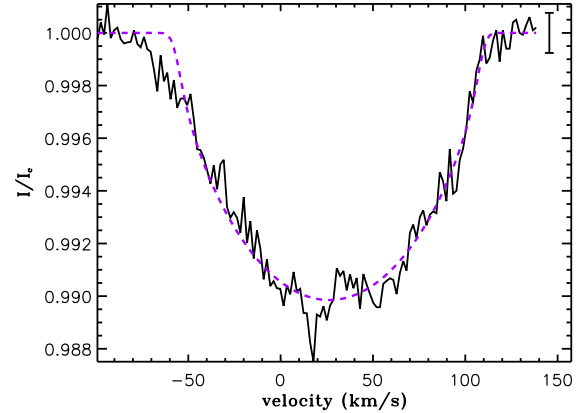


Figure A53. As Fig. A5 for the 2009 observation of HD 259431.

the Hipparcos photometric data (Perryman & ESA 1997) to derive the luminosity. The spectral energy distribution as well as mid-IR interferometric observations are well reproduced with an optically thick gaseous disk (Kraus et al. 2008).

The spectrum of HD 259431 is strongly contaminated with variable CS features. The few metallic lines that are not contaminated are well fit with an effective temperature $T_{\text{eff}} = 14000 \pm 1000$ K, consistent with the work of Hernández et al. (2004). The cores of the Balmer lines, from H ϵ to H γ , are superimposed on a double-peaked emission profile, with a narrow central absorption that is deeper than the emission. In H δ and H γ narrow blueshifted absorption components appear in the blue part of the CS emission. H β displays a double-peaked emission profile, with a strong central absorption that goes below the continuum, and a blueshifted narrow absorption superimposed on the blue wing of the emission. H α shows a strong double-peaked emission profile. The Ca II K lines shows a broad emission superimposed on a narrow absorption that could be of IS origin. Most of the metallic lines display broad double-peaked emission profiles, with a relatively faint central absorption. The central absorption is much stronger in the lines of multiplet 42 of Fe II. The red part of the He I lines at 5875 Å and 6678 Å are greatly changed between March 2007 and February 2009: the profile of 2007 is much broader on the red part, while the blue wing stayed unchanged. The red part of these He lines in 2009 is consistent with the predicted photospheric profile. While the O I 777 nm triplet shows a single-peaked emission profile, the Paschen lines and the O I 8446 Å and Ca II IR triplets display strong double-peaked emission profiles, with central absorptions that are faint and narrow in the O I triplet and in the Paschen lines, but stronger and broader in the Ca II triplet.

We have cleaned the mask in order to reject the lines contaminated with CS features. The resulting three LSD I profiles display photospheric shape, and can be fitted with a photospheric function, giving consistent $v \sin i$. However, the profiles from 2007 and 2010 are much noisier than that of 2009, so that a combination of the three profiles did not improve the $v \sin i$ determination of the star compared to determination from the 2009 profile alone. We therefore decided to fit only the profile of 2009 with a single photospheric function. The result is shown in Fig. A53.

A54 HD 275877 (=XY Per)

XY Per illuminates the bright nebosity VdB 24 (van den Bergh 1966b). It is a strong visible and near-IR photometric variable star (e.g. Oudmaijer et al. 2001), and belongs to the UXOR class of stars (Mora et al. 2004), whose the prototype is HD 293782 = UX Ori (Sec. A61). For the same reasons as in the case of UX Ori, we used the photometric data of Oudmaijer et al. (2001) at the brightest magnitude, together with the Hipparcos parallax (Perryman & ESA 1997), to determine the luminosity of the star. We did not use the new Hipparcos parallax of van Leeuwen (2007) as it is totally inconsistent with the old one, and with the effective temperature of the star. The near-IR excess observed in XY Per is typical of the Herbig Ae/Be class of objects (Eiroa et al. 2001).

The spectrum of XY Per is strongly contaminated with CS features, as is common for UXOR-type stars. Uncontaminated, lines and the wings of the Balmer lines are consistent with $T_{\text{eff}} = 9000 \pm 500$ K, corresponding to the spectral classification of Mora et al. (2001). Most of the metallic lines, including the Ca II K line, as well as the core of the Balmer lines are superimposed on strong CS absorption. Emission is also observed in the wings of the CS absorption in the core of H β . H α displays a double-peaked emission profile, with a deep narrow central absorption that goes below the continuum. The He I lines at 5875 Å, 6678 Å and 7065 Å, and the O I 777 nm triplet show inverse-P Cygni profiles, with weak blue emission, and a strong central absorption. The O I 8446 Å triplet is also much stronger than predicted. The Ca II IR triplet shows double-peaked emission lines, with very strong and narrow central absorptions. The core of the Paschen lines may be contaminated with CS emission.

We have cleaned the mask in order to reject the lines contaminated with CS features. The resulting LSD I profiles shows photospheric shapes still slightly contaminated with emission on both the blue and red sides. After a careful examination of the spectrum, the few lines not obviously contaminated with CS features are found to have a V shape, consistent with the LSD I profiles. Both profiles are well fitted with a photospheric plus Gaussian functions, giving consistent $v \sin i$. However, because the profile from 2009 is relatively noisy, including it in the fit together with the profile from 2006 did not improve the $v \sin i$ determination of the star. We therefore decided to only fit the profile of 2006 with a single photospheric function and two Gaussian functions. The result is shown in Fig. A54.

A55 HD 278937 (= IP Per)

According to its Galactic coordinates and its proper motions (from the Tycho-2 catalogue, Høg et al. 1998, 2000), IP Per is very likely associated with the Per OB 2 association situated at a distance of ~ 320 pc (de Zeeuw et al. 1999). IP Per is a photometric variable; the variations are assumed to be caused by moving circumstellar material which shadows the star when it crosses the line of sight (Miroshnichenko et al. 2001). Therefore, the minimum magnitude is very likely close to the true magnitude of the star. We used the photometric data of Miroshnichenko et al. (2001) at the brightest magnitude to derive the luminosity of the star. A large IR excess is clearly seen in the spectral energy distribution, which can be reproduced with a two-temperature disk model, as in other HAeBe stars (Miroshnichenko et al. 2001).

The spectrum of IP Per is consistent with the temperature and gravity determination of Folsom et al. (2012, $T_{\text{eff}} = 8500$ K,

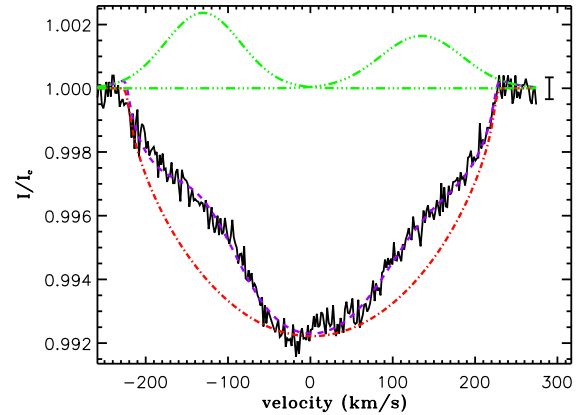


Figure A54. As Fig. A5 for the 2006 observation of XY Per.

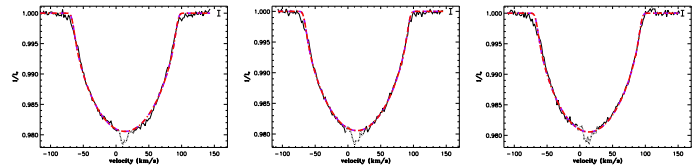


Figure A55. As Fig. A5 for the Feb. 21st 06 :26 (left), 21st 07 :50 (middle), and 22nd (right) 2005 observations of IP Per.

$\log g = 4.1 \pm 0.2$). Only few CS features are observed in its spectrum. Weak emission fills the core of H γ , while the core of H β is superimposed on a faint single-peaked emission. H α displays a single-peaked emission profile of type VI. The He I 5875 Å line shows a faint inverse-P Cygni profile in the observation of Feb. 21st 2005, while the He I lines at 5875 Å and 6678 Å show broad double-peaked emission profiles in the observations of Feb. 20th 2005. The O I 777 nm triplet is stronger than predicted, and emission is observed in the wings of the profile in the observations of Feb. 20th.

We have calculated the LSD profiles without performing a special cleaning to the Kurucz mask. The three LSD I profiles display generally photospheric shapes, superimposed, in the core, on a faint and narrow absorption of unknown origin. A careful look at the spectra leads to the conclusion that this absorption could be present in all the metallic lines, but is lost in the noise, and thus cannot be corrected by cleaning the mask. We therefore fit the three profiles, simultaneously, with a photospheric function, but excluding the data points inside the cores. The result is shown in Fig. A55.

A56 HD 287823

From its Galactic coordinates (Perryman & ESA 1997), HD 287823 might be part of the Orion OB1 association, situated at a distance of ~ 375 pc (Blaauw 1964; Brown et al. 1994). The strong near-IR excess observed in the direction of HD 287823 reveals the presence of an optically thick inner disk around the star, as for many HAeBe stars (Hernández et al. 2005).

In our spectrum, we detect the spectral lines of a companion of almost the same projected rotational velocity, with a large enough radial velocity separation from the primary that the two spectra are well separated. The lines are sharp enough that we needed to in-

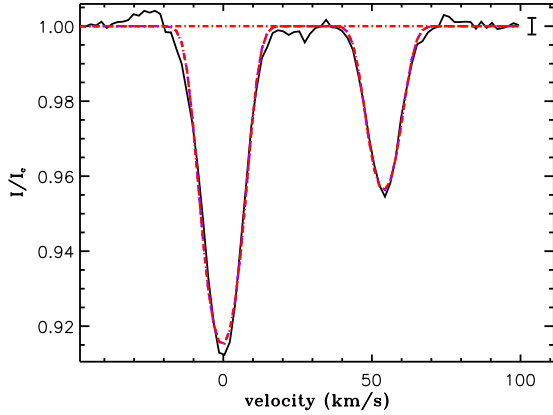


Figure A56. As Fig. A5 for HD 287823

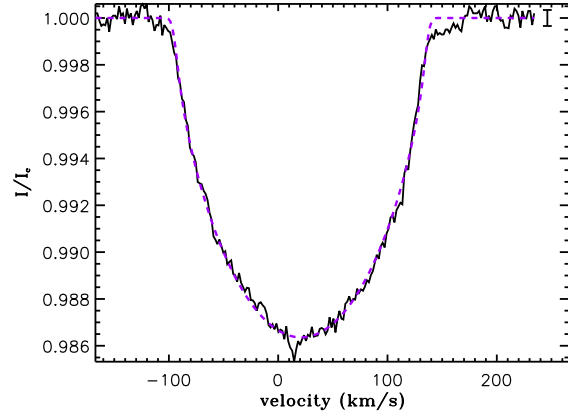


Figure A57. As Fig. A5 for HD 287841

clude macroturbulent velocities which we set to 2 km.s^{-1} . We find that our spectra are well reproduced with effective temperatures of 10000 K and 7000 K for the primary (P) and secondary (S) respectively, and with a ratio of radii R_P/R_S equal to 1.5, leading to a ratio of the luminosities : $L_P/L_S = 9.4$. We used the Hipparcos photometric data (Perryman & ESA 1997) to derive the luminosity of the system, $\log(L/L_\odot) = 1.83$, then the luminosity of each component : $\log(L_P/L_\odot) = 1.79$ and $\log(L_S/L_\odot) = 0.82$.

Doering & Meixner (2009), from IRAS observations, report the detection of an IR companion at a distance of 2.4 arcsec. The ESPaDOnS aperture being 1.6 arcsec, either the IR companion is the same as the spectroscopic companion observed in our spectrum, which means that the secondary has moved closer to the primary between the IRAS observations and ours, or the IR companion is not the same as the spectroscopic companion, and HD 287823 would therefore be a triple system.

Circumstellar features are only observed in few lines : weak emission is present in the core of $H\alpha$ and $H\beta$, while the wings of the O I 8446 Å and Ca II IR triplets seem to be in emission. We used the Kurucz mask of 10 000 K, more suitable for the primary that dominates the flux of the system, to calculate the LSD profile of the binary. While the line ratio of the LSD profile of the primary with respect to the secondary cannot be used for a determination of the luminosity ratio, the $v \sin i$ and v_{rad} of both components can still be retrieved from the fit of the LSD profile of the binary. We used the same method as for HD 152404 = AK Sco, to fit the profile of the binary, and the result is shown in Fig. A56.

A57 HD 287841 (= V346 Ori)

HD 287841 is part of the Orion OB 1a association (Hernández et al. 2005), situated at a distance of 375 pc (Brown et al. 1994). We used the Hipparcos photometric data (Perryman & ESA 1997) to derive the luminosity of the star. The spectral energy distribution in the near-IR is consistent with the presence of an optically thick inner disk around the star, as is found for most HAeBe stars (Hernández et al. 2005).

The spectrum of HD 287841 is consistent with the temperature and gravity determination of Bernabei et al. (2009, $T_{\text{eff}} = 7550 \pm 250 \text{ K}$, $\log g = 3.5 \pm 0.4$). CS features are only observed in few spectral lines. The core of $H\beta$ is contaminated with weak emission, while the core of $H\alpha$ is superimposed on a single-peaked emission

line. The O I 777 nm triplet is stronger than predicted, and emission might be present in the cores of the Paschen lines.

We have calculated the LSD profiles without performing a special cleaning to the Kurucz mask. The LSD I profile displays a photospheric shape that fits very well with a photospheric function. The result is shown in Fig. A57.

A58 HD 290409

HD 290409 is part of the Orion OB 1 star forming region (Vieira et al. 2003), situated at a distance $\sim 375 \text{ pc}$ (Brown et al. 1994). The near-IR excess observed in the direction of the star is similar to that observed for other Herbig Ae/Be stars (Doering & Meixner 2009).

Near-IR observations of HD 290409 reveal variability that could be due to a companion (Doering & Meixner 2009). In our spectrum we distinguish two components, one with an effective temperature around $9000 \pm 500 \text{ K}$ that provides a fit to the Balmer lines, and a second component that accounts for the metallic lines, at a temperature around 5000 K. By applying the LSD method with a mask for 9000 K, we obtain the LSD I profile of a binary star with a rapidly rotating primary, and a secondary rotating more slowly, consistent with the observed spectrum. We used the same method as in the case of HD 152404 = AK Sco to compute the synthetic composite spectrum of a binary star. We find that our spectrum is well reproduced with effective temperatures of 9000 K and 5000 K for the primary (P) and secondary (S), respectively, and with a ratio of radii R_P/R_S equal to 1.5. We also estimate the ratio of the luminosity : $L_P/L_S = 23.6$. We used the photometric data of Vieira et al. (2003) to derive the luminosity of the system : $\log(L/L_\odot) = 1.32$, and then the luminosity of each component : $\log(L_P/L_\odot) = 1.30$ and $\log(L_S/L_\odot) = -0.07$. The secondary is therefore a PMS solar-type star, and does not belong to the HAeBe-class.

Few CS features are observed in the spectrum. The cores of the Balmer lines, from $H\epsilon$ to $H\beta$, are superimposed on a redshifted CS absorption of increasing depth with wavelength. In addition, emission is observed in the wings of the CS absorption in $H\beta$. $H\alpha$ displays a complex emission profile. The O I 777 nm triplet is stronger than predicted, and the cores of the Paschen lines seem to be superimposed on faint and narrow single-peaked emission lines.

We used the Kurucz mask of 9000 K, more suitable for the dominant primary, to compute the LSD profiles of the binary. The resulting I profile shows photospheric shapes for both stars, super-

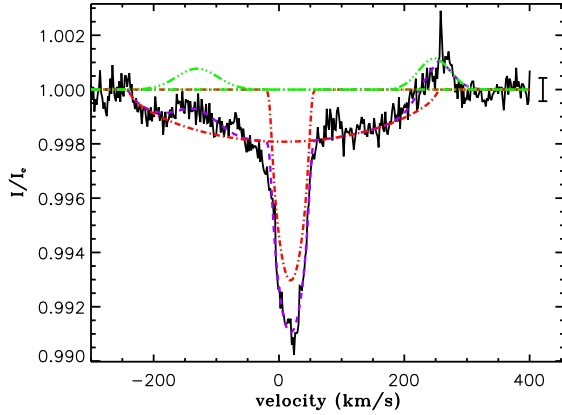


Figure A58. As Fig. A5 for HD 290409

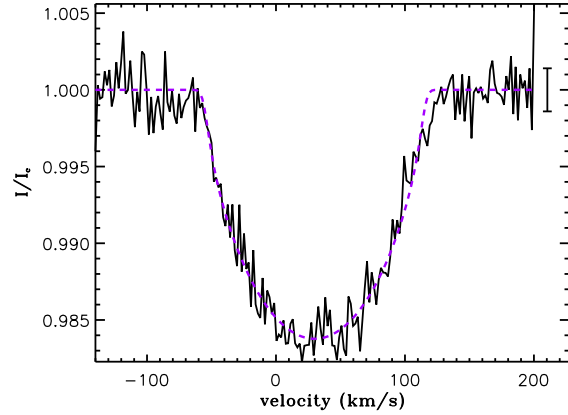


Figure A59. As Fig. A5 for HD 290500

imposed on weak emission. We used the same method as AK Sco to fit the LSD profile of the binary, but we also added two Gaussian functions in order to fit the CS emission. The result is shown in Fig. A58. We tried to eliminate the CS contamination by cleaning the mask, and fit the I profile with only the sum of two photospheric functions, but the results were much noisier and did not improve the determination of the $v \sin i$ of the two stars.

A59 HD 290500

HD 290500 is part of the Orion OB 1 star forming region (Vieira et al. 2003), situated at a distance ~ 375 pc (Brown et al. 1994). We used the photometric data of Guetter (1979) to derive the luminosity of the star. The near-IR excess observed in the direction of the star is similar to that observed around other Herbig Ae/Be stars (Doering & Meixner 2009).

The metallic lines of the spectrum are well fit with an effective temperature $T_{\text{eff}} = 9000 \pm 500$ K, consistent with the spectral type of the Henry Draper Extension Charts (HDEC) catalogue (Nesterov et al. 1995). The spectrum of HD 290500 is only slightly contaminated with CS features. The core of $H\beta$ is superimposed on a P Cygni profile. $H\alpha$ displays a double-peaked emission profile of type VI, with a narrow and strong central absorption. The O I 777 nm triplet is stronger than predicted, and the He I lines at 5875 Å and 6678 Å show inverse-P Cygni profiles. The spectrum longward of 8000 Å is too noisy to be analysed.

We have cleaned the mask in order to reject the lines contaminated with CS features. The LSD resulting I profile displays a photospheric shape well fitted with a photospheric function. The result is shown in Fig. A59.

A60 HD 290770

HD 290770 is part of the belt of Orion OB1 (Guetter 1976), situated at a distance of 375 pc (Brown et al. 1994). We used the photometric data of Vieira et al. (2003) to derive the luminosity of the star. The near-IR excess observed in the direction of the star is similar to that observed for other Herbig Ae/Be stars (Doering & Meixner 2009).

The spectrum of HD 290770 is almost without photospheric lines. This could be due to the combination of a high temperature and a large $v \sin i$. While the Balmer lines seem to be consistent with an effective temperature $T_{\text{eff}} = 10000$ K, the few photospheric

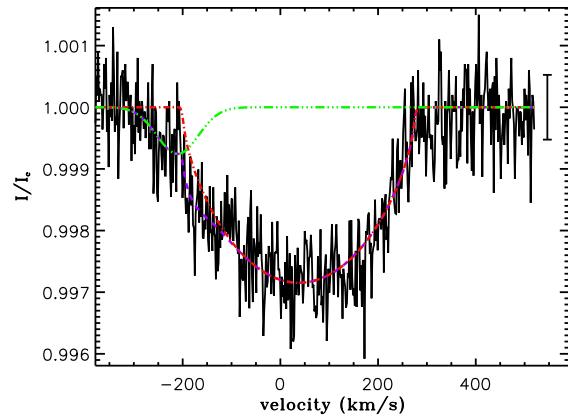


Figure A60. As Fig. A5 for HD 290770

lines that do not seem to be contaminated with CS features, and that are useful for temperature determination, such as the Ca II K and He I 4026 Å lines, are strongly in favour of an effective temperature $T_{\text{eff}} = 12000$ K. We therefore adopted a temperature of 11000 ± 1000 K, consistent with the temperature determination of Vieira et al. (2003).

Few circumstellar features are observed in the spectrum of HD 290770. The cores of the Balmer lines, from $H\theta$ to $H\beta$, are superimposed on a single-peaked emission line of increasing amplitude with wavelength. From $H\epsilon$ to $H\beta$ a blueshifted absorption component appears in the core of the profiles. $H\alpha$ displays a single-peaked emission profile of type VI, superimposed on two weak absorption components in the blue wing of the emission profile. The He I 4471 Å line is contaminated with emission, while the He I lines at 5875 Å, 6678 Å, and 7065 Å show broad double-peaked emission profiles. The O I 777 nm triplet is stronger than predicted. The O I 8846 Å triplet is in emission, and single-peaked emission lines are superimposed on the core of the Paschen lines.

We have cleaned the mask in order to reject the lines contaminated with CS features. The resulting LSD I profile displays a photospheric shape with weak CS contamination in the blue wing. We fit the profile with a photospheric function and a Gaussian function. The result is shown in Fig. A60.

A61 HD 293782 (= UX Ori)

UX Ori is part of the Orion OB1d association, situated at a distance of 375 pc (Brown et al. 1994). UX Ori is the prototype star of the UXOR-type objects, which are found to be strongly irregular photometric variables. The Hipparcos magnitudes (Perryman & ESA 1997), in the Tycho V_T system, vary from 8.6 mag to 11.0 mag. Corresponding to the PMS nature of HAeBe stars, this variability is assumed to be caused by moving circumstellar material, shadowing the star when it crosses the line of sight (Mora et al. 2002). Therefore the brightest magnitude observed by Hipparcos is very likely close to the true magnitude of the star. In order to convert the magnitudes ($V_T = 8.6$ mag, $B_T = 9.7$ mag) from the Tycho to the Johnson system, we used the calibration formula 1.3.20 of the Hipparcos and Tycho catalogues (Perryman & ESA 1997, p.57), and we find $V = 8.53$ mag and $(B - V) = 0.615$ mag.

The spectrum of UX Ori is very specific to the UXOR-type stars, and is strongly contaminated with transient circumstellar absorption and emission features in the Balmer lines and also in the metallic lines. Most of the photospheric profiles of the metal lines are contaminated with strong redshifted absorption, sometimes superimposed on blueshifted emission. Mora et al. (2002) argue that these absorption lines come from large bodies in the circumstellar disk of these stars. $H\alpha$ shows a double-peaked emission profile of type VI, with a redshifted central absorption that goes below the continuum. The cores of the other Balmer lines, from $H\epsilon$ to $H\beta$, are superimposed on redshifted absorption and blueshifted emission, both of which increase as the wavelength increases. The Ca II K line is much stronger than predicted, and displays a V-shape. The He I lines at 5875 Å and 6678 Å show inverse P Cygni profiles. The O I 777 nm and O I 8446 Å triplets show also inverse P Cygni profiles, but with very weak blue emission, and very strong red absorption. The Ca II IR triplet also displays P Cygni profiles, while faint blue-shifted emission is present in the cores of the Paschen lines. The wings of the Balmer lines and those metallic lines which are not contaminated with emission are consistent with the temperature and gravity determination of Mora et al. (2002, $T_{\text{eff}} = 9250 \pm 500$, $\log g = 4.0$).

We first calculated the LSD profiles without performing a special cleaning to the Kurucz mask, resulting in a strongly contaminated I profile. We have cleaned the mask in many ways, without improvement of the I profile. We therefore choose to fit the contaminated I profile by rejecting from the fit the contaminated part of the profile. The result is shown in Fig. A61.

A62 HD 344361 (= WW Vul)

WW Vul is an isolated Herbig Ae star, at a distance of ~ 700 pc, as estimated by Montesinos et al. (2009). WW Vul is an UXOR star (Mora et al. 2004), a class of stars that are known to be strong photometric variable. Strong variability was confirmed by Herbst & Shevchenko (1999), who find an amplitude of variation going up to 2.15 mag for WW Vul. We used the photometric data of these authors to compute the luminosity of the star.

WW Vul displays CS contamination in the spectral lines, similar to other UXOR stars. The lines not contaminated with CS features are consistent with the temperature determination of Mora et al. (2004, $T_{\text{eff}} = 9500$ K). Most of the photospheric lines, including Ca II K, and the Balmer lines from $H\eta$ to $H\beta$, are superimposed on strong redshifted absorption features, and sometimes show emission as well. $H\alpha$ displays a double-peaked emission pro-

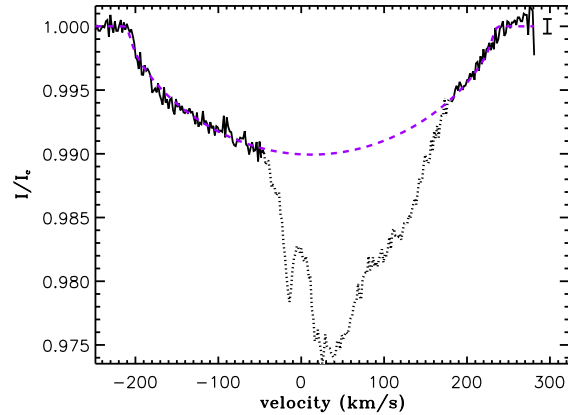


Figure A61. As Fig. A5 for HD 293782 (=UX Ori)

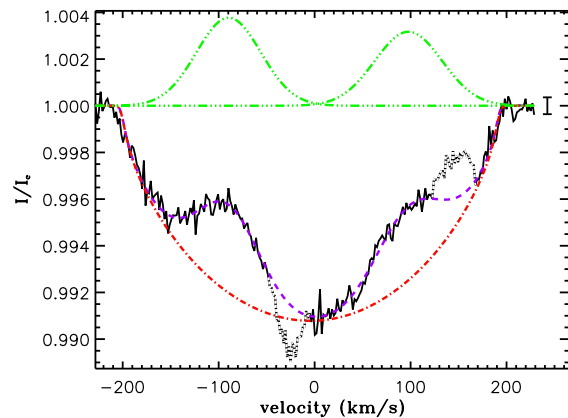


Figure A62. As Fig. A5 for the 2005 observation of HD 344361 (= WW Vul).

file of type VI, with a redshifted central absorption that goes below the continuum. The He I lines at 5875 Å, 6678 Å, and 7065 Å, as well as the O I 8446 and Ca II IR triplets show inverse P Cygni profiles. The O I 777 nm triplet is much stronger than predicted, and the cores of the Paschen lines are filled with emission.

We have calculated the LSD profiles without performing a special cleaning to the Kurucz mask. Both profiles display photospheric shapes with CS contamination, and can both be fitted with a photospheric function and Gaussian functions, giving consistent $v \sin i$. However, because the profile of 2007 is much noisier than the earlier observation, inclusion of these data did not improve the $v \sin i$ determination of the star, when combined with the profile of 2005. We therefore decide to fit only the profile from 2005 with a single photospheric function and two Gaussian functions. The result is shown in Fig. A62.

A63 LkH α 215

LkH α 215 is associated with the reflection nebulae NGC 2245 (Magakian 2003), situated at a distance of 900 pc (Oliver et al. 1996). We used the photometric data of (Herbst & Shevchenko 1999) to derive the luminosity of the stars. LkH α 215 possesses

strong near-IR excess that has been attributed by Hillenbrand et al. (1992) to a circumstellar accretion disk.

The spectrum of LkH α 215 contains two kind of lines : (i) broad, very shallow and rare lines, always superimposed on the second kind of lines ; (ii) sharp and very deep lines, that have shifted in radial velocity between the 2008 and the 2009 observations. Circumstellar emission in many metallic lines as well as a large $v \sin i$ are assumed to be at the origin of the first kind of lines. The second kind of lines is assumed to come from a slow rotator with a high metallicity. In spite of the peculiarity of this spectrum, as well as its low SNR, we attempted to determine the effective temperature of both stars. From the wings of the Balmer lines as well as the presence of few He I lines, we find that a temperature around 14000 K fits the lines of the fast rotator satisfactorily, which we assume to be the primary component. The lines of the slow rotator, the secondary component, seem to be produced by a photosphere at 14000 K, as well. However these lines are much deeper than those predicted by a solar composition synthetic spectrum. Varying the gravity and the effective temperature within reasonable ranges does not improve the fit. A strong metallicity is therefore more likely to be the cause of the large depth of these lines. While our temperature determination is highly uncertain, the SB2 nature of LkH α 215 appears firmly established, and we will therefore consider it as a binary in the following.

Due to the uncertain determination of the temperature of both stars, and the low SNR of our data, we are not able to constrain usefully the luminosity ratio of the two components. As both stars seem to have similar temperatures, and are very young, it is reasonable to assume that they have a common origin and a similar age, and therefore similar luminosities. The luminosity ratio could therefore be close to 1.

The spectrum of LkH α 215 is contaminated with circumstellar features. As mentioned above, we suspect that the absence of many metallic lines, as well as the faintness of others, are not only due to a large $v \sin i$, but also to contamination by CS emission. We also observe emission in the cores of the Balmer lines from H ϵ to H γ . H β displays a double-peaked emission profile of type VI with a central absorption that goes well below the continuum. H α shows a double-peaked emission profile of type V (according to Beals 1953), with a redshifted central absorption that reaches the continuum. The O I 8446 Å triplet displays a double-peaked emission profile, while the Ca II IR-triplet shows a single-peaked emission line. The Paschen lines seem to be filled with emission, and superimposed on deep and narrow central absorption.

We have cleaned the mask in order to reject the lines contaminated with CS features, to compute the LSD profiles of the binary. The I profile of 2009 is much less noisy than the profile of 2008. The result is that while both components are visible in the profile of 2009, only the secondary component is visible in the profile of 2008 (Fig. A63 left). In Fig. A63 (left), we show the shift in radial velocity of the secondary component from 2008 (black full line) to 2009 (red dashed line). Due to the low SNR of the profile of 2008, we did not use it to determine the $v \sin i$ of the primary, but we nevertheless fit it to determine the radial velocity of the secondary component in 2008. The $v \sin i$ of both components as well as the radial velocity of the primary and the radial velocity of the secondary in 2009 have been determined from the fit of the 2009's profile. While we tried to eliminate the lines contaminated with emission, we still have a small contamination in the 2009 profile that we could not improve. We therefore fit the profile with a photospheric function for a binary (as in HD 152404 = AK Sco) and a Gaussian function. The result is shown in Fig. A63.

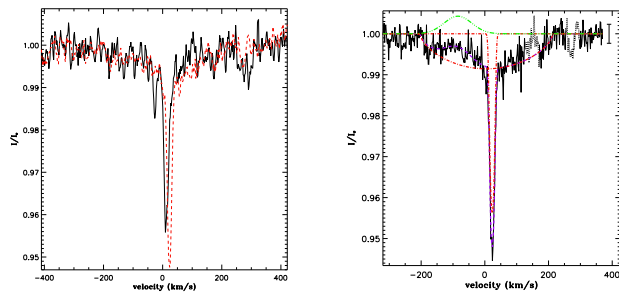


Figure A63. Left : LSD I profiles of LkH α 215 observed on Apr. 15th 2008 (black full line) and Mar. 11th 2009 (red dashed-line). Note the shift in radial velocity of the secondary. Right : As Fig. A5 for the Mar. 11th 2009 observation of LkH α 215.

A64 MWC 1080

The MWC 1080 system is a small stellar group embedded within the dark cloud LDN1238. Using the local standard of rest velocity of this dark cloud ($v_{\text{LSR}} = -30.3 \text{ km.s}^{-1}$) determined by Levreault (1985), and the revised prescription for calculating kinematic distances of Reid et al. (2009) to estimate the distance of the system at about 2300 pc. The most luminous star, MWC 1080 (V628 Cas), has been classified as a B0e star with a flat optically thick circumstellar disk (Wang et al. 2008).

The ESPaDOnS spectrum of MWC 1080 is totally contaminated with emission, sometimes superimposed on circumstellar absorption. No photospheric lines is detected in the spectrum. All the Balmer lines display P Cygni profiles of type IV, except H α which shows a P Cygni line of type III. We are therefore not able to give an estimate of the effective temperature of the star, or to confirm the spectral type of Hillenbrand et al. (1992). In the absence of photospheric lines $v \sin i$ can not be determined.

A65 VV Ser

VV Ser is located in the Serpens molecular cloud, situated at a distance of 260 pc (Straizys et al. 1996). We used the photometric data of Herbst & Shevchenko (1999) to compute the luminosity of the star. Based on its spectral energy distribution, VV Ser has been classified as a group I object by Hillenbrand et al. (1992), one of a class of objects that are surrounded with flat optically thick accretion disk.

The spectrum of VV Ser is strongly contaminated with circumstellar features, and has been classified as an UXOR-type star (Pontoppidan et al. 2007). CS absorption components and sometimes emission are superimposed on the photospheric profiles of many metallic lines (including Ca II K). The cores of the Balmer lines from H η to H γ are also superimposed on blueshifted CS absorption, with emission on the blue side of the CS absorption. Both emission and absorption increase with increasing wavelength. H β displays a double-peaked emission profile of type VI, with a slightly blueshifted central absorption that goes well below the continuum. H α shows a double-peaked emission profile of type V, with a slightly blueshifted central absorption that almost reaches the continuum. The He I lines at 5875 Å, 6678 Å, and 7065 Å display inverse P Cygni profiles with very strong absorption. The O I 777 nm triplet is much stronger than predicted, while the O I 8446 Å triplet has a double-peaked emission profile. Double-peaked emission profiles are also superimposed on the cores of the Paschen lines, while the Ca II IR-triplet displays

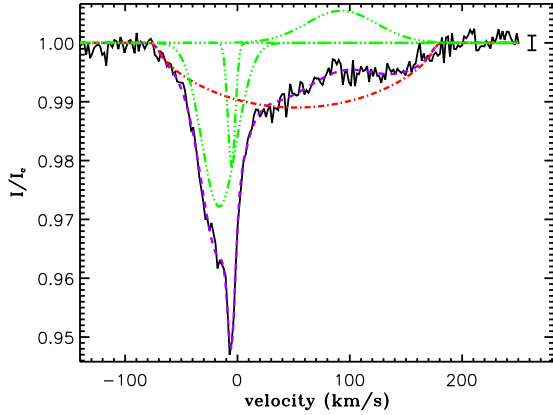


Figure A64. As Fig. A5 for VV Ser.

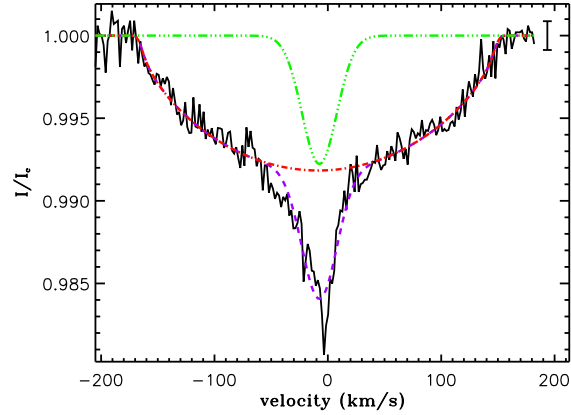


Figure A65. As Fig. A5 for VX Cas.

double-peaked emission profiles with very strong central absorption. The wings of the photospheric profiles are consistent with the effective temperature determination of Hernández et al. (2004, $T_{\text{eff}} = 14000 \pm 2000$).

We have calculated the LSD profiles without performing a special cleaning to the Kurucz mask. The resulting LSD I profile is contaminated with circumstellar features. We tried to clean the mask, without improving the I profile. We therefore fit the contaminated I profile with a photospheric function and 3 Gaussian functions modelling the circumstellar components. The result is shown in Fig. A64.

A66 VX Cas

VX Cas is an UX Orionis star situated at a distance of 620 pc (Montesinos et al. 2009). We used the photometric data of Herbst & Shevchenko (1999) to determine the luminosity of the star. VX Cas possesses a strong IR excess due to thermal emission from its circumstellar dust (Shakhovskoi et al. 2003).

The spectrum of VX Cas is well fit with an inconsistent with the effective temperature of Hernández et al. (2004, $T_{\text{eff}} = 9500 \pm 1500$ K). Most of the metallic lines (including Ca II K) are superimposed on blueshifted CS absorption components. Blueshifted CS absorption is also observed in the core of the Balmer lines from H ϵ to H β . In addition, emission is present in the wings of the CS absorption in H γ and H β . H α displays a double-peaked emission profile of type VI, with a slightly blueshifted central absorption that reaches the continuum. The He I lines at 5875 Å and 6678 Å, as well as the O I 777 nm triplet, are much broader and much deeper than predicted. Although the spectrum above 8000 Å is quite noisy, it appears that the Ca I IR triplet may be in emission, and emission may fill the core of the Paschen lines.

We have calculated the LSD profiles without performing a special cleaning to the Kurucz mask. The resulting LSD I displays a photospheric profile superimposed on a narrow central circumstellar absorption. We tried to clean the mask by rejecting, as far as possible, the contaminated lines. The result gives a profile which is still contaminated with the CS absorption, and with a much lower SNR. We therefore decided to fit the profile with the highest SNR, with a photospheric function plus a Gaussian function. The result is shown in Fig. A65.